Helsinki University of Technology Signal Processing Laboratory
Teknillinen korkeakoulu Signaalinkäsittelytekniikan laboratorio
Espoo 2007 Report 61

ANALYSIS AND COMPENSATION OF NONLINEAR POWER AMPLIFIER EFFECTS IN MULTI-ANTENNA OFDM SYSTEMS

Fernando Hugo Gregorio

Dissertation for the degree of Doctor of Science in Technology to be presented with due permission of the Department of Electrical and Communications Engineering for public examination and debate in Auditorium S2 at Helsinki University of Technology (Espoo, Finland) on the 19th of November, 2007, at 12 o'clock noon.

Helsinki University of Technology
Department of Electrical and Communications Engineering
Signal Processing Laboratory

Teknillinen korkeakoulu
Sähkö- ja tietoliikennetekniikan osasto
Signaalinkäsittelytekniikan laboratorio

Distribution:
Helsinki University of Technology
Signal Processing Laboratory
P.O. Box 3000
FIN-02015 HUT
Tel. +358-9-451 3211
Fax. +358-9-452 3614
E-mail: Mirja.Lemetyinen@tkk.fi
Webpage: http://wooster.tkk.fi

ISBN 978-951-22-9000-0 (Printed)
ISBN 978-951-22-9001-7 (Electronic)
ISSN 1458-6401

Multiprint
Espoo 2007

ABSTRACT OF DOCTORAL DISSERTATION	HELSINKI UNIVERSITY OF TECHNOLOGY P.O. BOX 1000, FI-02015 TKK http://www.tkk.fi

Author Fernando Hugo Gregorio

Name of the dissertation

Analysis and compensation of nonlinear power amplifiers effects in multi-antenna OFDM systems

Manuscript submitted 08.06.2007	Manuscript revised 27.09.2007

Date of the defence 19.11.2007

☐ Monograph ☒ Article dissertation (summary + original articles)

Department Electrical and Communications Engineering

Laboratory Signal Processing Laboratory

Field of research Digital Signal processing in wireless communication systems

Opponent(s) Prof. Markus Rupp (Vienna University of Technology) and Docent Mikko Valkama (Tampere University of Technology)

Supervisor Risto Wichman

Instructor Stefan Werner

Abstract

The high peak to average power ratio (PAPR) levels associated with multicarrier systems require the use of linear power amplifiers (PA) with large dynamic range. Unfortunately, linearity and power efficiency are two conflicting specifications for practical PAs. However, systems with high power efficiency are required, for example, in case of battery operated mobile terminals.Thus, the PA needs to operate in a high power efficiency region which compromises the linearity constraints. The evaluation of the effect of nonlinear amplification on the system performance is an important issue that must be considered in a realistic system design.

This thesis first addresses the performance analysis of multiuser OFDM systems (space division multiple access (SDMA)-OFDM) employing nonlinear PAs. Bit error probability (BEP) and capacity expressions are derived for an OFDM system with diversity, assuming a memoryless PA. Moreover, BEP expressions are derived for an orthogonal space-time coded (OSTBC)-OFDM system that include the effect of a broadband nonlinear PA and imperfect memory compensation. Thereafter, techniques to reduce the effects of power amplifier distortion are proposed. We consider techniques that can be implemented either in the receiver, the transmitter, or as a combination of both, all with the same goal of relieving the linearity constaints and improving the power efficiency.

A low PAPR OFDM implementation is addressed where subcarriers are allocated to different users in such a way that the generated intermodulation distortion is kept at minimum. Then, we propose the combination of multiuser detection and nonlinear distortion mitigation techniques. Initially, knowledge of the PA model (modelled as memoryless) is required for the implementation. The extension to broadband PAs and to PA model estimation in the receiver are also made. Efficient channel estimation strategies are developed that work in the presence of nonlinear distortion. Finally, a split predistorter structure to remove nonlinear distortion caused by a broadband PA is proposed. The idea is to reduce the transmitter complexity by distributing the predistorter tasks such that the transmitter compensates for the static nonlinearity, and the receiver equalizes the PA memory.

Keywords Nonlinear power amplifiers, OFDM, PAPR, nonlinear distortion

ISBN (printed) 978-951-22-9000-0	ISSN (printed) 1458-6401
ISBN (pdf) 978-951-22-9001-7	ISSN (pdf)
Language English	Number of pages 133 + app. 69

Publisher Helsinki University of Technology, Signal Processing Laboratory

Print distribution Helsinki University of Technology, Signal Processing Laboratory

☒ The dissertation can be read at http://lib.tkk.fi/Diss/isbn9789512290017

VÄITÖSKIRJAN TIIVISTELMÄ	TEKNILLINEN KORKEAKOULU PL 1000, 02015 TKK http://www.tkk.fi

Tekijä Fernando Hugo Gregorio

Väitöskirjan nimi
Epälineaaristen tehovahvistimien suorituskykyanalyysi ja epälineaarisuuksien kompensointi usean antennin OFDM-järjestelmissä

Käsikirjoituksen päivämäärä 08.06.2007	Korjatun käsikirjoituksen päivämäärä 27.09.2007

Väitöstilaisuuden ajankohta 19.11.2007

☐ Monografia	☒ Yhdistelmäväitöskirja (yhteenveto + erillisartikkelit)

Osasto Electrical and Communications Engineering

Laboratorio Signal Processing Laboratory

Tutkimusala Tietoliikenteen signaalinkäsittely

Vastaväittäjä(t) Prof. Markus Rupp (Vienna University of Technology) and Docent Mikko Valkama (Tampere University of Technology)

Työn valvoja Prof. Risto Wichman

Työn ohjaaja Dr. Stefan Werner

Tiivistelmä

Lähetystehon suuri vaihtelu monikantoaaltojärjestelmissä asettaa tiukkoja vaatimuksia tehovahvistimille. Vahvistimien lineaarisen alueen pitää olla suuri, mikä johtaa huonoon hyötysuhteeseen ja suureen tehonkulutukseen vahvistimen operoidessa lineaarisella alueella. Jos vahvistimen hyötysuhde halutaan pitää korkeana, kuten esimerkiksi akuilla toimivissa kannettavissa päätelaitteissa, vahvistettu signaali väistämättä vääristyy. Näiden epälineaaristen vääristymien kompensointi on tärkeä osa langattomien tietoliikennejärjestelmien suunnittelua.

Tässä työssä tarkastellaan epälineaaristen tehovahvistimien vaikutusta monen käyttäjän OFDM- järjestelmiin ja näiden vaikutusten kompensointia lähettimessä ja/tai vastaanottimessa, kun päätelaitteissa voi olla useampia antenneja. Lähettimessä vääristymien epäedullista vaikutusta vähennetään lomittelemalla lähetettyjä kantoaaltoja eri lähetysantennien kesken. Vastaanottimessa monen käyttäjän ilmaisu yhdistetään vääristymien kompensointiin ja kanavaestimointiin. Lopuksi työssä kehitetään algoritmi, jossa vääristymien kompensointi jaetaan lähettimen ja vastaanottimen kesken. Työssä myös johdetaan vastaanottimen virhetodennäköisyyslausekkeet ja kanavan kapasiteettilausekkeet erilaisille systeemimalleille, kun lähetetty signaali on vääristynyt epälineaarisesti.

Asiasanat tietoliikennetekniikka, tehovahvistin, OFDM, moniantennitekniikka

ISBN (painettu) 978-951-22-9000-0	ISSN (painettu) 1458-6401
ISBN (pdf) 978-951-22-9001-7	ISSN (pdf)
Kieli Englanti	Sivumäärä 133 + app. 69

Julkaisija Helsinki University of Technology, Signal Processing Laboratory

Painetun väitöskirjan jakelu Helsinki University of Technology, Signal Processing Laboratory

☒ Luettavissa verkossa osoitteessa http://lib.tkk.fi/Diss/isbn9789512290017

Acknowledgements

The work constituting this thesis was carried out in the Signal Processing Laboratory at Helsinki University of Technology during the years 2003 - 2007. The Signal Processing in Telecommunications research group is a member of SMARAD, which is a Center of Excellence accredited by the Academy of Finland.

I wish to express my gratitude to my former supervisor, Prof. Timo Laakso for his continuous encouragement, guidance and support during the course of this work. I am also grateful to my current supervisor Prof. Risto Wichman for his support and advice during the last period of my work.

I wish to express many thanks to my instructor and co-author D. Sc. Stefan Werner for his support and constructive criticism that improved my work and the technical quality of my publications. Stefan gave me a great support during these four years being very well-disposed and willing to help every single time I needed correction, advice, and improvements for my drafts. Special thanks to his guidance and constant encouragement.

Then, I would like to thank the thesis pre-examiners Dr. Dhammika Jayalath and Docent Dr. Mikko Valkama, for their constructive and helpful comments.

I really appreciate the support of Prof. Juan Cousseau from Universidad Nacional del Sur, Argentina, who was my M. Sc. degree supervisor and is co-author in many scientific papers. I consider him as my father in the academic world.

Furthermore, I would like to thank all my colleagues and co-workers at the Signal Processing Laboratory. Very special thanks to my friend Eduardo Zacarías for our endless conversations. Additionally, I am grateful to Gilda Jantunen (ex Gámez), Mobien Shoaib, Mei Yen and Cássio Ribeiro for all the constructive and relaxing discussions.

Many thanks go to our laboratory secretaries Mirja Lemetyinen and Anne Jäskeläinen, and the GETA coordinator Marja Leppäharju; they were always eager to help in their best mood in every-day practical issues that made my and my family's life easier in Finland.

I am also thankful to the Argentinean community in Finland, especially Sergio's, Matias', Markus', Temmu's, and Timo's families for the joyful moments spent together as well as for their unconditional help during difficult

times.

The thesis work was partially funded by ALβAN, European Union Programme of High Level Scholarships for Latin America. Identification Number: E03D19254AR and Helsinki University of Technology postgraduate scholarship. The financial support from Nokia Foundation, Finnish Cultural Foundation, and Ella and Georg Ehrnrooth Foundation is gratefully acknowledged.

I wish to express my gratitude to my family's wholehearted support. First of all it goes to my parents, Hugo and María Elisa; and my parents in law, Hilda and Carlos. At the same time to my blood siblings and in laws Soledad, Belen, Juan Pablo, Sergio, and Alicia, for their tireless encouragement during all this time.

Last, but not least, to my beloved wife Patricia and our lovely daughters Manuela, Delfina, and Luisa, who followed me on this fantastic adventure: many thanks for providing me with a more colorful life outside the research work and the happiness in my life, *Muchisimas gracias!*.

I dedicate this thesis to Patricia and The Powerpuff Girls, Manuela, Delfina, and Luisa.

Espoo, November 2007

Fernando Gregorio

A Patricia, Manuela, Delfina y Luisa

Contents

List of original publications

P1: F. Gregorio, T.I. Laakso and R. Wichman. Comparison of clustered and antenna interleaving OFDM in multiple-antenna systems with amplifier nonlinearities, in *Proceedings of the IEEE Signal Processing and Communications 2004, SPCOM 2004,* pp. 111-114, December 2004, Bangalore, India.

P2: F. Gregorio and T.I. Laakso. Novel carrier allocation for multiuser OFDM system with amplifier nonlinearities, in *Proceedings of the European Signal Processing Conference, EUSIPCO 2005,* September 2005, Antalya, Turkey.

P3: F. Gregorio, J. Cousseau and T.I. Laakso. Receiver cancellation of nonlinear power amplifier distortion in SDMA-OFDM systems, in *Proceedings of the IEEE International Conference on Acoustics, Speech, and Signal Processing, ICASSP 2006,* pp. IV 325-328, May 2006, Toulouse, France.

P4: F. Gregorio, S. Werner, J. Cousseau and T.I. Laakso. Channel estimation for multiuser OFDM systems in the presence of power amplifier nonlinearities, in *Proceedings of the International Symposium on Personal Indoor and Mobile Radio Communication, PIMRC 2006,* September 2006, Helsinki, Finland.

P5: F. Gregorio, S. Werner, J. Cousseau and T.I. Laakso. Receiver cancellation technique for nonlinear power amplifier distortion in SDMA-OFDM systems, *IEEE Transactions on Vehicular Technology*, vol. 56, no.5, pp. 2499 - 2516. September 2007.

P6: F. Gregorio, S. Werner, J. Cousseau and R. Wichman. Split predistortion approach for reduced complexity terminal in OFDM systems, in *Proceedings of the Vehicular Technology Conference, VTC 2007,* pp. 2697-2701, April 2007, Dublin, Ireland.

P7: F. Gregorio, S. Werner, J. Hämäläinen, R. Wichman and J. Cousseau. BEP analysis of OSTBC-OFDM systems with broadband PA and imperfect memory compensation, to appear in *IEEE Communications Letters*, 2007.

P8: F. Gregorio, S. Werner, J. Cousseau and R. Wichman. Broadband power amplifier distortion cancellation with model estimation in the receiver, in *Proceedings of the IEEE International Workshop on Signal Processing Advances for Wireless Communications, SPAWC 2007,* June 2007, Helsinki, Finland.

Abbreviations and symbols

Abbreviations

ADSL	Asymmetric Digital Subscriber Line
ACI	adjacent channel interference
ACPR	adjacent channel power ratio
A/D	analog to digital conversion
AM/AM	amplitude to amplitude conversion
AM/PM	amplitude to phase conversion
AWGN	additive white Gaussian noise
BS	base station
CALLUM	combined analog locked loop universal modulator
CDF	cumulative distribution function
CCDF	complementary cumulative distribution function
CDMA	code division multiple access
COFDM	clustered orthogonal frequency division multiplexing
CP	cyclic prefix
CSI	channel state information
D/A	digital to analog conversion
DAB	Digital Audio Broadcasting
DAR	decision-aided reconstruction
DFT	discrete Fourier transform
DMT	discrete multitone modulation
DSP	digital signal processing
DSL	digital subscriber lines
DVB	Digital Video Broadcasting
EDGE	Enhanced Data-rates for Global Evolution
EER	envelope elimination and restoration
FFT	fast Fourier transform
FDM	frequency division multiplexing
FDMA	frequency division multiple access
FEQ	frequency domain equalizer
GaAs FET	gallium arsenide field effect transistor
HSDPA	High Speed Downlink Packet Access

i.i.d.	independent identically distributed
IBI	inter block interference
IBO	input back-off
IDFT	inverse discrete Fourier transform
IF	intermediate frequency
IMD	intermodulation distortion
IMP	intermodulation products
ISI	intersymbol interference
IMT	International Mobile Telecommunications
IP3	third order interception point
KV	Kautz-Volterra
LiNC	linear amplification with nonlinear components
LMS	least mean square
LS	least squares
LUT	look-up table
MAI	multiple access interference
MAP	maximum a posteriori
ML	maximum likelihood
MIMO	multiple-input multiple-output
MMSE	minimum mean square error
OBO	output back-off
OFDM	orthogonal frequency division multiplexing
OSTBC	orthogonal space time block code
PDF	probability density function
PA	power amplifier
PAE	power amplifier efficiency
PAPR	peak to average power ratio
PD	predistorter
PANC	power amplifier nonlinearities cancellation
PIC	parallel interference cancellation
PICR	peak to interference-to-carrier ratio
PSD	power spectral density
PTS	partial transmit sequence
QPSK	quadrature phase-shift keying
QAM	quadrature amplitude modulation
RF	radio frequency
r.v.	random variable
SC-CP	single carrier system with cyclic prefix
SDMA	space division multiple access
SNDR	signal to noise and distortion ratio
SNR	signal to noise ratio
SFC	space frequency coding
SIC	successive interference cancellation
SISO	single-input single-output

STC	space time coding
SSPA	solid state power amplifier
TDMA	time division multiple access
TI	tone injection
TR	tone reservation
TWTA	traveling wave tube amplifier
VBLAST	Vertical Bell Laboratories Layered Space-Time Architecture
UWB	ultra wide band
WCDMA	Wideband CDMA
WLAN	wireless local access network
WiMAX	Worldwide Interoperability for Microwave Access
WiFi	Wireless Fidelity
3G	third generation
4G	fourth generation

Symbols

$\|\mathbf{x}\|$	euclidean norm of vector $\mathbf{x}$
$\|x\|$	absolute value of scalar x
A_s	saturation output amplitude
$E\{x\}$	expectation of random variable x
j	imaginary unit
exp	exponential function
F_a	AM/AM conversion
F_p	AM/PM conversion
$g(\cdot)$	Memoryless PA transfer function
$\mathbf{G}_{cp}$	cyclic prefix insertion matrix
K_L	Linear gain of the PA
k	OFDM subcarrier index
min	minimum
max	maximum
n	OFDM symbol index
N	Number of OFDM subcarriers
$\mathbf{Q}_N$	IDFT matrix
$\mathbf{Q}_N^{\mathrm{H}}$	DFT matrix
$\mathbf{R}_{cp}$	cyclic prefix removal matrix
$\mathcal{X}$	frequency domain scalar
$\boldsymbol{\mathcal{X}}$	frequency domain vector
$\boldsymbol{\mathcal{X}}$	frequency domain matrix
x	time domain scalar
$\mathbf{x}$	time domain vector
$\mathbf{X}$	time domain matrix
x^*	complex conjugate of x

$\mathbf{X}^{\mathrm{T}}$	transpose of a matrix $\mathbf{X}$
$\mathbf{X}^{\mathrm{H}}$	Hermitian transpose of a matrix $\mathbf{X}$
$\hat{x}$	estimate of x
v	cyclic prefix length
ν	clipping level
σ_n^2	variance of noise sequence
σ_x^2	variance of input sequence
σ_d^2	variance of nonlinear distortion sequence
σ_c^2	variance of memory compensation error

Chapter 1

Introduction

1.1 Motivation

New generations of wireless communication systems require high data rate transmission in order to fulfill the requirements for multimedia communication. Bandwidth-intensive multimedia applications have boosted the evolution of wireless technology, e.g., mobile television service via Digital Video Broadcasting (DVB) and wireless teleconferencing. An open issue that the new technology needs to solve to enable ubiquitous broadband wireless communications is the integration of wireless LAN (WLAN) and Bluetooth with advanced wireless technologies such as 3.5G High-Speed Downlink Packet Access (HSDPA), DVB, WiFi, WiMAX, and sensor networks.

The majority of the new communication systems are adopting multicarrier techniques, in particular Orthogonal Frequency Division Multiplexing (OFDM), which are effective techniques for combating multipath fading and enable high data rate transmissions over mobile wireless channels. OFDM has been standardized in several wired and wireless systems, such as IEEE802.11a/g wireless LAN [1,2], HIPERLAN/2 [3], Digital Audio Broadcasting (DAB) [4], DVB [5] and Digital Subscriber Lines (DSL) [6]. OFDM also allows the allocation of several user bands dividing the spectrum in groups, referred to as multiband (MB) OFDM. The advantages of MB OFDM are exploited in the WiMedia MB-OFDM standard [7] developed for ultra wide band (UWB) communication systems [8, 9].

OFDM provides high spectral efficiency and robustness against time dispersive channels [10, 11]. In multicarrier systems, the modulation is performed on a block-by-block basis, with a guard interval between the blocks. By transmitting several symbols in parallel, the symbol duration is increased thereby reducing the effects of intersymbol interference (ISI) caused by the dispersive fading channel. Under the assumption that the channel delay spread is shorter than the guard interval (implemented as a circular extension), the convolution between the transmitted data and the channel

becomes circular. This means that the received frequency domain signal is simply the point-wise multiplication of the input signal and the channel coefficients in frequency domain. Then, the transmitted symbols can be recovered by a simple single-tap equalizer for each subcarrier allowing the implementation of simple receiver structures.

OFDM also supports adaptive modulation techniques where the constellation size on each subcarrier depends on the channel conditions [12, 13]. The subcarriers with high signal-to-noise ratio (SNR) values employ more constellation points than subcarriers with low SNR. Using adaptive bit loading, the achievable bit rate of a multicarrier system is always larger or equal to that of a single-carrier system with cyclic prefix (SC-CP) operating over the same channel and bandwidth [14].

To achieve the performance advantages of adaptive modulation, channel state information (CSI) is required at the transmitter. The mismatch between the CSI at the transmitter and the real channel affects the reliability of the allocation method. As a consequence the feedback channel link carrying the CSI need to be carefully designed [15].

To achieve tolerable levels of error probability and immunity against time and frequency selective fading, channel coding is necessary. Channel coding can be implemented in either time domain or frequency domain. Block, convolutional and turbo codes are the most used coding methods in the majority of the wireless standards [16]. They can be combined with interleavers to improve the system performance in the presence of burst errors.

The implementation of OFDM in conjunction with multi-antenna techniques is a promising way to efficiently use the radio spectrum extending the capacity of mobile communication systems, see, e.g., [17–22]. Multi-antenna OFDM technologies are suitable for dynamic multiuser resource allocation [23] that exploits system diversities in time, frequency and space through an intelligent management of bandwidth allocation, multiple access, scheduling, and power and rate adaptation. In a multiuser system, the implementation of multiuser OFDM that assigns dynamically the subcarriers according to the channel conditions shows an effective improvement in the system performance [24] when compared with fixed multiple-access schemes such as time division multiple access (TDMA) and frequency division multiple access (FDMA) [25].

Multi-antenna OFDM systems are implemented by evolving standards as IEEE802.11n and IEEE802.16 WMAN, and is a potential candidate in the standardization of IMT-Advanced mobile cellular systems.

The implementation of an OFDM transceiver is depicted in Figure 1.1. At the transmitter, the input bits are mapped onto appropriate symbols, based on the modulation used on the corresponding subcarrier, then grouped and processed by the inverse discrete Fourier transform (IDFT). The parallel output of the IDFT is converted to a serial stream of OFDM symbols

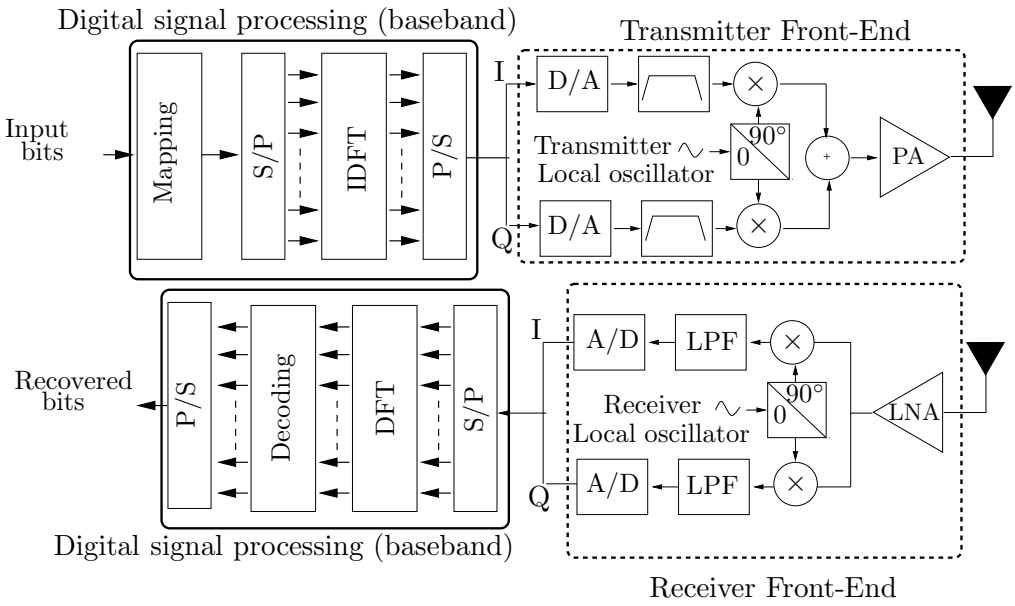

Figure 1.1: OFDM transceiver architecture

.

and separated into real (in-phase) and imaginary (quadrature-phase) components (I and Q), and then converted into an analog baseband signal using a digital-to-analog converter (D/A). Thereafter the analog signal is filtered by two reconstruction filters. Finally, the I and Q channels are translated to the carrier frequency and amplified. In the transmitter two principal parts can be identified: a digital block that operates at baseband frequency, and an analog block, referred to as the RF front-end, that operates at radio frequency. The RF front-end consists of components that need to be carefully designed to ensure a proper system operation.

At the receiver, the received signal is first amplified by a low noise amplifier (LNA). Analog in-phase and quadrature demodulators (I/Q demodulator) are used to down-convert the received signal to baseband. Thereafter, the signal is filtered and converted to digital domain where it is demodulated, equalized and decoded to recover the original transmitted symbols.

Several impairments of the RF front-end block can have a major impact on the system performance:

1. Power amplifier with nonlinear transfer functions: real PA has a nonlinear response that creates in-band and out-of-band distortion that not only reduces the system performance but also creates interference on adjacent channels.

2. In-phase and quadrature (I/Q) imbalances: an amplitude or phase mismatch between the I and Q branches in the front-end analog pro-

cessing leads to a limited image attenuation.

3. Phase noise: the presence of random phase noise in the local oscillators causes constellation rotation and intercarrier interference (ICI).

4. Carrier frequency offset: created by mismatch between the carrier frequency of the oscillators in the transmitter and the receiver and by Doppler shift due to movility.

This thesis focuses on the first impairment and deals with the compensation and analysis of OFDM systems employing nonlinear PAs. Carrier frequency offset, I/Q imbalance, and phase noise are briefly reviewed in Chapter 2.

The high peak to average power ratio (PAPR) associated with the OFDM signal is an important drawback in the search of a power efficient communication system [26]. The high dynamic range of the OFDM signal requires a linear PA, that in general shows poor results in terms of power efficiency.

Figure 1.2a shows the amplitude distribution of two OFDM signals, where signal s_0 has a high dynamic range and signal s_1 is a scaled version of s_0 with reduced variance. Figure 1.2b illustrates a typical transfer function of a nonlinear PA. Three PA operation regions can be seen from this figure: a linear region where the output signal is a scaled version of the input signal ($P_0 < P_{in} < P_L$), a nonlinear region where the PA gain decreases ($P_L < P_{in} < P_{sat}$), and a saturation region where the output signal reaches the maximum value ($P_{in} > P_{sat}$). Finally, the power efficiency as a function of the input signal power is plotted in Figure 1.2c. From the figures we can infer that s_0 will cause the PA to operate in the saturation region. One way to force the operation of the PA into the linear region, is to scale the input signal (back-off), like in the case of signal s_1. It will reduce the signal fluctuations and the PA will operate mostly in the linear region with low levels of nonlinear distortion. However, as is illustrated in Figure 1.2c, PAs are more power efficient when operating close to the saturation region. Similarly, the closer to saturation the PA is driven, the larger the amount of nonlinear distortion, which will degrade the system performance.

It is clear that there is a trade-off between the allowed level of nonlinear distortion and the system power efficiency. An illustration of the out-of-band distortion and in-band distortion created by a solid state power amplifier operating at different back-off levels, is shown in Figure 1.3.

In order to maintain tolerable levels of bit error rate (BER) and adjacent channel interference (ACI) while increasing the power efficiency performance, we will need to consider techniques for compensating the nonlinear distortion. This compensation can be done at the transmitter or at the receiver. When the compensation is applied at the transmitter, the signal to be transmitted is modified before passing it to the power amplifier. Several approaches exist that modify the signal before transmission and the most

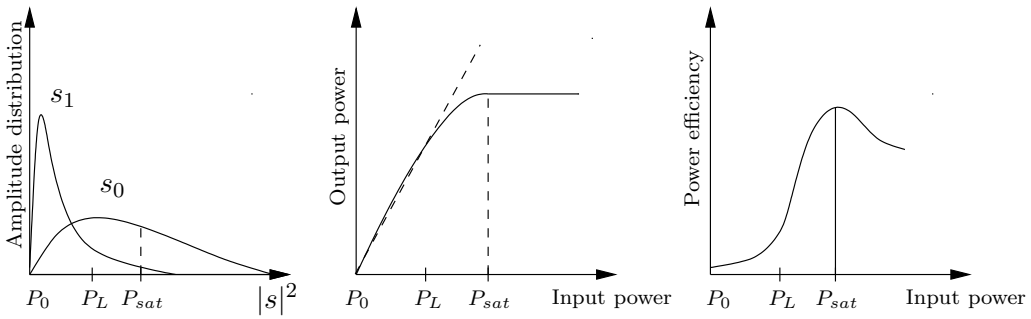

Figure 1.2: a) Amplitude distribution of two OFDM signals, original signal s_0 and signal s_1 which is a scaled version of (back-off) s_0, b) PA transfer function, and c) power amplifier efficiency

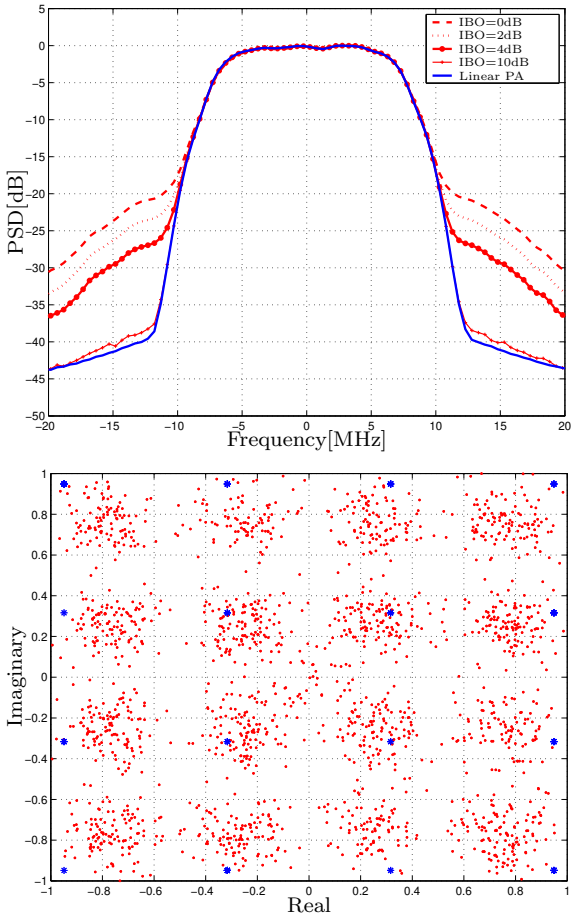

Figure 1.3: Out-of-band distortion and in-band distortion created by a solid state power amplifier (SSPA) operating at different back-off levels

well known methods are PAPR reduction techniques [27] which reduce the signal variance and allow the PA to operate in a power efficient region, PA linearization and predistortion [28–31]. Techniques applied in the receiver side include postdistortion [32] and iterative detection techniques [33, 34].

From a performance point-of-view (e.g., BER and power efficiency) it may be preferable to mitigate the nonlinear distortion at the transmitter. However, limited power consumption and hardware complexity can motivate a receiver cancellation technique. This is typically the case in uplink transmission where the base station has more resources in terms of power and computational complexity.

1.2 Scope of this thesis

The goal of the thesis is to characterize the performance of multi-antenna OFDM systems that employ nonlinear (or power efficient) power amplifiers for signal transmission. The performance is evaluated through theoretical analysis and simulations. New signal processing techniques are developed that can reduce nonlinear distortion before the signal detection. We consider techniques suitable for implementation at the transmitter and at the receiver, as well as hybrid solutions. Practical issues like channel and PA parameters estimation are taken into account. Other issues related with practical implementations such as synchronization, I/Q imbalance, and phase noise are not addressed in this thesis.

1.3 Contributions and organization of this thesis

The contributions of this thesis are in the area of power amplifier distortion cancellation and reduction techniques with applications in wireless OFDM systems.

This thesis deals with the performance losses experienced by an OFDM system when a nonlinear PA is employed. The performance measurements of interest are bit error probability (BEP) and capacity. One of the contributions of this thesis, reported in P5, is the derivation of closed-form expressions for BEP and channel capacity for multi-antenna OFDM systems with diversity for the case of memoryless PA. In P7 a closed-form solution for bit error probability of an orthogonal space time block code (OSTBC)-OFDM system with imperfect memory compensation is derived. These analyses motivate the implementation of PA distortion cancellation techniques in order to improve system performance.

The implementation of low PAPR OFDM techniques, such as clustered OFDM and antenna interleaving OFDM, is addressed in P1. To reduce the intermodulation distortion (IMD) a novel carrier allocation technique, implemented in the transmitter, has been developed in P2.

The constraints of reduced-size and power efficient user devices, motivate to move the computationally intensive tasks, such as nonlinearity cancellation techniques, to the base station receiver, where more resources are available in terms of power consumption and hardware complexity. A novel iterative power amplifier distortion cancellation technique has been developed for multiple-antennas systems in publications P3 and P5. The combination of channel estimation and iterative power amplifier distortion cancellation technique to obtain accurate channel estimates is developed in P4.

When broadband signals are considered, the PA frequency response is nonflat over the system operation bandwidth. In this case, memory effects need to be taken into account in the design of PA distortion cancellation techniques. To cope with this problem, the original cancellation technique presented in P3 is extended to the case of a broadband PA. We also consider the problem of PA parameter estimation in the receiver. These important issues are treated in P8.

Another contribution of this thesis is a split predistorter (SPD) structure for broadband PA, that is presented in P6, allowing a low complexity solution. The reduced implementation complexity is obtained by distributing the predistorter tasks such that the transmitter compensates for the static nonlinearity, and the receiver equalizes the PA memory.

This thesis is organized as follows. Chapter 2 gives an overview of OFDM systems including the single- and multiple-antenna cases. System models are introduced and the PAPR problem associated with OFDM systems is discussed. A brief review of power amplifier models including memoryless and broadband PAs is presented in the second part of Chapter 2.

In Chapter 3 an analysis of the nonlinear distortion effects on the performance of OFDM systems is presented. The end of the chapter presents the contributions of the thesis which includes error probability and system capacity analysis for multiuser OFDM systems.

Chapter 4 deals with power amplifier distortion mitigation techniques that are applied before transmission. A literature survey of different mitigation techniques is given including predistortion techniques, power back-off and PAPR reduction methods. The chapter ends with a brief review of the thesis contributions made in this area.

Chapter 5 introduces power amplifier distortion mitigation techniques applied in the receiver. A novel iterative power amplifier distortion cancellation technique for single-antenna and multiple-antenna systems is described at the end of the chapter.

Finally, Chapter 6 summarizes the results and contributions of the thesis.

1.4 Summary of publications

The thesis consists of an introductory part and eight original publications. Two papers are related with PAPR reduction techniques implemented in the transmitter. Five are dealing with receiver cancellation of power amplifier distortion. The cases of memoryless and broadband (with memory) PAs as well as the problem of PA model estimation in the receiver are treated. Performance analysis, in particular bit error probability and capacity, for an SDMA-OFDM system that employs a nonlinear power amplifier is carried out in one article. One publication addresses the performance degradation of an OSTBC-OFDM system when imperfect PA memory estimates are used in the equalization process. Finally, a split-predistorter structure is presented in one paper, where the nonlinear compensation of a broadband PA is performed in both the transmitter and the receiver.

In P1, the use of clustered OFDM (COFDM) and antenna interleaving OFDM (AIOFDM) techniques for PAPR reduction is evaluated in a WLAN system that employs a memoryless power amplifier. Results show that COFDM and AIOFDM reduce the linearity constraints in the power amplifier, thus increasing the power efficiency.

Publication P2 presents a new carrier allocation method that reduces the intermodulation distortion between different carriers in a multiuser OFDM system. A new user that enters the system is assigned subcarriers such that the resulting second and third-order intermodulation distortion interfering with other users is kept to a minimum. Simulation results show that the proposed technique is able to reduce the required back-off level, increasing the amplifier power efficiency.

Publication P3 introduces a novel receiver cancellation technique that reduces the nonlinear effects created by a memoryless power amplifier. The proposed technique is implemented for a multiuser OFDM-SDMA system. The basic idea of the proposed technique is the following. With an initial estimate of the user symbols, the distortion effects can be estimated if the PA model is known. After that, the nonlinear distortion can be removed from the received signal and new and improved symbol estimates can be obtained. This procedure can be repeated in an iterative manner to obtain almost undistorted estimates. This technique improves power efficiency in the order of 30%.

The estimation of the channel is seriously affected by the nonlinear distortion. Moreover, accurate channel estimates are required in SDMA systems to separate the users, in particular when large constellation sizes are used. This practical issue is addressed in P4, where a new channel estimation approach is combined with iterative distortion cancellation technique. An initial channel estimation is carried out in frequency domain followed by time domain processing of the received signal. In the time domain step, the equalized signals from the frequency domain processing is used to re-

move the nonlinear distortion and to improve the initial channel estimate. Simulations verify that the combined channel estimation and nonlinear cancellation strategy has a performance close to the case of perfectly known channel.

Publication P5 is one of the main publications of this thesis. The iterative distortion cancellation technique proposed in P3 is further developed. The novel technique was evaluated for stationary and time-varying channels. Theoretical BEP and capacity expressions that includes nonlinear distortion effects were derived for an SDMA-OFDM system employing a least-squares receiver for user separation. The theoretical results can be readily extended for other kinds of systems with diversity.

Publication P6 presents a split predistorter structure to overcome the high complexity problems related to the conventional predistortion approach. A low complexity memoryless predistorter in the transmitter is used for nonlinear distortion compensation and a postcompensation filter at the receiver that jointly equalizes PA memory and channel effects.

In Publication P7, a performance analysis is carried out for an OSTBC-OFDM system for the case when a broadband nonlinear power amplifier with memory is used. The analysis include the effects of nonlinear distortion and imperfect PA memory equalization. Closed-form expressions for the BEP are obtained for cases when PA memory is compensated at the transmitter or the receiver.

Publication P8 deals with the issues related to the PA model estimation necessary for the receiver cancellation technique in P3-P5. In this work, the more practical problem of estimating and tracking the PA model in the receiver is addressed moving the computationally involved PA identification to the receiver.

All the simulation software for all the original papers of this dissertation was written solely by the author. The author has been responsible for developing the original ideas and writing all the papers. Co-authors have been supervising the work and provided guidance for the theoretical proofs.

Chapter 2

System Model

This chapter presents the basic OFDM system and power amplifier (PA) models used throughout this thesis. Advantages and challenges of OFDM are briefly discussed. Initially we consider the case of a single-antenna OFDM system, i.e., the receiver and the transmitter are equipped with a single antenna. Thereafter, we extend the model to a multiuser space division multiple access (SDMA)-OFDM system and discuss multiuser receiver structures. Later, RF power amplifier classes are briefly described and, finally, we describe the most common models encountered in the literature for modelling narrowband and broadband power amplifiers.

2.1 Introduction

OFDM techniques were proposed as a means of counteracting the distortion created by dispersive radio channels by turning frequency selective channels into a set of flat parallel sub channels (tones) [10, 11, 35]. By transmitting several symbols in parallel, the symbol duration is increased reducing the effects of ISI caused by the dispersive fading channel. Therefore, OFDM is an effective technique for combating multipath fading and for high data rate transmission over mobile wireless channels.

If each tone has sufficiently narrow bandwidth, the multipath fading can be characterized as flat and the equalization process is reduced to a single tap per subcarrier. Reduced complexity equalization is an important advantage, compared with the complicated equalization structures required for single-carrier systems.

OFDM can be viewed as a form of frequency division multiplexing (FDM). OFDM allows the spectrum of each tone to overlap, and since each tone is orthogonal with every other tone, they do not interfere with each other resulting in a high spectral efficiency.

One of the major advantages of OFDM is the possibility to adaptively distribute the transmission load among different subchannels to achieve

an optimum transmission rate. Adaptive modulation takes advantage of the frequency selectivity and time variation of the multipath channel by adapting the transmitted signal spectrum to achieve maximum throughput [12, 13, 36, 37]. The many advantages of OFDM, added to the capacity of dynamic multiuser resource allocation [24] that exploit system diversities through intelligent management of bandwidth allocation, multiple access, scheduling, and power and rate adaptation, make OFDM a strong candidate for future communication systems.

Over the years, several fundamental works based on OFDM or similar multicarrier approaches have been published, see, e.g., [38–42]. However, implementation limitations delayed its practical application. The implementation of the fast Fourier transform (FFT) and the introduction of digital signal processing (DSP) techniques in modem design made the use of OFDM practical in a wide variety of applications.

In recent years, many wired and wireless standards have adopted OFDM. Discrete Multi-Tone (DMT) techniques [43], a particular implementation of OFDM, has been adopted as standard for Asymmetric Digital Subscriber Line (ADSL) systems [6]. In the wireless network market, OFDM is part of IEEE 802.11a [1], 802.11g [2], and HiperLAN/2 [3] WLAN standards [16]. Long-term evolution 3G [44], IMT-Advanced [45], and mobile WiMAX [46] are also considering OFDM as a transmission technique.

In this thesis we address both the implementation of OFDM in a single antenna systems, or single-input single-output (SISO), and in multi-antenna systems, or multiple-input multiple-output (MIMO), where the latter provides an enhanced system capacity with excellent performance. The system model for the single antenna case is presented in Section 2.2. The extension to MIMO, and SDMA in particular, is treated in Section 2.3.

Employing OFDM in mobile communication systems is advantageous (as mentioned above) from the perspective of robustness to time-dispersive channels, high spectral efficiency, adaptive modulation and simple equalization structures. However, due to problems inherent to multicarrier systems new challenges arise that need to be addressed. One of these challenges is due to the high peak to average power ratio (PAPR) levels of OFDM signals, described in detail in Section 2.4. The high PAPR signals will generate nonlinear distortion on the communication channel when amplified by practical PAs with nonlinear response and finite amplitude ranges. The nonlinear distortion creates out-of-band emissions which interfere co-channel users and in-band distortion that causes self-interference. A reasonable question to ask is "why not then use linear PAs?". The reason is that linear PAs are power inefficient and costly. In fact, a dominating cost of practical networks is due to use of a highly linear power amplifier [47]. Section 2.5 provides a summary on RF power amplifiers categorization based on their operational topology. To assess the system performance, when nonlinear PA distortion is present, requires an accurate nonlinear model of the amplifier. Several PA models

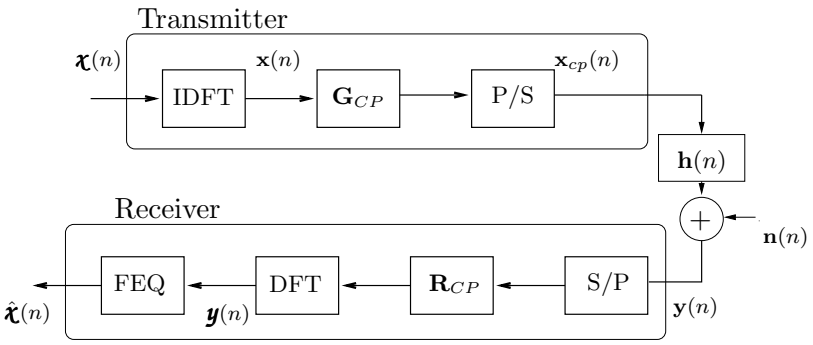

Figure 2.1: OFDM system model where $\mathbf{G}_{CP}$ and $\mathbf{R}_{CP}$ denote the cyclic prefix insertion and removal operation, P/S and S/P refer to parallel to serial and serial to parallel conversion respectively and FEQ is the frequency-domain equalizer.

have been proposed in the literature ranging from simple memoryless models, appropriate for narrow-band systems and low-power amplifiers, to more elaborated models required for modelling broadband PAs, where dynamic effects due to electrical and electro-thermal process need to be considered. Several PA models are briefly reviewed in Section 2.6.

Other challenges arising in practical implementation of OFDM systems are I/Q mismatch, phase noise and synchronization. These topics are treated in Section 2.7.

Notation: In this thesis, small boldface letters are used to denote vectors and capital boldface letters are used to denote matrices. In addition, standard font (Times Roman) is used for time-domain variables and calligraphic letters are used to denote frequency-domain variables. For example, $\mathbf{H}$, $\mathbf{h}$ and h denote a matrix, vector and scalar variable in the time domain. Their corresponding notations in the frequency domain are: $\boldsymbol{\mathcal{H}}$, $\boldsymbol{\hbar}$ and $\hbar$.

2.2 Single antenna OFDM system

The OFDM system under consideration has N subcarriers and consists of one single user. The mobile user and the base station are both equipped with a single antenna. A complete block diagram of an OFDM transceiver is illustrated in Figure 2.1.

To optimize the system data rate or the overall bit error rate, different modulation can be assigned to each subcarrier by using a bit loading algorithm, where the constellation size is a function of the subchannel quality, i.e., the subcarriers with high SNR use larger constellation size. The principal drawback of this adaptive modulation is that the transmitter needs to have channel state information (CSI). Coding and interleaver are applied

in practical OFDM systems to improve the system performance, achieving tolerable levels of error rate and immunity against fading channels. However, coding and interleaver are not considered in this section to simplify the model notation.

The sequence of input bits $\mathbf{b}$ are mapped onto appropriate symbols based on the constellation size associated to each subcarrier, $\chi(n,k)$ and grouped in blocks of N data symbol. Each of these blocks can be represented by a data symbol vector $\boldsymbol{\chi}(n) = [\chi(n,0), \chi(n,1), \cdots, \chi(n,N-1)]^T$ where n denotes the OFDM symbol index.

Next, the OFDM symbol is fed through the inverse discrete Fourier transform (IDFT) and the discrete-time OFDM sequence is obtained.

The time domain multicarrier signal $x(n,i)$, $i = 0 : N-1$ after the IDFT operation is given by

$$x(n,i) = \frac{1}{\sqrt{N}} \sum_{k=0}^{N-1} \chi(n,k) \exp\left(\frac{j2\pi ik}{N}\right) \quad 0 \leq i \leq (N-1) \tag{2.1}$$

where i denotes the sub-symbol index. In order to simplify the notation, the modulation process can be represented in matrix form as

$$\mathbf{x}(n) = \mathbf{Q}_N \boldsymbol{\chi}(n) \tag{2.2}$$

where $\mathbf{x}(n) = [x(n,0), \cdots, x(n,N-1)]^T$ is a $N \times 1$ vector constructed with the time domain OFDM signal in Eq. (2.1) and $\mathbf{Q}_N \in \mathbb{C}^{N \times N}$ represents the IDFT matrix and is given by

$$\mathbf{Q}_N = \begin{bmatrix} Q_{1,1} & \cdots & Q_{N,1} \\ Q_{1,2} & \ddots & Q_{N,2} \\ \vdots & \ddots & \vdots \\ Q_{1,N} & \ddots & Q_{N,N} \end{bmatrix} \tag{2.3}$$

whose the elements are given by

$$Q_{m,n} = \frac{1}{\sqrt{N}} \exp\left(\frac{j2\pi[m-1][n-1]}{N}\right) \tag{2.4}$$

To avoid ISI and inter block interference (IBI), a guard interval is used. The most common choice is to use a cyclic prefix (CP), i.e., to copy the last v samples to the beginning of the symbol, see Figure 2.2. If v is chosen larger than the channel length, ISI free reception is obtained. The choice of the cyclic extension is further motivated by the simple equalization in the receiver. Alternatively, the guard interval can be padded with zeros at the end of each modulated OFDM symbol [48]. In [49] the performance of OFDM with zero padding (ZP) and CP are compared in terms of PA clipping

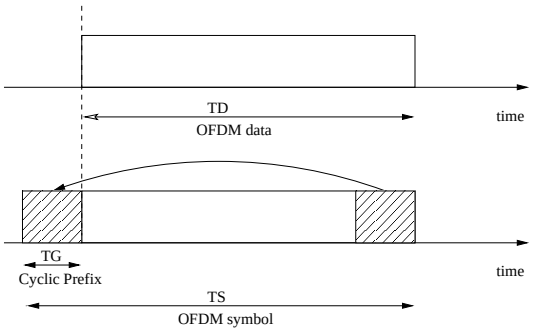

Figure 2.2: The principle of cyclic prefix (CP) in an OFDM system. T_S, T_g and $T_g + T_S$ refers to the durations of the data part, the cyclic prefix and the complete OFDM block respectively.

effects, showing that ZP introduces slightly more nonlinear distortion and, therefore, needs slightly increased power back-off reducing the overall power-efficiency.

The transmitted OFDM symbol can be expressed as

$$\mathbf{x}_{cp}(n) = \mathbf{G}_{cp}\mathbf{x}(n) = \mathbf{G}_{cp}\mathbf{Q}_N\boldsymbol{\chi}(n) \tag{2.5}$$

where $\mathbf{G}_{cp}$ is an $(N+v)\times N$ matrix that represents the cyclic prefix insertion operation and is given by

$$\mathbf{G}_{cp} = \begin{bmatrix} \mathbf{0}_{P\times(N-P)} & \mathbf{I}_P \\ \mathbf{I}_{N-P} & \mathbf{0}_{(N-P)\times P} \\ \mathbf{0}_{P\times(N-P)} & \mathbf{I}_P \end{bmatrix} \tag{2.6}$$

The sequence is transmitted through the wireless channel whose impulse response has L non-zero taps and is denoted by the $L \times 1$ vector $\mathbf{h}(n) = [h_1(n), h_2(n), \ldots, h_L(n)]^T$. In this work, the channel taps are assumed constant within one OFDM symbol, T_s (block fading assumption) and the channel impulse response (CIR) length is assumed to be shorter than the cyclic prefix length, i.e., $L < v$.

Under these assumptions, the received signal can be expressed as

$$\mathbf{y}(n) = \check{\mathbf{H}}(n)\mathbf{x}(n) + \mathbf{n}(n) \tag{2.7}$$

where $\check{\mathbf{H}}(n) = \mathbf{R}_{cp}\mathbf{H}(n)\mathbf{G}_{cp}$ is an $N \times N$ matrix, $\mathbf{R}_{cp}$ is an $N \times (N + v)$ matrix that denotes the CP removal operation, the $(N + v) \times (N + v)$ $\mathbf{H}(n)$ matrix represents the wireless channel and $\mathbf{n}(n)$ is a white Gaussian channel noise.

The cyclic prefix insertion/removal operation renders the convolution operation to a circulant convolution operation. Hence, the matrix $\check{\mathbf{H}}(n)$ can be written as

$$\check{\mathbf{H}}(n) = \begin{bmatrix} h_1(n) & 0 & \cdots & 0 & h_L(n) & \cdots & h_2(n) \\ h_2(n) & h_1(n) & 0 & \cdots & 0 & \ddots & \vdots \\ \vdots & h_2(n) & \ddots & 0 & \ddots & 0 & h_L(n) \\ h_L(n) & \vdots & \ddots & h_1(n) & \ddots & 0 & 0 \\ 0 & h_L(n) & \vdots & h_2(n) & \ddots & \ddots & 0 \\ \vdots & 0 & \ddots & & h_1(n) & 0 & 0 \\ 0 & \cdots & 0 & h_L(n) & \cdots & h_2(n) & h_1(n) \end{bmatrix}$$

The receiver sequence $\mathbf{y}(n)$ is split in blocks and the cyclic prefix associated with each block is removed.

Finally, the discrete Fourier transform (DFT) operation is performed on each of these blocks and the frequency-domain received signal is obtained

$$\boldsymbol{y}(n) = \mathbf{Q}_N^H \mathbf{y}(n) = \mathbf{Q}_N^H [\check{\mathbf{H}}(n)\mathbf{x}(n) + \mathbf{n}(n)] = \boldsymbol{\mathcal{D}}_h(n)\boldsymbol{\chi}(n) + \boldsymbol{n}(n) \tag{2.8}$$

where $\boldsymbol{\mathcal{D}}_h(n)$ is an $N \times N$ diagonal matrix created with the channel frequency response $\boldsymbol{\mathcal{D}}_h(n) = \text{diag}[\boldsymbol{h}(n)]$. The received sequence on the subcarrier k at time instant n can be expressed by

$$y(n,k) = h(n,k)\chi(n,k) + n(n,k) \tag{2.9}$$

where $h(n,k)$ is the channel frequency response and $n(n,k)$ is an additive noise. The noise component is the kth element of $\boldsymbol{n}(n) = \mathbf{Q}_N^H \mathbf{n}(n) = [n(n,1), n(n,2), \ldots, n(n,N)]^T$, whose elements are uncorrelated zero mean circular complex Gaussian because the DFT is an orthogonal linear transform.

Equation (2.9) demonstrates the advantage of the implementation of an OFDM system. The received data symbol $y(n,k)$ depends on the transmitted data $\chi(n,k)$ and channel frequency response $h(n,k)$. Recovering the transmitted symbol can be done using a single-tap frequency domain equalizer (FEQ). The soft estimate of $\chi(n,k)$ can be obtained as

$$\hat{\chi}(n,k) = w(n,k)y(n,k) \tag{2.10}$$

where $w(n,k)$ is the equalizer tap to be used on subcarrier k. For example, the equalizer coefficient for an *least squares* (LS) equalizer is given by $w(n,k) = 1/\hat{h}(n,k)$, where $\hat{h}(n,k)$ is an estimate of the channel frequency response. Alternatively, a minimum mean square error (MMSE) equalizer can be used to take into account noise amplification at frequencies where the channel has spectral nulls [50].

2.3 Multi-antenna OFDM system

A system employing multiple antennas at both the transmitter and the receiver is often referred to as a multiple-input multiple-output (MIMO) system. MIMO systems may be implemented in a number of different ways to obtain diversity gain to combat signal fading or capacity gain. V-BLAST techniques [51,52], and closed-loop techniques, where the knowledge of channel at the transmitter is exploited, provide an increase in the system capacity. MIMO-OFDM systems have been developed in order to improve the power efficiency by maximizing spatial diversity. SDMA [53–57], space-frequency coding (SFC) techniques [58] and space-time coding (STC) [59] are some of the most popular techniques.

This thesis focus on SDMA-OFDM systems and signal models for other multiplexing techniques can be found in [21, 58–61].

The multiuser SDMA-OFDM system under consideration has N subcarriers, and consists of one base station equipped with P antennas and L mobile users with a single transmit antenna. That results in a $P \times L$ MIMO-OFDM system. A block diagram of the SDMA-OFDM system is depicted in Figure 2.3. It is assumed that all users are transmitting independent signals simultaneously on all N subcarriers. The transmitted signal from user j at time instant n is given by

$$\mathbf{x}_j(n) = \mathbf{G}_{cp}\bar{\mathbf{x}}_j(n) = \mathbf{G}_{cp}\mathbf{Q}_N\boldsymbol{\chi}_j(n) \tag{2.11}$$

where the matrices $\mathbf{G}_{cp}$ and $\mathbf{Q}_N$ are defined in Eq. (2.6) and Eq. (2.3), respectively, and $\bar{\mathbf{x}}_j(n)$ is the IDFT of the modulated symbols, $\boldsymbol{\chi}_j(n) \in \mathbb{C}^{N\times 1}$, without the cyclic prefix.

The received signal at antenna i after removing the cyclic prefix, $\mathbf{y}_i(n)$, is formed by the superposition of the independently faded signals associated with the L users sharing the same space-frequency resource. The received signal, assumed to be corrupted by circular complex Gaussian noise $\mathbf{n}_i(n)$ at the array elements, is given by

$$\mathbf{y}_i(n) = \sum_{j=1}^{L} \mathbf{H}_{i,j}(n)\bar{\mathbf{x}}_j(n) + \mathbf{n}_i(n) \tag{2.12}$$

where $\mathbf{H}_{i,j}(n)$ is the $N \times N$ circulant time-domain (TD) channel matrix at time instant n, formed by the channel response vector $\mathbf{h}_{i,j}(n)$ for the link between user j and base station antenna i. The frequency-domain expression of the received signal is obtained by taking the DFT of Eq. (2.12).

Let $\boldsymbol{y}(n,k) = [y_1(n,k), \ldots, y_P(n,k)]^{\mathrm{T}}$ denote the vector of received signals at each antenna on subcarrier k. Then, the received signal vector for each subcarrier can be written as

$$\boldsymbol{y}(n,k) = \boldsymbol{\mathcal{H}}(n,k)\boldsymbol{\chi}(n,k) + \boldsymbol{n}(n,k) \tag{2.13}$$

where $\boldsymbol{\chi}(n,k) = [\chi_1(n,k), \ldots, \chi_L(n,k)]^{\mathrm{T}}$ is the vector containing transmitted signals from each user, $\boldsymbol{n}(n,k) \in \mathbb{C}^{P\times 1}$ is the additive noise assumed to be circular complex Gaussian with $E[\boldsymbol{n}(n,k)\boldsymbol{n}^{\mathrm{H}}(n,k)] = \sigma_n^2\mathbf{I}$ and $\boldsymbol{\mathcal{H}}(n,k) \in \mathbb{C}^{P\times L}$ is the multiuser channel transfer matrix given by [35]

$$\boldsymbol{\mathcal{H}}(n,k) = \begin{bmatrix} \mathcal{h}_{1,1}(n,k) & \mathcal{h}_{1,2}(n,k) & \ldots & \mathcal{h}_{1,L}(n,k) \\ \mathcal{h}_{2,1}(n,k) & \mathcal{h}_{2,2}(n,k) & \ldots & \mathcal{h}_{2,L}(n,k) \\ \vdots & \vdots & \ddots & \vdots \\ \mathcal{h}_{P,1}(n,k) & \mathcal{h}_{P,2}(n,k) & \ldots & \mathcal{h}_{P,L}(n,k) \end{bmatrix} \tag{2.14}$$

where $\mathcal{h}_{i,j}(n,k)$ denotes the channel response on subcarrier k at time n between antenna element i of the base station and user j.

An estimate $\hat{\boldsymbol{\chi}}(n,k)$ of the L user transmitted signals $\boldsymbol{\chi}(n,k)$ can be obtained by linearly combining the signals at the P receive antennas using a weight matrix $\boldsymbol{\mathcal{W}} \in \mathbb{C}^{P\times L}$:

$$\hat{\boldsymbol{\chi}}(n,k) = \boldsymbol{\mathcal{W}}^{\mathrm{H}}\boldsymbol{y}(n,k) \tag{2.15}$$

The standard LS combiner $\boldsymbol{\mathcal{W}} = \boldsymbol{\mathcal{W}}_{LS}$ is given by [62]

$$\boldsymbol{\mathcal{W}}_{LS} = \boldsymbol{\mathcal{H}}(n,k)\left[\boldsymbol{\mathcal{H}}^{\mathrm{H}}(n,k)\boldsymbol{\mathcal{H}}(n,k)\right]^{-1} \tag{2.16}$$

The standard LS combiner requires the calculation of the left-inverse of $\boldsymbol{\mathcal{H}}$. A necessary condition for the existence of the inverse is that L columns of the matrix $\boldsymbol{\mathcal{H}}$ are linearly independent, and $P \geq L$ where P is the number of rows. In other words, the number of active users equipped with a single antenna must be lower than the number of receiver antennas. Similarly to SISO case, an MMSE detector can be used. This alternative exploits the available statistical knowledge of the noise and makes a trade-off between the multiuser interference and the measurement noise. The optimal MMSE weight is obtained as

$$\boldsymbol{\mathcal{W}}_{MMSE} = \left[\boldsymbol{\mathcal{H}}(n,k)\mathbf{P}_\rho\boldsymbol{\mathcal{H}}^{\mathrm{H}}(n,k) + \mathbf{I}\right]^{-1}\boldsymbol{\mathcal{H}}(n,k)\mathbf{P}_\rho \tag{2.17}$$

where matrix $\mathbf{P}_\rho$ is an $(L \times L)$ diagonal matrix of form $\mathtt{diag}(\rho_1, \ldots, \rho_L)$ with $\rho_j = \sigma_j^2/\sigma_n^2$ being the SNR of user j.

Other multiuser detection techniques previously developed for code-division-multiple-access (CDMA) can be applied in SDMA-OFDM transceivers, e.g., successive interference cancellation (SIC), parallel interference cancellation (PIC) and maximum likelihood (ML) detection [62]. These techniques are nonlinear and require *a priori* knowledge of the remaining users. For a comprehensive treatment of multiuser detection techniques including, linear and nonlinear methods, see, e.g., [62–65]. The application of

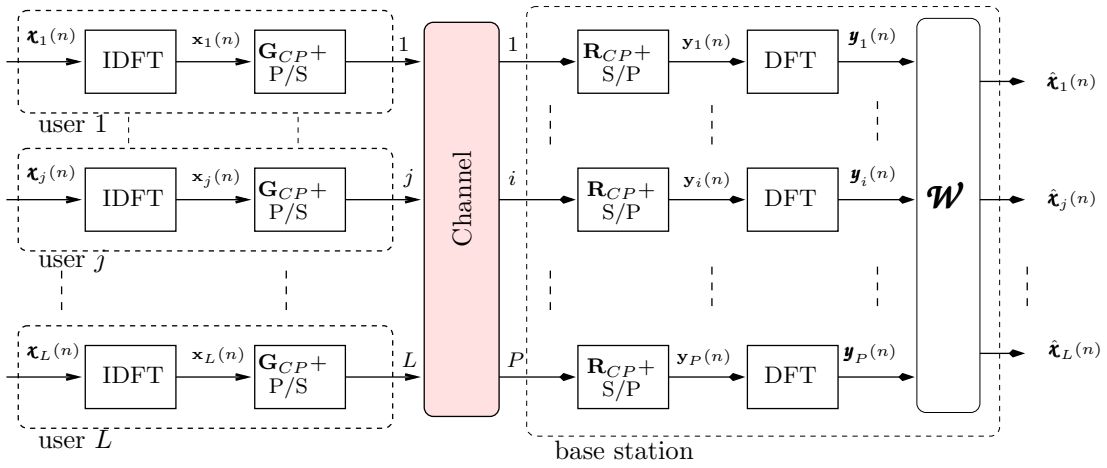

Figure 2.3: SDMA-OFDM system with L single-antenna users and a base station with P receive antennas.

multiuser detection techniques in SDMA-OFDM is described in [35] which includes comparisons and practical issues such as implementation complexity.

2.4 PAPR in OFDM systems

OFDM transceivers are more susceptible to the impairments in the front-end implementation than single-carrier systems. The high PAPR problem associated with multicarrier signals is one of the principal impairments in the implementation of OFDM systems. The linear operation of the PA over a large dynamic range imposes a considerable implementation cost and a reduced power efficiency.

The time domain OFDM signal is constituted by the sum of N complex exponential signals, see Eq. (2.1). The phase and the amplitude of these signals are determined by the random symbols on the different subcarriers.

The PAPR is defined as

$$PAPR = \frac{\max_{0\leq n\leq N-1} |x(n)|^2}{E[|x(n)|^2])} \tag{2.18}$$

where $x(n)$ is the time domain OFDM signal sampled at symbol rate. The PAPR for the case of a continuous-time waveform $x(t)$ is given by Eq. (2.18) by simply replacing $x(n)$ with the continuous waveform $x(t)$. The PAPR of discrete-time sequences (sampled sequences) determines the complexity of the hardware required for digital signal processing, e.g., the quantization bits of analog-to-digital (A/D) and digital-to-analog (D/A) converters. The

majority of the PAPR reduction techniques are applied on the discrete time signal. Consequently the PAPR defined for discrete time signal is a more useful measure. In general we have $PAPR_d \leq PAPR_c$, where $PAPR_d$ and $PAPR_c$ denote the PAPRs of the discrete-time sequence and the continuous-time signal, respectively [66].

Large values of PAPR are obtained when the signals add coherently. An OFDM system with N subcarriers gets a peak power that is N times the average power. Although in practice, fully coherent addition for the maximum value is highly improbable.

Seeing the OFDM signal as a sum of N independent and identically distributed random variables each with mean value μ and variance σ^2, the Central Limit Theorem tells us that the probability density function (pdf) of this sum approaches that of a Gaussian variable, with expected value $E[x(n)] = N\mu$ and variance $Var[|x(n)|] = N\sigma^2$. That is, the pdf of the OFDM signal may be approximated as $\mathbf{N}(N\mu, N\sigma^2)$ for N large. In other words, the more carriers, the larger the variance, or, equivalently the larger the PAPR.

The large PAPR levels increases the implementation complexity (number of bits) of the A/D and the D/A converters such that large peaks can be represented with good precision. In addition, to avoid nonlinear distortion at these high-level peaks, the power amplifier must be linear over a large dynamic range (at worst N times the average power used for transmission). The linearity and efficiency of a power amplifier are mutually exclusive specifications [67]. Consequently, the power efficiency of an OFDM system is seriously affected by its PAPR characteristics

Several approaches have been developed to obtain the distribution of the PAPR of an OFDM signal [68–70]. All these approaches assume that the OFDM signal can be approximated by a complex Gaussian random process. Under the Gaussian assumption, the probability that the PAPR is below a threshold λ is given by the cumulative distribution function (CDF)

$$Pr\left\{PAPR[x(n)] \leq \lambda\right\} = [1 - \exp(-\lambda)]^N \tag{2.19}$$

For the case of band-limited OFDM signals, Eq. (2.19) is too optimistic. A more accurate approximation of the cumulative distribution for high levels of PAPR, derived in [69], gives the following closed-form approximation

$$Pr\left\{PAPR[x(n)] \leq \lambda\right\} \approx \exp\left[-\sqrt{\frac{\pi\lambda}{3}}\exp(-\lambda)\right] \tag{2.20}$$

Figure 2.4 plots the complementary cumulative distribution function (CCDF), $1 - Pr\left\{PAPR[x(n)] \leq \lambda\right\}$ employing Equations (2.19) and (2.20) for $N = 64$ and $N = 1024$. In practical OFDM systems, the signals are amplified by a PA which is peak-power limited. If the envelope of the transmitted signal is larger than the PA's saturation point in time instant n, the

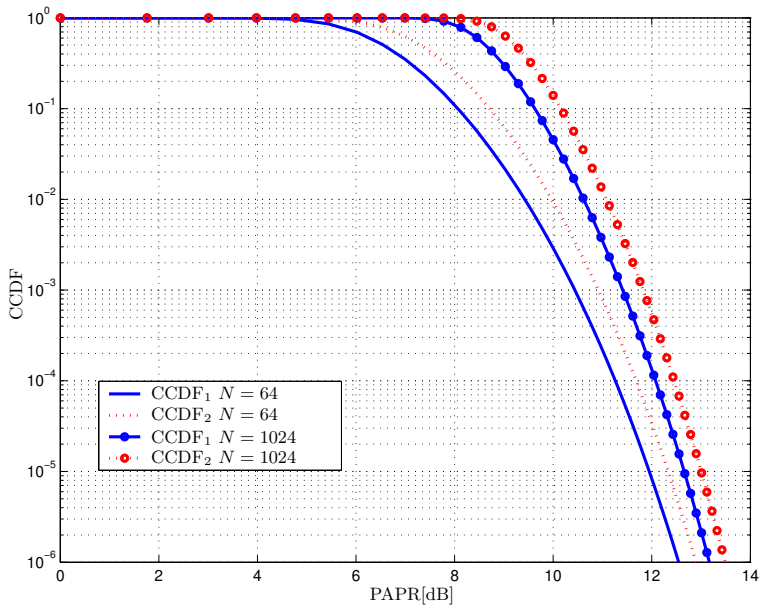

Figure 2.4: Complementary Cumulative Distribution Function (CCDF) of PAPR distribution for $N = 64$ and $N = 1024$ calculated using Eq. (2.19) (CCDF$_1$) and a more accurate approach, Eq. (2.20), (CCDF$_2$).

signal at this instant will be clipped creating nonlinear distortion increasing the BER and the interference over adjacent users. A reasonable clipping probability level, for reduced system degradation, is 10^{-4} [71] obtained with a $PAPR = 12$ dB for $N = 1024$ (see Figure 2.4). It means that PA is operating 12 dB above the average input power, an operation point where the PA has low power efficiency.

Reducing the PAPR levels allows the PA to operate in a more power efficient region. As a consequence, several PAPR reduction techniques have been proposed for OFDM systems. A brief review of PAPR reduction techniques will be presented in Chapter 4.

2.5 RF power amplifiers

Power amplifiers can be categorized based on their circuital configuration and operational topology. The most commonly used classification for PA are A, B, AB, and C operations. This classification depends on the operation point of the amplifier defined by its collector current (bipolar transistors) or drain current (field effect transistors). These classes provide a good indication of linearity and power efficiency [29].

The power efficiency is a measure that tells how effectively an amplifier

converts the power drawn from the DC supply to useful power at the output. That is,

$$PAE = \frac{P_o}{P_{dc}} \tag{2.21}$$

where P_o is the output power and P_{dc} is the power from the DC supply.

Figure 2.5 illustrates the operation points, Q, for the described classes considering a PA employing a bipolar transistor where I_c and V_{be} denotes the collector current and the voltage base-emitter respectively.

The operation point Q and input signal level in class A PAs are chosen such that the output signal varies through the complete cycle of the input signal, i.e., the conduction angle, θ_c, is 360° degrees. They operate at constant current independently of the input signal level reaching a maximum efficiency of 50 % for a continuos wave signal. The low power efficiency constraints its application to low-power systems and where high linear amplification are required, e.g., multicarrier systems.

A more power efficient solution at the expense of linearity is obtained by class B operation where the output signal varies through half a cycle of the input signal. A single-ended class B PA amplifies only 180° degrees of the input signal (half cycle), thus producing significant distortion. A push-pull configuration that uses two transistors operating in antiphase, each amplifying one half of the input signal, is often implemented reducing the distortion level. By using a class B amplifier a maximum power efficiency of 78.5 % can be obtained.

Class B PA introduces crossover distortion due to the imperfect transition between the off and on operations of the active device which is not tolerable in most applications. To solve this problem, an intermediate solution between class A and class B amplifier, class AB, can be used which has a conduction angle larger than 180° as depicted in Figure 2.5. In class AB amplifiers the bias current is set at DC level over zero reducing the crossover effects with small loss of efficiency.

Class C amplifiers are biased to operate with conduction angles less than 180° degrees presenting good efficiency but poor linearity. The application of these amplifiers is restricted to systems that require high efficiency levels and are not concerned with nonlinear effects.

To conclude this review and to simplify the comparison, the characteristics of the described PA classes are summarized in Table 2.1.

2.6 Power amplifier models

Practical and power-efficient amplifiers will have a nonlinear response unless the PA is operating far from the saturation point. Therefore, accurate

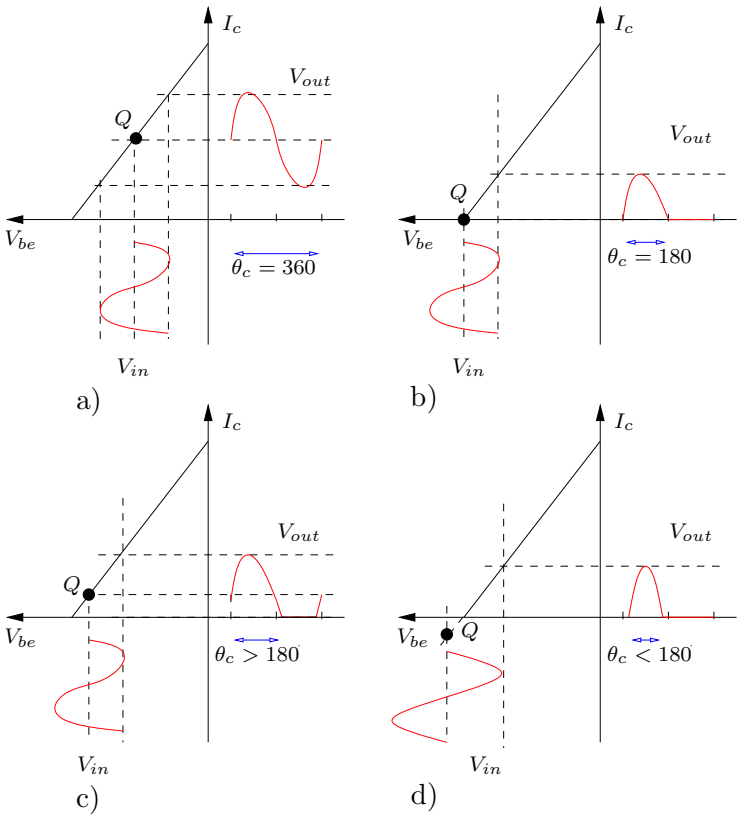

Figure 2.5: Illustrations of operation points of the different PA classes: a) Class A, b) Class B, c) Class AB and, d) Class C.

Table 2.1: Characteristics of PA classes

	Class A	Class B	Class AB	Class C
Conduction angle θ_c	360°	180°	$> 180°$	$< 180°$
Power efficiency	$\leq 50\%$	78.5%	$\leq 78.5\%$	$78.5\% - 100\%$
Nonlinear distortion	Very low	High	Low	Very High

nonlinear models for the amplifier are important when studying the system performance.

Higher-level transference models, or behavioral models (black-box models), in which no *a priori* knowledge of the PA's internal composition is assumed, provide good accuracy with reasonable complexity for simulation and analysis purposes. These empirical models are developed based on a set of selected input-output observations and offer a compact representation of the PA characteristics. Models based on detailed physical descriptions of the PA [72], i.e. transistor parameters, are not addressed in this work.

In the following we briefly review the more representative approaches. Characterization of PA behavior based on measurements are initially addressed. In the second part, memoryless models are described. The more representative models, polynomial, Saleh and solid state, are described. Thereafter, more realistic models including memory effects are presented. In particular, Volterra, Wiener, Hammerstein, Wiener-Hammerstein and memory polynomial models are described.

2.6.1 Characterization of PA behavior based on measurements

In the following, the concepts of 1 dB compression point obtained by using a single-tone input signal and third order interception point obtained by using a two-tone input signal are described. Both parameters are commonly used to characterize the PA behavior.

Single-tone measurements

Assuming a PA modelled by using a third-order polynomial with real-valued coefficients a, the output signal can be expressed as

$$y(t) = a_1 x(t) + a_2 x(t)^2 + a_3 x(t)^3 \tag{2.22}$$

where $x(t)$ is the input signal, a_1,a_2 and a_3 are real valued coefficients and $y(t)$ is the output of the PA. Replacing the input signal by single-tone signal expressed as $x(t) = Csin(w_1 t)$ in Eq. 2.22. At the output of the PA new spectral components will be created:

- Fundamental w_1 with amplitude: $a_1 C + (3a_3/4)C^3$.
- Second Harmonic $2w_1$ with amplitude: $(a_2/2)C^2$
- Third Harmonic $3w_1$ with amplitude: $(a_3/4)C^3$
- DC component with amplitude $(a_2/2)C^2$

From these spectral components we can conclude that the nonlinear PA transfer function generates spectral components and also affects the gain at the fundamental frequency.

At low signal levels the output is governed by the linear term. However, when the input power is increased the third-order component modifies the linear response of the fundamental signal. This effect creates an amplitude-dependent gain. These results give a common measurement to quantize the level of nonlinearity: 1 dB compression point. In the 1 dB compression point the gain characteristic of a nonlinear amplifier deviates 1 dB from the gain of an ideal amplifier.

Two-tone measurements

When using a multitone input signal, the output of the PA will be constituted by the fundamental components as well as harmonics and intermodulation products.

Considering a two-tone input signal $x(t) = C(sin(w_1 t) + sin(w_2 t))$ that is amplified by a third-order polynomial, see Eq. (2.22) ($a_2 = 0$ is assumed to simplify the analysis because even terms can be disregarded in narrow band systems).

The output of the PA can be written as

$$\begin{aligned} y(t) &= (a_1 C + (9a_3/4)C^3)[(sin(w_1 t) + sin(w_2 t))] \text{ , fundamental} \\ &+ (3/4C^3 a_3)[(sin((2w_1 - w_2)t) + sin((2w_2 - w_1)t))] \text{ , IMP} \\ &- (3/4C^3 a_3)[(sin((2w_1 + w_2)t) - sin((w_1 + 2w_2)t))] \text{ , IMP high frequency} \\ &- (1/4C^3 a_3)[(sin(3w_1 t) + sin(3w_2 t))] \text{ , harmonics} \end{aligned} \tag{2.23}$$

where the harmonics components and the IMPs of high frequency ($2w_1 + w_2$ and $w_1 + 2w_2$) can be removed with a simple low-pass filters.

In general, the IMP products at frequencies $2w_1 - w_2$ and $2w_2 - w_1$ are inside the operation bandwidth and can not be removed.

The interception point is a simple parameter commonly used to quantize the intermodulation phenomenon. In particular, the input third-order intersection point (IIP3) is where the extrapolated linear gain and distortion products cross.

The IIP3 and 1dB compression point characteristics are depicted in Figure 2.6 for a PA modelled using a third-order polynomial. In this figure, the third-order intermodulation suppression parameter, $IS3$ is also indicated for a particular working point, P_{i_Q}, P_{o_Q}.

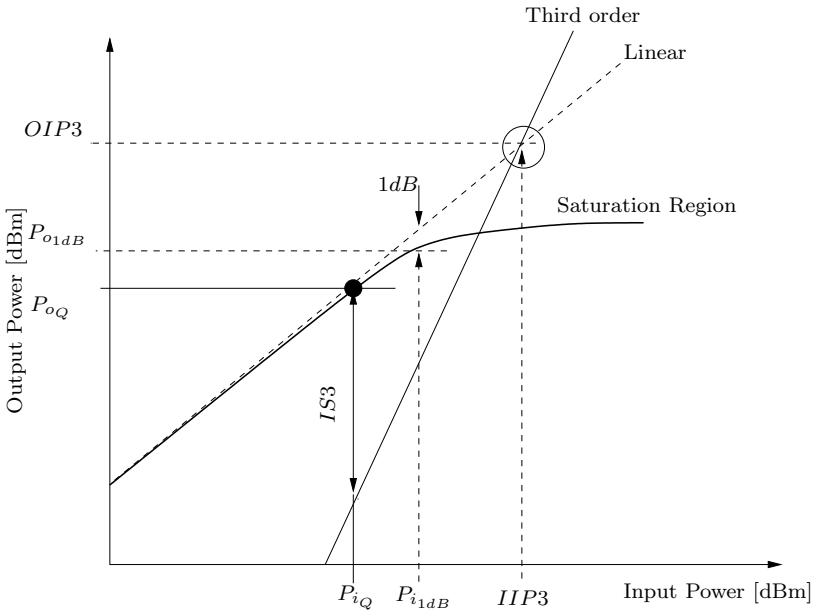

Figure 2.6: Illustration of input third-order intersection point (IIP3), output third order intersection point (OIP3), and 1dB compression point($P_{i_{1dB}}$,$P_{o_{1dB}}$). $IS3$ denotes the third-order intermodulation suppression for a particular working point P_{i_Q}, P_{o_Q}.

2.6.2 Memoryless PA models

If the PA has a flat frequency response characteristics over its entire working frequency range, or the communication system is narrow-band and if electro-thermal memory effects [73] are neglected, the PA can be modelled as a memoryless system. Memoryless power amplifiers are completely characterized by their AM/AM (amplitude to amplitude) and AM/PM (amplitude to phase) conversions which depend only on the current input signal value. Several memoryless PA models has been proposed to define the behavior of memoryless PAs. These models are fitted to AM/AM and AM/PM measurements obtained using a power-swept single tone input signal.

Considering the complex envelope $x(n)$ of the PA input, the complex envelope of a memoryless PA output $y(n)$ can be modelled as

$$y(n) = g[x(n)] = F_a(|x(n)|) \exp\{j(arg[x(n)] + F_p[|x(n)|])\} \tag{2.24}$$

where $F_a(\cdot)$ and $F_p(\cdot)$ are the AM/AM and AM/PM characteristics respectively.

Many models are tailored for a particular type of PA. For example, the Saleh model is good for modelling high-power amplifiers such as traveling-wave tube amplifiers (TWTAs). The Saleh model is, however, inaccurate

to model GaAs FET based amplifiers (solid state) which are useful for low and medium power levels. In this case a solid state power amplifier (SSPA) model is used that only takes in account the AM/AM conversion.

The measurements based models mentioned above are indeed useful, e.g., when setting up a simulation environment to assess the system performance. However, when designing signal processing techniques, that need to model the PA directly (or indirectly) and use this model to remove the PA induced nonlinear distortion, other parametric models that are not restricted to an specific PA type are useful. The most extensively used model is the polynomial model which renders simplified analysis and efficient design of nonlinear equalizers or distortion cancellation techniques (see, Chapter 4 and 5).

Saleh model

The Saleh model [74] used to model TWTA is a simple static PA model with only four parameters. The AM/AM and AM/PM characteristics are, respectively, given by

$$F_a(|x(n)|) = \frac{a_0|x(n)|}{1 + a_1|x(n)|^2} \tag{2.25}$$

$$F_p(|x(n)|) = \frac{b_0|x(n)|}{1 + b_1|x(n)|^2} \tag{2.26}$$

where a_0, a_1, b_0, and b_1 are positive real numbers. The Saleh model has been extensively applied in the evaluation of predistorters and linearization techniques, see, e.g., [75].

Solid State Power Amplifier (SSPA) model

Due to different input-output amplitude and phase characteristics of TWTA and SSPA [76], the Saleh model is not accurate for modelling the SSPA in the saturation region. The phase distortion of a typical SSPAs is much smaller than that of the TWTAs and is, therefore, neglected in the SSPA model defined as [77]

$$F_a(|x(n)|) = \frac{|x(n)|}{\left[1 + \left(\frac{|x(n)|}{A_s}\right)^{2p}\right]^{1/2p}} \tag{2.27}$$

$$F_p(|x(n)|) = 0 \tag{2.28}$$

where p defines the smoothness of the transition from linear operation to saturation and A_s is the saturation output amplitude.

For large values of p, the SSPA model approaches the soft limiter model that is commonly used to represent the clipping operation [68] to reduce the dynamic range of the OFDM signal. The soft limiter model is specified as

$$F_a(|x(n)|) = \begin{cases} |x(n)| & |x(n)| < A_s \\ A_s & |x(n)| > A_s \end{cases} \tag{2.29}$$

Related to the limiter model, we can define the clipping level ν

$$\nu = \frac{A_s}{\sqrt{E\{|x(n)|^2\}}} \tag{2.30}$$

where $\sqrt{E\{|x(n)|^2\}}$ is the RMS value of the OFDM signal.

Figure 2.7 illustrates the AM/AM and AM/PM curves for the SSPA model with $p = [0.5, 2, 10, 100]$ and the Saleh model with $a_0 = 2.1587$, $a_1 = 1.1517$, $b_0 = 4.033$ and $b_1 = 9.1040$. From this figure we see that the SSPA model with $p > 10$ resembles the limiter model which is useful for nonlinear distortion analysis. Larger levels of nonlinearity in both AM/AM and AM/PM curves for the TWTA are observed.

Memoryless polynomial model

The behavior of a memoryless PA can be described using a Taylor series with complex coefficients. The baseband output of the PA can be expressed as [78]

$$y(n) = x(n) \sum_{k=0}^{K} a_{2k+1} |x(n)|^{2k} \tag{2.31}$$

where K is the order of the polynomial function with coefficients a_{2k+1}. Only odd-order coefficients are considered because the signal generated from the even order terms are far from the carrier frequency and do not contribute to the baseband output.

A distinction between memoryless and quasi-memoryless can be done based on the coefficients a_{2k+1} [79, 80]. In case of real valued coefficients, only AM/AM conversion is modelled, and the polynomial represents a strictly memoryless PA [81]. For complex valued coefficients a_{2k+1}, AM/PM and AM/AM are modelled. In this case, the polynomial models a quasi-memoryless PA. In this thesis, the term memoryless includes both strictly memoryless and quasi-memoryless PAs.

The inclusion of the even-order term can improve the model accuracy, as is shown in [78]. In this case, the baseband output signal becomes

$$y(n) = x(n) \sum_{k=1}^{K} a_k |x(n)|^{k-1} = \sum_{k=1}^{K} a_k \Phi_k(x(n)) \tag{2.32}$$

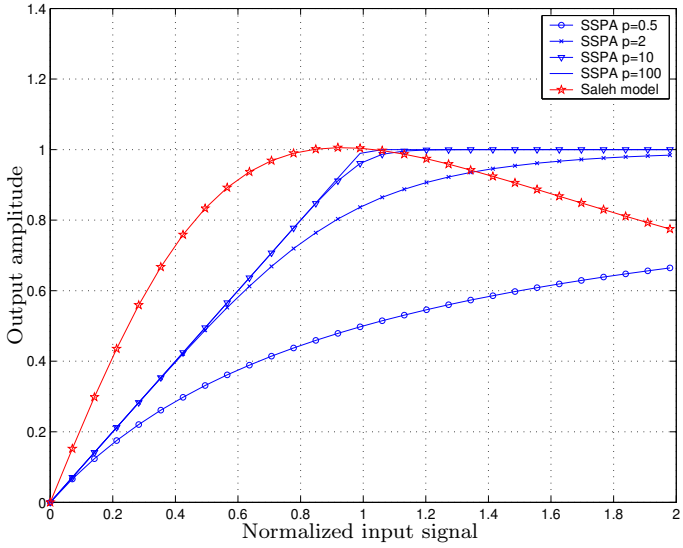

(a) AM/AM

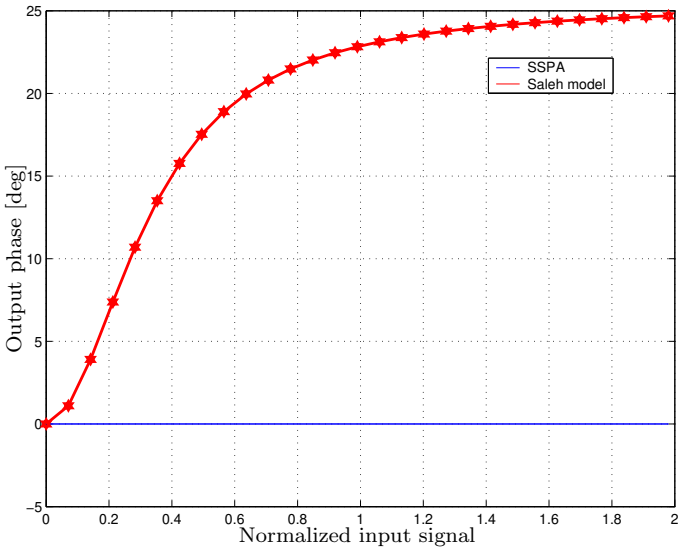

(b) AM/PM

Figure 2.7: AM/AM and AM/PM curves for SSPA model for $p = [0.5, 2, 10, 100]$ and Saleh model with $a_0 = 2.1587$, $a_1 = 1.1517$, $b_0 = 4.033$, and $b_1 = 9.1040$.

where $\Phi_k(x(n)) = |x(n)|^{k-1}x(n)$ is a basis set.

To extract the PA parameters $\{a_k\}_{k=1}^{K}$ based on a set of N input-output measurements at instants $\{n_i\}_{i=1}^{N}$, we define the respective input and output vectors as $\mathbf{x} = [x(n_1), \cdots, x(n_N)]^T$ and $\mathbf{y} = [y(n_1), \cdots, y(n_N)]^T$.

Defining the basis function $\mathbf{\Phi}_k(\mathbf{x}) = [\Phi_k(x(n_1)), \cdots, \Phi_k(x(n_N))]^T$ and the $N \times K$ matrix $\mathbf{\Phi} = [\mathbf{\Phi}_1(\mathbf{x}), \cdots, \mathbf{\Phi}_K(\mathbf{x})]$, the PA coefficients can be obtained as

$$\hat{\mathbf{a}}_{LS} = [\hat{a}_1, \cdots, \hat{a}_k]^T = (\mathbf{\Phi}^H\mathbf{\Phi})^{-1}\mathbf{\Phi}^H\mathbf{y} \tag{2.33}$$

For the case of large values of K, the regressor matrix $(\mathbf{\Phi}^H\mathbf{\Phi})^{-1}$ is ill-conditioned and may cause numerical instability [80]. A good measure for the numerical stability is the condition number of matrix $\mathbf{\Phi}^H\mathbf{\Phi}$ defined as $|\lambda_{max}/\lambda_{min}|$, where λ_{max} and λ_{min} are the largest and smallest eigenvalues of $\mathbf{\Phi}^H\mathbf{\Phi}$, respectively.

In general, matrix $\mathbf{\Phi}^H\mathbf{\Phi}$ has a high condition number due to the large correlation between the columns of this matrix. The sources of this large correlation are the high correlation of the nonlinear polynomials and the correlation of the data samples at different time instants.

In order to solve the numerical instability problem, an orthogonal polynomial basis [82] can be used that is robust in the presence of quantization noise and finite-precision errors [83]. Using orthogonal polynomials effectively reduces the high correlation of the nonlinear polynomial, thus improving the numerical stability.

Memoryless PA - linearized model

Based on the Bussgang's theorem [84], the output of a nonlinear memoryless PA excited by a Gaussian distributed signal $x(n)$ can be represented by the scaled version of the original signal plus an additive noise term [85], i.e.,

$$y_{NL}(n) = K_L x(n) + d(n) \tag{2.34}$$

where the distortion term $d(n)$ is uncorrelated with $x(n)$ and K_L is the attenuation factor. The equivalent block diagram is illustrated in Figure 2.8.

For the case of high clipping levels (i.e., few clipping events per OFDM symbol), the nonlinear distortion can be modelled as impulsive noise [86]. This case is not treated in the thesis mainly because it assumes that the PA is mostly operating in its linear region.

2.6.3 Broadband PA models

In broadband applications, the PA frequency response is no longer flat over the frequency operation region [88]. As a result, the power gain at a given

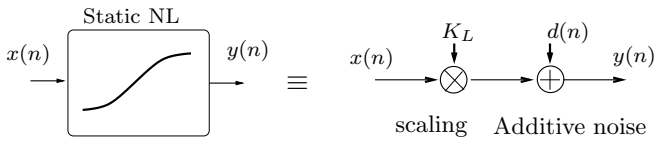

Figure 2.8: Equivalent nonlinear model [87] for the nonlinear distortion where $x(n)$ is the distortion-free input signal vector, K_L is the gain of the PA and $d(n)$ is the nonlinear distortion.

time instant depends on previous input signal values leading to a nonlinear system with memory.

Memory effects are in general associated to group delay, frequency response of matching networks and nonlinear capacitance of the transistors [89]. Other dynamic effects of the PA are due to electro-thermal effects [90]. The transistor self-heating phenomenon was investigated in [73] and it was concluded that self-heating effects are important when considering narrowband signals. For the case of broadband signals, the electrical effects due to the non flat response are more pronounced than the electro-thermal effects.

In this thesis we consider behavioral models that describe the PA as a black box which is not tailored to any specific physical phenomenon [91–95]. Behavioral models are simplifications of general Volterra models and are sometimes represented with a cascade combination of one or two linear filters and a memoryless nonlinearity, which is the case for the Wiener, the Hammerstein, and the Wiener-Hammerstein models.

In [96], the identification capability of several PA models is evaluated for WCDMA and LDMOS EDGE power amplifiers. For both PAs, Wiener and Hammerstein models show a good match with the input-output measurements. Compared with Volterra models, the simplified structures provide a more robust estimation. Saleh memoryless model, included in this analysis, shows poor modelling results.

Volterra models

The Volterra model is appropriate for modelling weakly nonlinear systems [97]. The relationship between the input $x(n)$ and the output $y(n)$ complex value signals is represented in discrete-time domain by the $2M-1$ order Volterra series as

$$y(n) = \sum_{k=0}^{M-1} \sum_{l_1=0}^{L} \cdots \sum_{l_{2k}=0}^{L} h_{2k+1}(l_1, l_2, \cdots, l_{2k+1}) \prod_{i=1}^{k+1} x(n-l_i) \prod_{i=k+2}^{2k+1} x^*(n-l_i) \tag{2.35}$$

where $h_{2k+1}(l_1, l_2, \cdots, l_{2k+1})$ represents the baseband equivalent Volterra kernels and L is the memory length.

Volterra series is certainly general with the added feature of being linear in the parameters. However, as with conventional Taylor series it converges slowly. Volterra series are unattractive for real-time application due to the number of coefficients required, which increases exponentially with L and M. In practice the series need to be truncated which may lead to ill-conditioned identification. Several approaches appear in the bibliography to reduce the number of Volterra parameters, see [98, 99]. Hammerstein, Wiener, Wiener-Hammerstein and memory polynomial models can improve the situation with fewer parameters [100].

Wiener models

The Wiener model is constituted by a linear filter $\mathbf{b} = [b_0, \cdots, b_{L_b-1}]$, here assumed FIR, followed by a static nonlinearity $g(\cdot)$, see Figure 2.9a. It can be described by the following equations

$$z(n) = \sum_{l=0}^{L_b-1} b_l x(n-l) \tag{2.36}$$

$$y(n) = z(n) \sum_{k=0}^{K} a_{2k+1} |z(n)|^k \tag{2.37}$$

where b_l are the coefficients of the linear block, and a_{2k+1} are the odd-order coefficients of the polynomial that describes the memoryless nonlinearity. Other representatives for the static nonlinearity, like piecewise linear functions, can be also used, e.g., [101].

A drawback of the Wiener model that arises in the model identification, is the fact that the model is nonlinear with respect to the parameters of the linear filter [96, 102]. Therefore, the output signal $y(n)$ cannot be explicitly written as a function of the input signal $x(n)$.

Hammerstein models

The Hammerstein model is composed by a memoryless nonlinearity followed by a linear filter, Figure 2.9b. The output of a Hammerstein system can be expressed as

$$z(n) = x(n) \sum_{k=0}^{K} a_{2k+1} |x(n)|^k \tag{2.38}$$

$$y(n) = \sum_{l=0}^{L_c-1} c_l z(n-l) \tag{2.39}$$

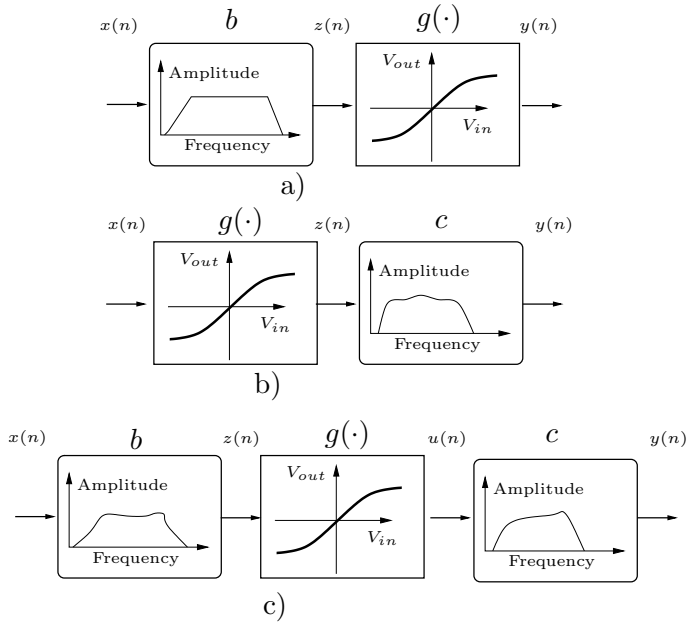

Figure 2.9: a) Wiener model, b) Hammerstein model and c) Wiener-Hammerstein model, where **b** and **c** represent the linear dynamic blocks and $g(\cdot)$ the static nonlinear block.

where $c_l = [c_0, \cdots, c_{L_c-1}]$ are the impulse response values of the linear block **c**.

The Hammerstein model is linear in the memory parameters as opposed to the Wiener model, which greatly simplifies its identification.

Wiener-Hammerstein models

A more general memory model is the Wiener-Hammerstein model, which is the cascade of the Wiener and Hammerstein structures, Figure 2.9c. The output of a Wiener-Hammerstein structure is specified by the following set of equations

$$z(n) = \sum_{l=0}^{L_b-1} b_l x(n-l) \tag{2.40}$$

$$u(n) = z(n) \sum_{k=0}^{K} a_{2k+1} |z(n)|^k \tag{2.41}$$

$$y(n) = \sum_{l=0}^{L_c-1} c_l u(n-l) \tag{2.42}$$

Memory-polynomial model

The memory polynomial model is constructed using the diagonal kernels of the Volterra series. Considering a baseband linear-cubic model represented with Volterra series [103], the output of the system is given by

$$y(n) = \sum_{l=0}^{L} h_1(l)x(n-l) + \sum_{l_1,l_2,l_3=0}^{L} h_3(l_1,l_2,l_3)x(n-l_1)x(n-l_2)x^*(n-l_3) \tag{2.43}$$

where $h_1(l)$ is the linear kernel and $h_3(l_1,l_2,l_3)$ is the cubic kernel.

The third-order memory-polynomial model is obtained by setting $h_3(l_1,l_2,l_3) = 0$ except for the diagonal $l_1 = l_2 = l_3$, i.e.,

$$y(n) = \sum_{l=0}^{L} \left[h_1(l)x(n-l) + h_3(l,l,l)x(n-l)|x(n-l_2)|^2\right] \tag{2.44}$$

The advantage of the memory-polynomial is that the number of coefficients is on the order of $L+1$ enabling its use in real-time applications.

Other polynomial models can be found in the literature. For example, the orthogonal memory-polynomial [82] that can alleviate the instability problem associated with the conventional polynomial models, and the Generalized memory polynomial [100] which combines the memory polynomial with additional cross terms improving estimation algorithm stability at a small increase of the computational complexity.

2.7 Other issues in practical OFDM systems

This thesis is devoted to find solutions that characterize and improve the system performance when nonlinear PAs are employed. There exist other challenges when implementing an OFDM system. We end this chapter with a brief review of three important topics not discussed in the rest of the thesis, namely, I/Q imbalance [104–106], phase noise [10,107] and synchronization.

2.7.1 I/Q Mismatch

When direct conversion is used to down-convert a signal from radio frequency (RF) to baseband, the band of interest is directly translated to zero frequency and filtered to suppress nearby interferer. Low implementation complexity is the main advantage of using a direct conversion structure when compared with other receiver structures such as superheterodyne. Unfortunately, in direct conversion receivers the baseband signal are severely distorted by imbalances in the In-phase and Quadrature (I/Q) branches [105,106,108].

Assuming an I/Q imbalance in the direct conversion receiver, the complex-valued baseband signal can be written as [104]

$$x' = \alpha x + \beta x^* \tag{2.45}$$

where x' is the signal affected by the I/Q imbalance, x is the signal before I/Q distortion, $*$ denotes complex conjugate, and α and β are given by

$$\alpha = \cos(\Delta\theta) + j\epsilon \sin(\Delta\theta) \tag{2.46}$$

$$\beta = \epsilon \cos(\Delta\theta) - j \sin(\Delta\theta) \tag{2.47}$$

with $\Delta\theta$ and ϵ being the phase and amplitude imbalances between the I and Q branches.

In the context of an OFDM system, let us denote the frequency domain OFDM symbol $\boldsymbol{\chi}$ and the time domain transmitted symbols by $\mathbf{x} = \mathbf{Q}\boldsymbol{\chi}$, where $\mathbf{Q}$ represents the IDFT operation. In the receiver, the recovered symbol after the down-conversion and DFT operations, neglecting the channel noise (AWGN channel with high SNR), can be expressed as

$$\hat{\boldsymbol{\chi}} = \mathbf{Q}^H \mathbf{x}' = \mathbf{Q}^H(\alpha\mathbf{x} + \beta\mathbf{x}^*) = \alpha\boldsymbol{\chi} + \beta\boldsymbol{\chi}^{\triangle} \tag{2.48}$$

where $\boldsymbol{\chi}^{\triangle}$ denotes the frequency domain representation of the complex conjugate $\mathbf{x}^*$.

The frequency domain representations of $\mathbf{x}^*$ and $\mathbf{x}$ are related as [104]

$$\boldsymbol{\chi} = \begin{bmatrix} \chi(1) \\ \chi(2) \\ \vdots \\ \chi(N/2) \\ \chi(N/2+1) \\ \chi(N/2+2) \\ \vdots \\ \chi(N) \end{bmatrix}, \boldsymbol{\chi}^{\triangle} = \begin{bmatrix} \chi^*(1) \\ \chi^*(N) \\ \vdots \\ \chi^*(N/2+2) \\ \chi^*(N/2+1) \\ \chi^*(N/2) \\ \vdots \\ \chi^*(2) \end{bmatrix}$$

From the point of view of an ideal channel, the effects of I/Q imbalances are clear: 1) the recovered constellation is scaled by a factor α and, 2) a scaled version of the mirror image of the constellation is added.

The I/Q impairments are even worse in a more realistic context where imperfect channel estimation and synchronization are taken into account. Furthermore, for large constellation sizes, I/Q imbalances become even more problematic.

A thorough review of I/Q imbalances in SISO and MIMO-OFDM systems can be found in [104]. Both I/Q imbalance compensation and nonlinear distortion compensation using adaptive interference cancellation are addressed in [109] in a realistic context based on real-world receiver front-end signals.

2.7.2 Phase noise

Oscillators are used to modulate the baseband information onto an RF carrier. The noise that originates from oscillator nonidealities appears in the baseband signal as additional phase and amplitude modulation [10].

The phase noise $\theta(n)$ is defined as the difference between the phase of the carrier f_c and the phase of the local oscillator f_o [107]. Assuming that there is no deterministic offset in the system, the phase noise can be modelled as a zero-mean random process, characterized by its power spectral density (PSD). The contribution of the phase noise can be viewed as an additional multiplicative effect of the channel, like fast and slow fading.

In case of OFDM systems, the multiplication of the received time domain signal with a time varying channel function is equivalent to convolving the frequency domain OFDM signal spectrum with the frequency domain channel transfer function. Under the assumption that the bandwidth of the phase noise is wider than the subcarrier spacing, the convolution results in intercarrier interference (ICI) affecting the system performance [110]. This is different than for the case of a single carrier system where the phase noise only reduces the effective SNR. The sensitivity to phase noise for single carrier and multicarrier systems was evaluated in [111, 112]. A more detailed analysis on phase noise in OFDM systems can be found in [113, 114]. I/Q mismatch and phase noise impact in MIMO-OFDM systems is evaluated in [115].

2.7.3 Synchronization: Timing and carrier frequency offset

Synchronization is a fundamental task that needs to be considered in the implementation of any digital communication system. The synchronization problem in OFDM systems requires different approaches considering the cases of broadcast systems or circuit switched systems and burst mode systems (packet switched systems). In burst mode systems, the synchronization has to be acquired during a short period of time after the start of the packet, whereas a broadcast and circuit switched systems that transmit data continuously can spend several symbols to obtain an accurate synchronization [116]. Synchronization errors can be either frequency, timing or both.

OFDM is robust to timing errors as long as the timing offset remains in the boundaries of the cyclic prefix. In this case, the orthogonality of the transmission is maintained that allows a simple equalization at the receiver. It is important to mention that the system robustness against channel delay spread is reduced because one portion of the cyclic prefix is employed to accommodate the timing offset. When the timing offset is too large and the boundaries of the cyclic prefix are exceeded, ISI and ICI are created and the orthogonality is partially lost [68][Ch.5.2.4].

Timing offset in OFDM is not as critical as in single-carrier systems [16], however, it should be compensated in order to keep it small compared with the length of cyclic prefix. A number of approaches to estimation of timing offset in OFDM systems have been presented in the literature. In general, the timing is determined by noticing that the correlation of the signal with a delayed version of itself will reach a peak when the repeated pattern is located. A thorough review of synchronization in multiuser OFDM systems can be found in [117]

One of the main drawbacks of OFDM systems is its sensitivity to carrier frequency offsets (CFOs) caused by the frequency mismatch between the local oscillators in the receiver and the transmitter together with the Doppler shift due to mobility. CFO will cause a loss of orthogonality between OFDM carriers and can degrade significantly the system performance if not estimated and compensated. This happens especially when the subcarrier spacing is small and data rates are high.

The system model presented in Section 2.1 assumes perfect carrier synchronization. If CFO is considered, the received signal vector in frequency domain can be written by [118]

$$\boldsymbol{y}(n) = \mathbf{Q}_N^H \mathbf{V}(\Delta_f(n)) \mathbf{Q}_N \boldsymbol{\mathcal{D}}_h(n) \boldsymbol{\chi}(n) + \boldsymbol{n}(n) \tag{2.49}$$

where $\boldsymbol{\mathcal{D}}_h(n)$ is a $N \times N$ diagonal matrix created with the channel frequency response $\boldsymbol{\mathcal{D}}_h(n) = \text{diag}[\boldsymbol{h}(n)]$ and

$$\mathbf{V}(\Delta_f(n)) = \text{diag}\left\{1, \exp\left(\frac{j2\pi\Delta_f(n)}{N}\right), \ldots, \exp\left(\frac{j2\pi(N-1)\Delta_f(n)}{N}\right)\right\} \tag{2.50}$$

is an $N \times N$ diagonal matrix that includes the normalized frequency offset Δ_f, $0 \leq \Delta_f \leq 1$.

We see from Equation 2.49 that for the case of perfect frequency synchronization (i.e., $\Delta_f = 0$), $\mathbf{V}(\Delta_f(n))$ will equal the identity matrix, and the received signal can be decoded by simple frequency domain equalization. On the other hand, when $\Delta_f \neq 0$, matrix $\mathbf{Q}_N^H \mathbf{V}(\Delta_f(n)) \mathbf{Q}_N$ is no longer diagonal, thus creating ICI.

The harmful effects of CFO are illustrated in Figure 2.10. We see that in the absence of CFO, each subcarrier waveform is sampled at its peak value where all other carrier waveforms are zero (i.e., ICI is zero). However, for a non-zero CFO, the carrier waveforms of adjacent subcarriers will no longer be sampled at zero crossings resulting in ICI.

Several techniques have been proposed to estimate and compensate CFO. They can be divided into data-aided and non-data-aided techniques depending on whether or not a training sequence is used.

Data-aided techniques are based on pilot symbols or preamble embedded into the transmitted signal. These techniques are commonly used in burst mode systems. The use of a preamble sequence, as in WLAN systems,

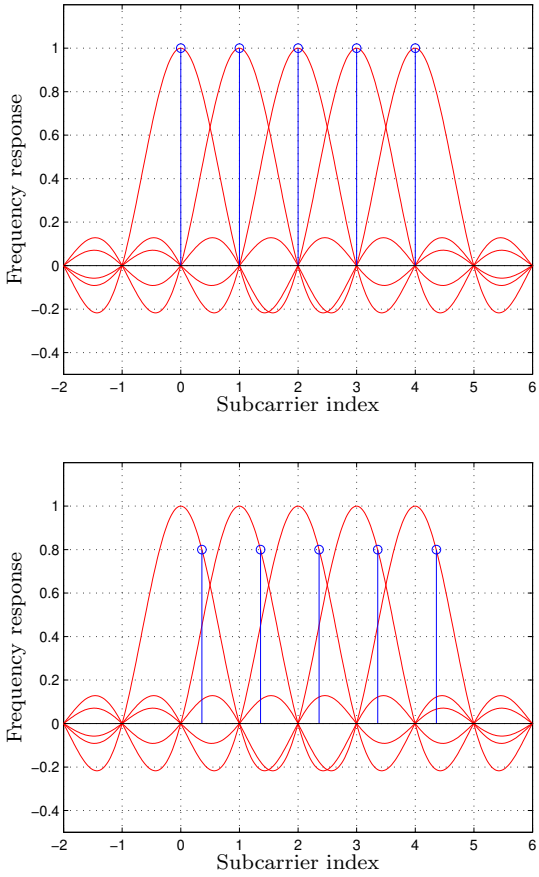

Figure 2.10: Effects of carrier frequency offset in an OFDM system. No CFO, i.e., $\Delta_f = 0$, ideal sampling position,i.e., each subcarrier waveform is sampled at its peak value where all other carrier waveforms are zero (top). CFO with $\Delta_f \neq 0$, the sampling instant is shifted reducing the amplitude and creating ICI (bottom).

allows the receiver to use maximum likelihood algorithms to estimate the CFO [119–122].

Non-data-aided methods employ the inherent structure of the OFDM symbols. CFO estimation techniques that exploit the properties of the cyclic prefix are addressed in [123, 124]. A CFO estimation method based on null subcarriers is addressed in [125].

Chapter 3

Analysis of power amplifier distortion effects in OFDM systems

This chapter gives an overview on the effects of the nonlinear distortion created by a real power amplifier to the performance of an OFDM communication system. Initially an analysis of bit error probability (BEP) and channel capacity for a SISO-OFDM system is introduced. Thereafter, a literature review on out-of-band distortion is presented.

Finally, the contributions of this thesis are enumerated. Expressions for BEP and capacity of an SDMA-OFDM system affected by a memoryless nonlinear amplifier are derived. The case of broadband PA and imperfect memory compensation in an OSTBC-OFDM system is described in the last part of the chapter.

3.1 Introduction

The amplification of a non-constant envelope signal by a power-efficient amplifier may cause nonlinear distortion affecting the system performance. The resulting nonlinear distortion can be categorized into two types: out-of-band distortion and in-band (or signal waveform) distortion. In-band distortion produces inter carrier interference increasing the bit error rate, or equivalently reducing the system capacity. Out-of-band distortion appears as a spectral regrowth, hence causing adjacent channel interference. In summary, the in-band distortion is affecting the own signal reception and the out-of-band distortion is affecting other users in the system. In other words, it is important to have a good idea of the levels of these two distortions in system design.

Therefore, it is desirable to have at hand closed-form expressions of bit error probability and capacity that include the effect of the PA induced

distortion. These expressions are then useful to evaluate whether some kind of nonlinear distortion compensation technique should be implemented or not to obtain a power efficient system with good performance.

In the following sections the effects of the in-band and the out-of-band distortion are analyzed for single-antenna and multi-antenna OFDM systems. The effects of PA memory are also considered.

The chapter ends with a brief review of the contributions of the thesis in the performance analysis of an OFDM system employing nonlinear PAs. One of the contributions of this thesis is the analysis and derivation of closed-form expressions for bit error probability and channel capacity for multiuser OFDM systems, in particular for SDMA-OFDM systems. Another is the derivation of an expression for the BEP of an OSTBC-OFDM system subject to nonlinear distortion and memory compensation errors.

3.2 BEP and capacity degradation

The analysis presented in this chapter is based on the assumption that the distortion caused by the PA can be modelled as an additive Gaussian noise whose variance depends on the input signal and the nonlinear PA characteristics [87, 126–129]. This assumption is realistic for low clipping levels, i.e., several clipping events per OFDM symbol. Figure 3.1, extracted from P5, illustrates the validity of this assumption and shows a Gaussian complementary cumulative distribution function (CCDF) with an adequate variance, and the simulation results for an OFDM system with $N = 512$ subcarriers and QPSK modulation. These curves show good agreement when clipping levels ν are lower than 6 dB.

Assuming that the nonlinear distortion is additive and Gaussian (more details in Section 2.6.2), the OFDM signal at the output of the memoryless nonlinear PA $g[\cdot]$ can be written as,

$$\mathbf{x}^g(n) = g[\mathbf{x}(n)] = K_L\,\mathbf{x}(n) + \mathbf{d}(n) \tag{3.1}$$

where the first term $\mathbf{x}(n)$ is the distortion-free input signal vector (see Eq. (2.5)) and K_L is the gain of the linear part (scaling factor) that verifies $K_L \leq 1$. The second term $\mathbf{d}(n)$ is the nonlinear distortion which is a function of the modulated symbol vector $\boldsymbol{\chi}(n)$ and the power amplifier transfer function $g[\cdot]$. The nonlinear distortion term verifies

$$E[\mathbf{d}^*(n)\mathbf{x}(n)] = 0$$
$$E[\mathbf{d}(n)] = 0$$

The received signal after removing the cyclic prefix is given by

$$\mathbf{y}(n) = K_L\check{\mathbf{H}}(n)\bar{\mathbf{x}}(n) + \check{\mathbf{H}}(n)\mathbf{d}(n) + \mathbf{n}(n) \tag{3.2}$$

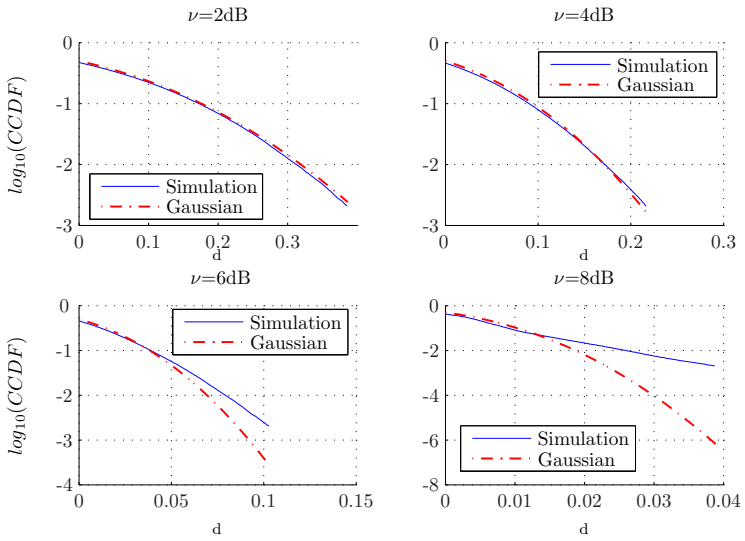

Figure 3.1: Complementary cumulative distribution function (CCDF) of distortion noise d for an OFDM system with $N = 512$ subcarriers and QPSK modulation equipped with an SSPA amplifier with smoothness factor $p = 2$ and clipping levels $\nu = [2, 4, 6, 8]$ dB.

where $\check{\mathbf{H}}(n)$ is the circular channel convolution matrix defined in Eq. (2.8). The frequency-domain expression of the received signal for each subcarrier can now be expressed as

$$y(n,k) = K_L h(n,k) x(n,k) + h(n,k) d(n,k) + n(n,k) \tag{3.3}$$

where $h(n,k)$ is, as in Chapter 2, the channel frequency response at subcarrier k. Assuming perfect channel estimation in the receiver, a soft estimate can be obtained by applying a zero-forcing equalizer and is given by

$$\hat{x}(n,k) = K_L x(n,k) + d(n,k) + \frac{n(n,k)}{\hat{h}(n,k)} \tag{3.4}$$

From Eq. (3.4) it is evident that the nonlinear distortion term $d(n,k)$ affects the decision variable in an additive way. Note that the distortion terms at different symbol instants are uncorrelated for a properly designed cyclic prefix, i.e., zero ISI. In general the nonlinear distortion terms are not necessarily statistically independent between subcarriers. However, based on the central limit theorem and considering large values of N, the nonlinear distortion terms $\{d(n,k)\}_{k=1}^{N}$ can be assumed as statistically independent [130].

The effective SNR at subcarrier k after equalization is

$$SNR(k) = \frac{K_L^2 \sigma_x^2}{\sigma_d^2 + \sigma_n'^2} \tag{3.5}$$

where $\sigma_d^2 = E[\mathcal{d}(n,k)\mathcal{d}^*(n,k)]$ (see P5, [87] for calculation details) and $\sigma_n'^2 = \sigma_n^2/|\mathcal{h}(n,k)|^2$. The variables K_L and σ_d^2 are functions of the employed PA model and can be analytically evaluated or obtained by simulations. For soft limiter PA model a closed-form solution is available [87], P5.

It is known that the BEP is a function of the modulation format and the SNR. For example, the BEP for the case of QPSK modulation is obtained as

$$P_e(k) = \frac{1}{2}\text{erfc}\left(\sqrt{SNR(k)}\right) = \frac{1}{2}\text{erfc}\left(\sqrt{\frac{K_L^2 \sigma_x^2}{\sigma_d^2 + \sigma_n'^2}}\right) \tag{3.6}$$

where erfc is the complementary error function defined as $\text{erfc}(x) = \frac{2}{\sqrt{\pi}} \int_x^\infty \exp(-t^2)dt$ [131, Sect. 8.250, Eq. (4)].

The channel capacity of a clipped OFDM system for the case of an AWGN channel was derived in [127] assuming that the distortion terms are uncorrelated additive Gaussian variables. The channel capacity of subcarrier k is then given by

$$C(k) = \log_2[1 + SNR(k)] = \log_2\left[1 + \frac{K_L^2 \sigma_x^2}{\sigma_d^2 + \sigma_n'^2}\right] \tag{3.7}$$

From Equation 3.7 we see the harmful effect of the nonlinear distortion that reduces the effective SNR due to the scaling factor $K_L^2 < 1$ and the additive noise term σ_d^2 in the denominator.

Assuming that the input power is equally distributed over each subcarrier (water filling is not implemented), the system capacity can be expressed as

$$C = \sum_{k=1}^{N} \log_2[1 + SNR(k)] \tag{3.8}$$

3.3 Out-of-band distortion

Standard regulations impose restrictions on the adjacent channel interference (ACI), usually measured using the adjacent channel power ratio (ACPR) parameter, defining spectral masks constraints. As a consequence, the PA operation point needs to be carefully chosen to meet the spectral mask. On the other hand, the PA operation point needs to be optimized in order to get the maximal power efficiency. These two constraints (power efficiency and ACI) are key factors in the design of the PA. Unfortunately,

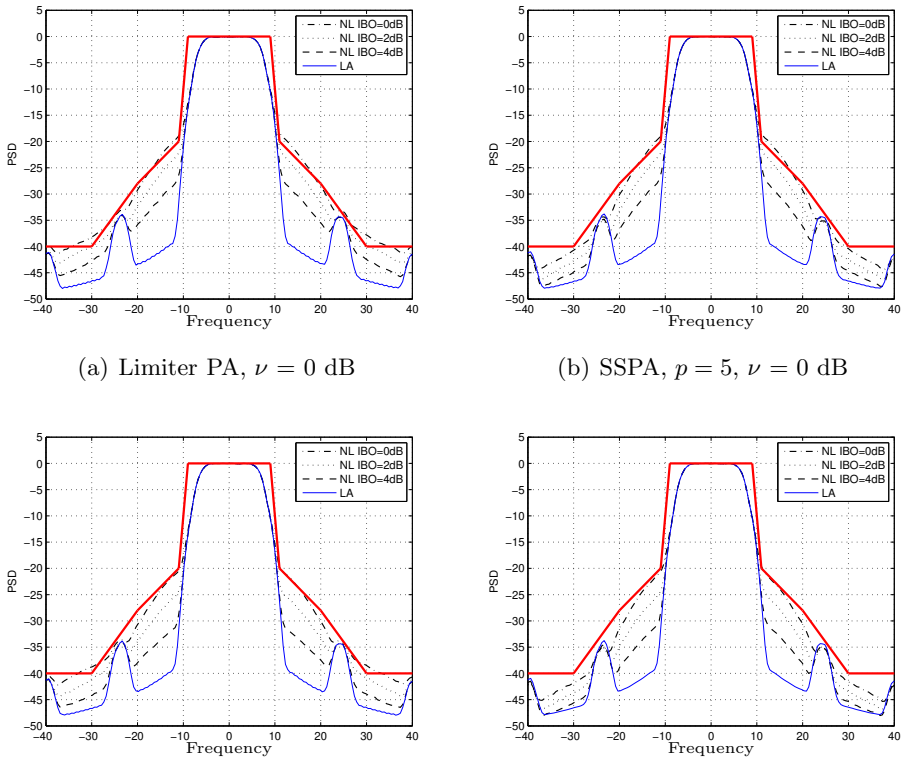

(a) Limiter PA, $\nu = 0$ dB

(b) SSPA, $p = 5$, $\nu = 0$ dB

(c) Limiter PA, $\nu = 1$ dB

(d) SSPA, $p = 5$, $\nu = 1$ dB

Figure 3.2: Out-of-band distortion for different PA models with clipping levels ν of 0 dB and 1 dB and back-off $IBO = 0, 2, 4$ dB. The WLAN spectral mask has a carrier spacing is 20 MHz, allocated in two frequency bands 5.15-5.35 GHz and 5.47-5.725 GHz [1].

efficiency and reduced ACI are two conflicting requirements, i.e., designs that limit the adjacent interference force the operation of the PA into a low power efficiency region.

To illustrate this concept, Figure 3.2 shows the transmission mask for HIPERLAN II and IEEE 802.11, which are available standards for WLAN. Both systems implement OFDM with similar parameters. The PSDs of nonlinear (NL) PAs (Limiter and SSPA models) are included with clipping levels ν of 0 dB and 1 dB and input back-off of $[0, 2, 4]$ dB. We see that the out-of-band distortion is below the transmit spectrum mask when the clipping level is $\nu = 1$ dB. In the case of $\nu = 0$ dB, the PA must work with back-off levels larger than 2 dB in order to fulfill the spectral mask requirements. Thus, the reduction of the ACPR comes at the expense of large back-off values which reduce the power efficiency of the PA.

The prediction of the spectral regrowth as a function of the PA param-

eters and modulation format has been an active research area for several years. Restricting the input signal to be Gaussian, a realistic assumption for OFDM systems, simplifies the theoretical analysis. Preliminary results employing this Gaussian assumption are found in [132] and [133] where a formula for the TWTA intermodulation was derived. In [134], the PA is modelled using complex power series, and a derivation of the ACPR and gain compression is presented. The extension to other PA models, like the Limiter and Cann's models, is presented by the same authors in [135] in the context of CDMA systems. ACPR prediction for a memoryless PA model is treated in [136] for narrow-band input signals (where the restriction on Gaussian input was removed), and in [137] for CDMA and OFDM signals. Closed-form expressions for ACPR for quasi-memoryless and memory polynomial PA are derived in [138]. Analysis of spectral regrowth for PA using Volterra models have been presented in [139, 140].

For more details on the topic of out-of-band distortion, please see the references cited in this section.

3.4 Contributions

This section summarizes the contributions of the thesis related to performance evaluation of OFDM systems subject to nonlinear PA distortion

BEP and capacity degradations for a multiuser SDMA-OFDM system employing a memoryless nonlinear PA are presented in the following. The obtained theoretical upper bound can be used for a realistic system design, whereas the upper bounds derived in [141] assuming a linear amplifier may yield too optimistic BEP values. Independently, and in parallel to our analysis, a simplified study of the symbol error rate (SER) performance was carried out in [142–144] for a MIMO-OFDM system subject to transmitter and receiver impairments. Closed-form expressions were provided for the SNR region (asymptotic error floor) and for low SNR (considering only signal scaling). We stress that our results, presented in this section, are more exact and are related to BER instead of SER. We provide closed-form expressions that are valid for more practical SNR values, ranging from medium to high SNR.

Finally, the BEP performance for a broadband OSTBC-OFDM with nonlinear distortion and imperfect memory compensation is analyzed.

3.4.1 BEP degradation in SDMA-OFDM systems with memoryless PA

In P5 a BEP analysis is carried out for a multiuser SDMA-OFDM system. Previous work on the subject was done by the author in [145]. However, a tighter approximation to the real case is obtained with the derivation obtained in P5.

The BEP derivation is based on the assumption that the distortion created by the PA can be modelled as an additive Gaussian noise with variance equal to σ_d^2 as was discussed in Section 3.2.

In order to simplify the analysis an uncorrelated MIMO channel (No correlation among the transmitting antennas nor among the receiving antennas) is assumed, i.e., the frequency-domain channel coefficients $\mathcal{H}_{i,j}(n,k)$ are samples of independent stationary, zero-mean and unit variance circular complex Gaussian distributed processes. Thus, the simplified model provides a lower bound of bit error probability in frequency selective channels.

Then using an LS detector for user separation in an SDMA-OFDM system equipped with P receive antennas in the base station and L users with a single antenna and assuming independent subcarrier modulation, the upper-bound of the error probability for a subcarrier k is given by

$$\begin{aligned} \bar{P}_e(k) \quad \leq \quad & \frac{1}{(P-L)!\bar{\gamma}^{P-L+1}} \sum_{m=0}^{\infty} \frac{(-1)^m (m+P-L)!}{m!} \Big(\frac{1}{\sigma_d^2}\Big)^{m+P-L+1} \\ & K_L^{2m} U_{P-L+m+1,\frac{P-L+2}{2}} \left(\frac{\sigma_a^2}{\sigma_d^2 \bar{\gamma}}\right) \end{aligned} \tag{3.9}$$

where $\bar{\gamma} = E[\gamma]$ is the average SNR, σ_a^2 is the energy of the complex-value data symbol, and $U_{P-L+m+1,\frac{P-L+2}{2}} \left(\frac{\sigma_a^2}{\sigma_d^2 \bar{\gamma}}\right)$ is the *Confluent Hypergeometric Function* [131, Sect. 9.211, Eq. (4)] defined as

$$U_{a,b}(z) = \frac{1}{\Gamma(a)} \int_0^{\infty} \exp(-zt) t^{a-1} (1+t)^{b-a-1} dt. \tag{3.10}$$

The advantage of the closed-form BEP solution is that it can be applied to calculate the performance of an SDMA-OFDM as well as other systems with diversity gain equal to $P-L$ without time consuming simulations. A closed-form solution for the calculation of σ_d^2 and K_L can be obtained for a soft limiter PA model (in Appendix A, P5).

In this analysis it is assumed that all users employ similar PAs. However, it is straightforward to extend these results to the case of different scaling factors and nonlinear distortion terms. In the particular case of SDMA systems, where each user is equipped with one transmit antenna, different PA parameters can be considered because each user is operating independently from other users. For MIMO systems where each user is operating with multiple antennas, the assumption of identical PA parameters is even more realistic.

Figure 3.3 illustrates BEP results of the LS detector obtained by theory and simulations for an SDMA-OFDM system ($L = 1$ to $L = 4$, $P = 4$) with QPSK modulation employing a nonlinear SSPA with clipping level $\nu = 1$ dB using an LS detector. The simulation parameters are summarized in Table 3.1.

As expected, the simulation results show lower BEP than the theoretical upper bound. For high SNR values, the BEP bound is tighter than in the low SNR region.

Extensive simulations, show that a close fit to the infinite sum of the original expression is obtained by employing only the first 20 to 30 terms.

Figure 3.4 shows the BEP results derived for the linear case obtained by using the results presented in [141], the nonlinear case obtained using Eq. (3.9) and BER results obtained by simulations. The case of an SDMA-OFDM system with $L = 2$ and $P = 4$ employing nonlinear SSPAs with clipping level $\nu = 1$ dB is considered. For a realistic BEP, e.g., $BEP = 10^{-2}$, Eq. (3.9) predicts the SNR with an error of 0.5 dB and the linear approach predicts the SNR value with a gap of 2.5 dB.

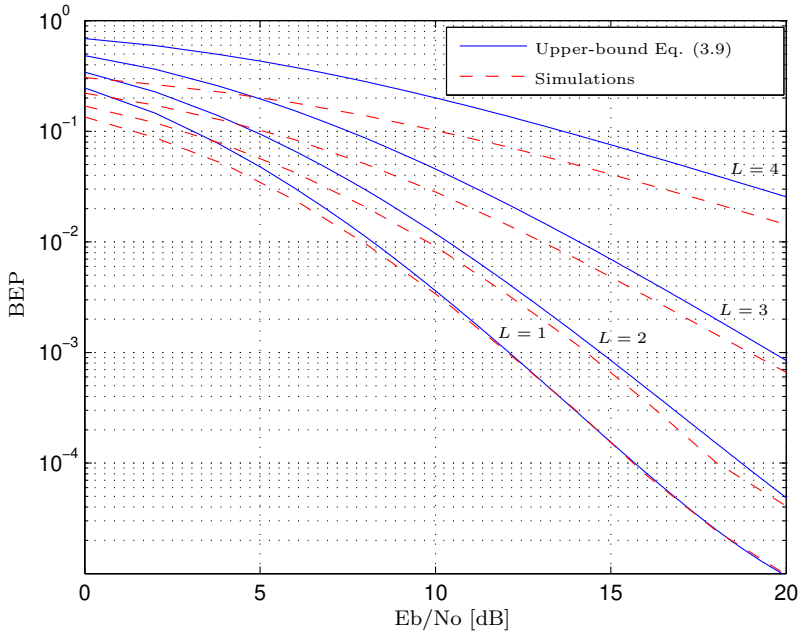

Figure 3.3: BEP versus E_b/N_o of a $P \times L$ SDMA-OFDM system with QPSK modulation, for the case of nonlinear SSPA with clipping level $\nu = 1$ dB using an LS detector.

3.4.2 Capacity degradation in SDMA-OFDM systems with memoryless PA

In the design of a communication system the effective data rate needs to be known in order to define the quality of service the system can offer. The case of single-user OFDM was already treated in Section 3.2 in the cited

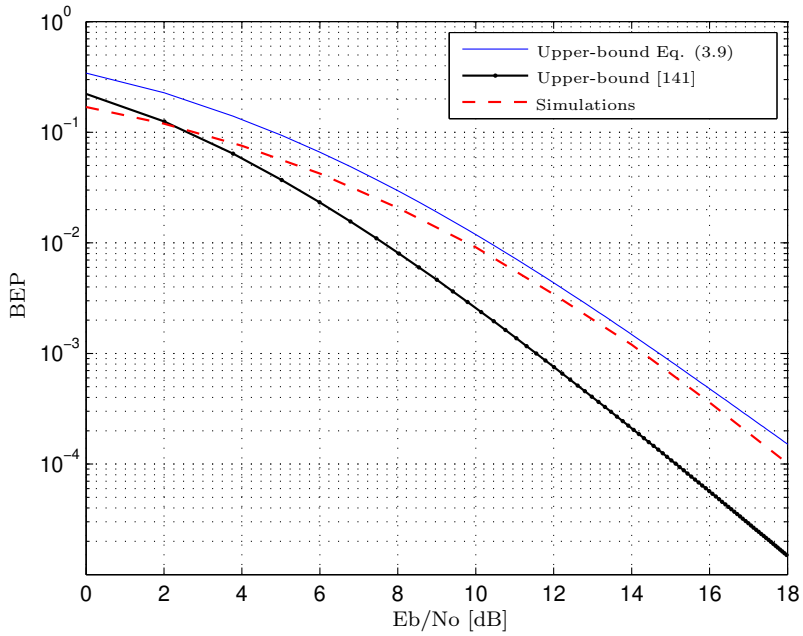

Figure 3.4: BEP versus E_b/N_o of an SDMA-OFDM system ($P = 4, L = 2$) with QPSK modulation employing nonlinear SSPAs with clipping level $\nu = 1$ dB using an LS detector. Analytical BEP results based on [141] (linear case) and [P5]. Simulation results are included for comparison.

references. Considering an SDMA-OFDM system employing an LS receiver, the capacity for user j is given by (see derivation details in P5)

$$C_{LS} = E\left[\log_2\left\{1 + \frac{\sigma_j^2}{\sigma_n^2[\boldsymbol{\mathcal{H}}^{\mathrm{H}}\boldsymbol{\mathcal{H}}]_{j,j}^{-1} + \sigma_d^2/K_L^2}\right\}\right] = E\left[\log_2\left\{1 + \frac{\sigma_j^2\gamma}{\sigma_a^2 + \sigma_d^2\gamma/K_L^2}\right\}\right] \tag{3.11}$$

where the instantaneous SNR $\gamma = (1/[\boldsymbol{\mathcal{H}}^{\mathrm{H}}\boldsymbol{\mathcal{H}}]_{j,j}^{-1})/\sigma_n^2$ is a χ^2-*distributed* variable with $2(P - L + 1)$ degrees of freedom. The capacity obtained by integrating Eq. (3.11) over a χ^2-*distribution* can be expressed as

$$C_{LS} = \int_0^\infty \log_2\left(1 + \frac{\sigma_j^2\gamma}{\sigma_a^2 + \sigma_d^2\gamma/K_L^2}\right)\frac{1}{(P-L)!\bar{\gamma}^{P-L+1}}\gamma^{P-L}\exp\left(-\frac{\gamma}{\bar{\gamma}}\right)d\gamma \tag{3.12}$$

This integral can be evaluated numerically. However, assuming a high SNR, the capacity can be approximated in closed form (see P5, Appendix

Table 3.1: Simulation parameters used for generating Figures 3.3 and 3.4.

System parameters	
Number of subcarriers	512
Cyclic prefix length	8
Modulation	QPSK
Clipping level	1 dB
Carrier frequency	5 GHZ
Bandwidth	20 MHZ
Channel parameters	
Type	Typical Urban
Channel delay profile	[0,1,2,3] μs
Power loss taps	[0,-1,-3,-9] dB
Mobile speed	5 km/h

C) and is given by

$$C_{LS}(k) \approx \log_2\left(1+\frac{1}{\sigma^2_{d'}}\right) - \frac{\sigma^2_d}{\ln(2)}\left[\ln(\beta)+\gamma_e-\exp(\beta)\right. \times \left.\left([1+\beta u(P-L)]\,\mathrm{E}i(-\beta)+\sum_{k=2}^{P-L}\frac{\beta^k\Gamma_I(1-k,\beta)}{k}\right)\right] \quad (3.13)$$

where $\beta = \frac{\sigma^2_d}{(\sigma^2_{d'}/K^2_L)\bar{\gamma}}$, γ_e is the Euler-Mascheroni constant ($\gamma_e = 0.5772\ldots$) [146], $\mathrm{E}i(\cdot)$ is the exponential integral function and $\Gamma_I(\cdot)$ is the incomplete gamma function [147]. The function $u(P-L)$ is the unit step function defined as $u(x) = 1\,\forall\, x > 0$ and $u(x) = 0\,\forall\, x \leq 0$.

The derivation was carried out under the same assumptions used for the BER derivation discussed in Section 3.4.1. The asymptotic capacity gives the upper-bound of the system capacity, and is obtained by evaluating the previous expression at high SNR

$$C^{\infty}_{LS}(k) = \lim_{\bar{\gamma}\to\infty} C_{LS}(k) = \log_2\left(1+\frac{K^2_L}{\sigma^2_{d'}}\right) \quad (3.14)$$

Figure 3.5 illustrates capacity results evaluated using Equation (3.13). Exact capacity values obtained using numerical evaluation of Eq. (3.12), asymptotic capacity (Eq. (3.14)) and capacity for the linear case are also included. From these results, we conclude that the nonlinear distortion limits the achievable system capacity.

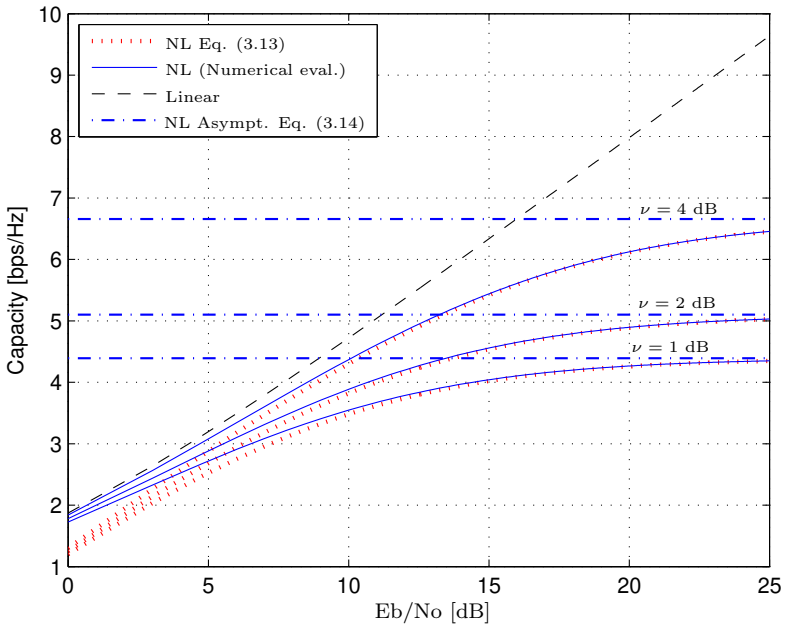

Figure 3.5: Capacity evaluation for an LS receiver with $L = 2$ users and $P = 4$ antennas, clipping levels of $\nu = 1$ dB, $\nu = 2$ dB and $\nu = 4$ dB. The exact value of capacity is obtained using numerical integration, the high SNR approximation is computed using Eq. (3.13), and the linear case was also included for comparison.

3.4.3 BEP in OSTBC-OFDM with nonlinear PA with imperfect memory effects compensation

In narrowband systems or when employing low-power amplifiers, memory effects in the PA can be neglected. In these cases, the PA can be modelled as a memoryless system. However, in the case of wideband communications systems, e.g., OFDM or WCDMA, or when employing high-power amplifiers, memory effects are introduced in the system.

The PA memory effects can be removed by applying predistortion with memory [82], memory precompensation at the transmitter side [148], or postcompensation at the receiver. The latter two approaches require that a sufficient power back-off is applied to the input signal so that the PA memory effects can be efficiently handled by a frequency domain equalizer, i.e., any presence of nonlinear distortion is neglected. Due to the non-flat frequency response of the broadband PA, estimation errors will naturally degrade the BER performance. It is important to note that both these solutions neglect the distortion due to the nonlinear input-output characteristics of the PA.

In practice, due to the large peak-to-average power ratio (PAPR) of the OFDM signal, nonlinear distortion will also be present.

In publication P7, BEP expressions are derived for an OFDM system with diversity, in particular for an OSTBC-OFDM system, that include the effect of a broadband nonlinear PA and imperfect memory compensation.

For the derivation of the BER expressions, the PA is assumed to be accurately represented by a Wiener model [100] and the distortion term is modelled as before like a Gaussian variable. The linear filter of the Wiener PA structure is modelled with an FIR filter $\mathbf{c}$ with L_c taps. The unbiased PA memory estimate can be modelled in frequency domain as

$$\hat{\mathcal{C}}(n,k) = \mathcal{C}(n,k) + \Delta_c(n,k) \tag{3.15}$$

where n is the OFDM symbol index, k is the subcarrier, $\Delta_c(n,k)$ is the modelling error assumed to be zero-mean complex Gaussian variable with variance $\sigma_c^2(n,k)$ independent of $\mathcal{C}(n,k)$.

In an $N_T \times N_R$ OSTBC-OFDM system affected by nonlinear amplification, the decision variable for the transmitted symbol $\mathcal{X}_j(n,k)$ at the output of the OSTBC-decoder, assuming perfect channel knowledge in the receiver, gives the same results as a Maximum Ratio Combining (MRC), i.e.,

$$\begin{aligned} \hat{\mathcal{X}}_j(n,k) &= \alpha(n,k)[K_L\,\mathcal{C}(n,k)\mathcal{X}_j(n,k) + \mathcal{D}_j(n,k)] + \mathcal{W}(n,k) \\ \alpha(n,k) &= \sum_{j=1}^{N_T}\sum_{i=1}^{N_R} |\mathcal{H}_{i,j}(n,k)|^2 \end{aligned} \tag{3.16}$$

where $\mathcal{W}(n,k)$ is a complex Gaussian variable with zero mean and variance $\alpha(n,k)\sigma_n^2$ created by the noise contribution from the N_R receive antennas at different time instants, $\mathcal{D}_j(n,k)$ is the nonlinear distortion (modelled as additive Gaussian noise), K_L is the linear multiplication factor. The decision variable is affected in an additive way by $\mathcal{D}_j(n,k)$ and scaled by the memory $\mathcal{C}(n,k)$. Both these effects may cause errors in the detection process.

As mentioned before, there are two options to remove the memory effects:

- Precompensation (transmitter): the signal to be amplified is pre-equalized in frequency domain with the unbiased memory estimate $\hat{\mathcal{C}}(n,k)$.
- Postcompensation (receiver side): the received signal is post-equalized in frequency domain using the unbiased memory estimate $\hat{\mathcal{C}}(n,k)$.

In the following equations time index n and subcarrier index k are dropped to simplify the notation. Applying precompensation, the effective SNR at subcarrier k is given by

$$\gamma_{PRE} = \frac{K_L^2\gamma}{[K_L^2\epsilon_1 + \sigma_d^2/\sigma_x^2\epsilon_2]\gamma + 1} \tag{3.17}$$

where $\gamma = \alpha\sigma_x^2/\sigma_n^2$ is a chi-square variable with $2N_TN_R$ degrees of freedom and ϵ_1 and ϵ_2, are given by

$$\epsilon_1 = \sum_{i=1}^{\infty} i!(\sigma_c^2/|\mathcal{C}|)^i,\ \epsilon_2 = |\mathcal{C}| \sum_{i=0}^{\infty} i!(\sigma_c^2/|\mathcal{C}|)^i \tag{3.18}$$

In the case of postcompensation, the effective SNR becomes

$$\gamma_{POS} = \frac{K_L^2\gamma}{[K_L^2\epsilon_1 + \sigma_d^2/\sigma_x^2\epsilon_2]\gamma + \epsilon_2} \tag{3.19}$$

Using the effective SNR equations, the bit error probability is derived for the precompensation and the postcompensation cases with imperfect memory model. The following closed-form solution for QPSK modulation at subcarrier k is given by

$$\begin{aligned}\bar{P}_e(k) &= \frac{1}{2K}\left\{1 - \frac{1}{(L+1)!\bar{\gamma}^L\sqrt{\pi}} \sum_{n=0}^{\infty} \frac{K_L^{1+2n}}{n!(1/2+n)}\right. \\ &\times \left(\frac{K_L^2\epsilon_1 + \sigma_d^2/\sigma_x^2\epsilon_2}{K}\right)^{n+L-1/2} \times \Gamma(n+L+1/2) \\ &\left.\times U_{n+L+1/2,L+1}\left(\frac{K}{\bar{\gamma}(K_L^2\epsilon_1 + \sigma_d^2/\sigma_x^2\epsilon_2)}\right)\right\}\end{aligned} \tag{3.20}$$

where $U_{a,b}(z)$ is the *Confluent Hypergeometric Function* previously defined in Eq. (3.10), the constant $K = 1$ for memory precompensation and $K = \epsilon_2$ for postcompensation, $\bar{\gamma} = E[\gamma]$ is the average SNR and $L = N_T \times N_R$.

The asymptotic BER, that provides the system error floor, is given by

$$\bar{P}_e^{\infty}(k) = \operatorname{erfc}\left(\sqrt{\frac{K_L^2}{(K_L^2\epsilon_1 + \sigma_d^2/\sigma_x^2\epsilon_2)}}\right) \tag{3.21}$$

Figure 3.6 shows the BEP curves obtained by simulations and by employing the first 30 terms of Eq. (3.20) for different values of memory compensation errors σ_c^2 without nonlinear distortion (clipping level $\nu = \infty$). These results allow us to conclude that memory effects must be accurately compensated and that the removal of nonlinear distortion (by linearization or memoryless predistortion) is not enough to ensure suitable BER levels.

Figure 3.7 illustrates the BEP curves for PA operating a clipping level of $\nu = 0$ dB.

The simulation parameters for both curves are summarized in Table 3.2.

Similar approach can be used for the derivation of other nonlinear models as, e.g., the Hammerstein and Wiener-Hammerstein models [100].

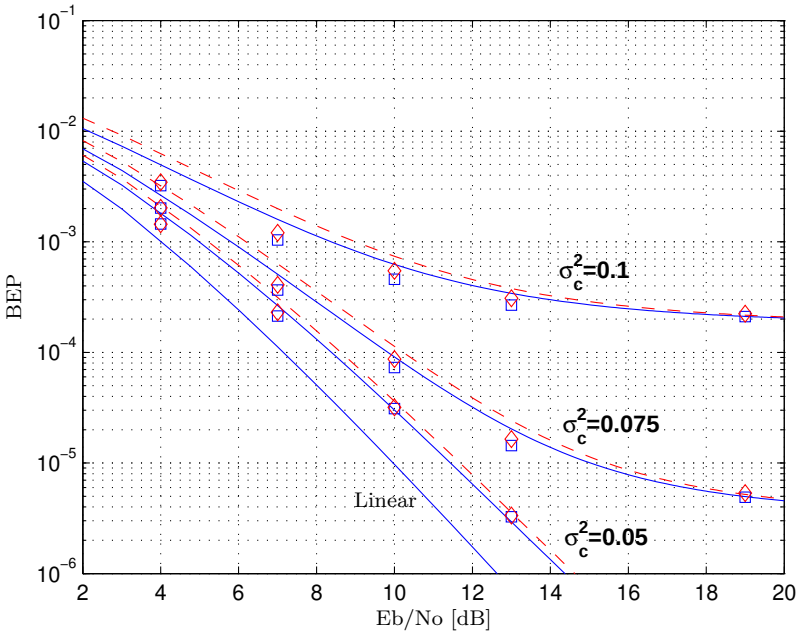

Figure 3.6: BEP versus Eb/No in a 2 x 2 OSTBC-OFDM system for different memory modelling error σ_c^2 with a Wiener-type nonlinear PA, clipping level $\nu = \infty$. Precompensation: theoretical (solid line) and simulation ('□'). Postcompensation: theoretical (dashed line) and simulation ('⋄').

Table 3.2: Simulation parameters used for generating Figures 3.6 and 3.7.

System parameters	
$N_T \times N_R$	2×2
Number of subcarriers	512
Cyclic prefix length	32
Modulation	QPSK
Clipping level	∞ , 0 dB
Carrier frequency	5 GHZ
Bandwidth	20 MHZ
Power amplifier	HMC409LP4 (modelled with a Wiener model)
Channel parameters	
Type	Typical Urban
Channel delay profile	[0,1,2,3] μs
Power loss taps	[0,-1,-3,-9] dB
Mobile speed	10 km/h

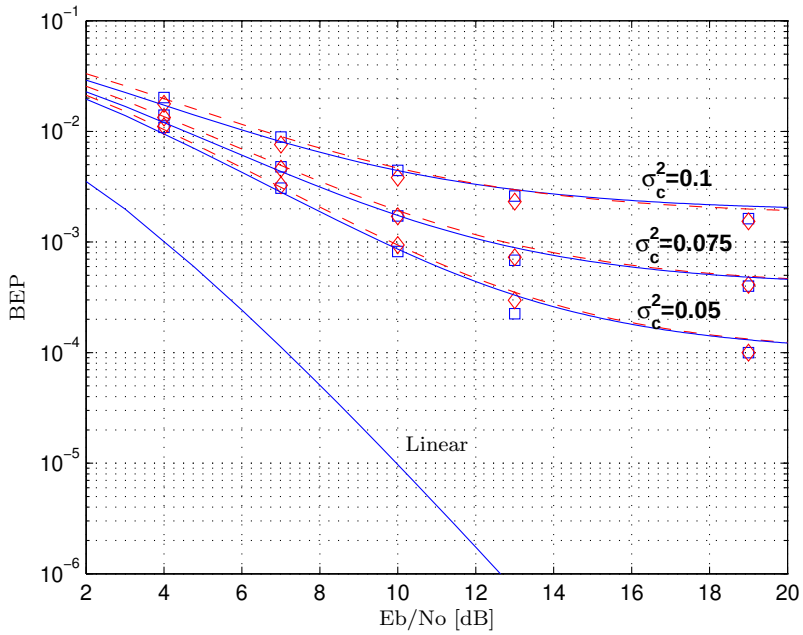

Figure 3.7: BEP versus Eb/No in a 2 x 2 OSTBC-OFDM system for different memory modelling error σ_c^2 with a Wiener-type nonlinear PA, clipping level $\nu = 0$ dB. Precompensation: theoretical (solid line) and simulation ('□').

Chapter 4

Power amplifier distortion compensation at the transmitter

This chapter presents an overview of various transmitter techniques for nonlinear distortion compensation where the goal is to obtain a system with tolerable levels of bit error rate (BER) and adjacent channel power ratio (ACPR). Initially back-off and PAPR reduction techniques are described. Thereafter, an overview of predistortion methods is presented. Finally, we review the contributions of this thesis related to transmitter techniques: a novel carrier allocation method with reduced intermodulation distortion, and a split predistorter structure for broadband PAs.

4.1 Introduction

To obtain a power efficient system with tolerable levels of BER and out-of-band distortion, the nonlinear PA distortion needs to be kept as low as possible while, at the same time, the PA is allowed to operate close to saturation. To achieve this goal we could think of a solution that compensates the nonlinear distortion at either the transmitter or the receiver. For the case of transmitter compensation, the signal to be transmitted is modified prior to the power amplifier. The most well known methods are PA linearization and PAPR reduction techniques.

Linearization techniques attempt to achieve an ideal linear power amplification [31], which enables the use of a nonlinear PA with good power efficiency. Nowadays, linearization techniques can be implemented using software defined radio systems, rendering cost and power efficient solutions (in particular at the base station) [28].

The different linearization techniques can be categorized into three groups: 1) Analog feedback methods that include RF feedback, envelope

feedback, polar feedback, and cartesian feedback techniques [29], 2) Feedforward methods where an auxiliary amplifier is used in the feedforward loop to generate IMD products that cancel those at the PA output [30] and, 3) Predistortion methods where the signal is distorted prior to the power amplifier.

The advantages of feedforward methods include large operation bandwidth and inherent stability. However, the rather complex implementation makes it difficult to add feedforward methods in existing power amplifiers. One advantage of predistortion is the possibility to design predistorters in baseband, thus taking advantage of a DSP implementation.

In addition to the above mentioned techniques, there are linearization techniques that modify the input signal to produce constant envelope signals so that the PA can be operated in the linear region. Examples of such techniques include, linear amplification with nonlinear components (LiNC) [149], envelope elimination and restoration (EER) [29], and combined analog locked loop universal modulator (CALLUM) [150]. These techniques were originally developed for analog implementation. However, the digital implementation operating at baseband frequencies solves the problems of high cost and hardware complexity associated to the analog processing [29]. Other transmitter compensation methods that can be used in conjunction with the linearization techniques are power back-off and PAPR reduction. Back-off techniques scale the original signal moving the operation point of the PA to the linear region. However, this solution decreases the PA power efficiency. PAPR reduction techniques give a more power efficient solution [151].

Companding techniques provide an alternative to improve the system performance when operating the PA in a power efficient region (i.e., close to saturation). When applying companding techniques, the baseband signals are compressed at the transmitter for reducing peak-to-average power (PAPR) and expanded at the receiver to remove the distortion caused by the compressing operation [152, 153].

In the following sections back-off and PAPR reduction techniques are described. Thereafter, predistortion techniques are presented. At the end of the chapter a brief review of the contribution of this thesis is presented.

4.2 Back-off

To ensure linear amplification, the input signal can be attenuated (a so-called power back-off is applied) to fit into the linear region of the power amplifier. The application of back-off results in a significant increase in the PA power specifications, i.e., the PA design is oversized, resulting in a reduced power efficiency [154]. For this reason, back-off is restricted to applications with low requirements of PA efficiency.

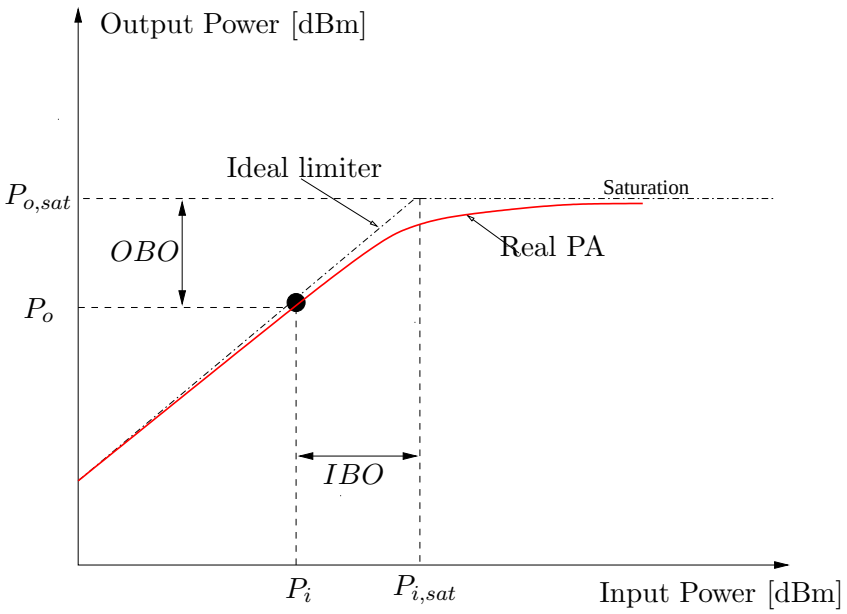

Figure 4.1: Definition of IBO and OBO.

The two quantities to measure the level of back-off are: input back-off (IBO), and output back-off (OBO). They are defined as

$$IBO = 10 \log_{10} \frac{P_{i,sat}}{P_i} \tag{4.1}$$

and

$$OBO = 10 \log_{10} \frac{P_{o,sat}}{P_o} \tag{4.2}$$

where $P_{i,sat}$ and $P_{o,sat}$ are the input and output saturation powers and P_i and P_o are the average power of the input and output signals. Either OBO or IBO can be used to specify the PA operation point. OBO is useful to quantify how much output power the amplifier generates compared with the maximal available power. Figure 4.1 illustrates the definition of IBO and OBO parameters.

As mentioned above, the application of back-off to linearize the system comes at the expense of a decreased power efficiency. Figure 4.2 illustrates the trade-off between linearity versus power efficiency. In this figure, power amplifier efficiency (PAE), output power P_o and amplifier gain versus the input power P_i are plotted for a typical low power amplifier (HMC409LP4) used for WLAN and WiMAX applications [155]. We see that for input signal powers between -20 to -5 dBm the PA is perfectly linear, but has a poor power efficiency. Operating the amplifier in the saturation region allows for

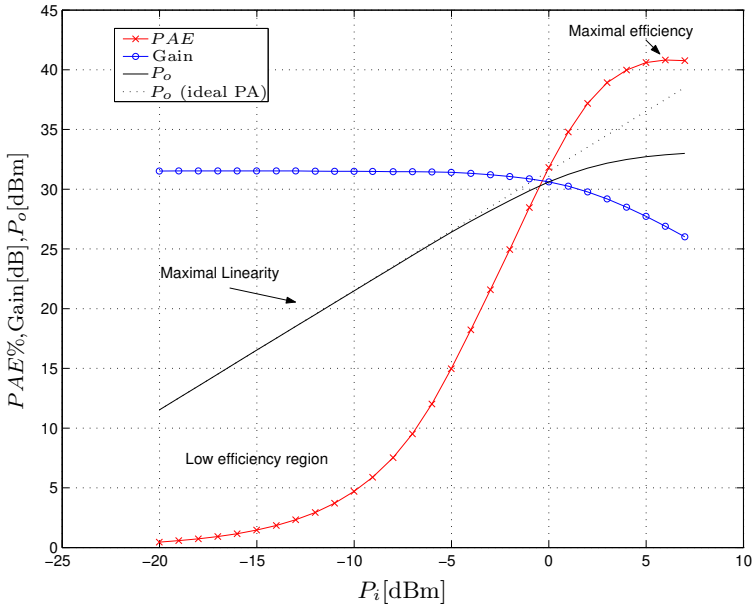

Figure 4.2: Curves of WLAN/WiMAX power amplifier. Curves of power amplifier efficiency (PAE) versus input power (P_i), power output (P_o) versus input power (P_i), and power gain versus input power (P_i).

a maximum power efficiency, however, sacrificing linearity. The situation is even worse when high-power amplifiers are considered [154].

The linearity and power efficiency constraints have initiated the development of more advanced compensation techniques that are described in the next sections.

4.3 PAPR reduction techniques

In this section, a brief review of the most well-known PAPR reduction techniques is provided.

PAPR reduction techniques reduces the envelope fluctuations of the signal to be transmitted by the PA. The easiest way to reduce the PAPR is to clip the signal at the transmitter. This clipping operation distorts the original signal increasing the out-of-band radiation and the bit error rate. Several approaches exist that reduce the PAPR without creating distortion noise, so called *distortionless* techniques. The most well-known techniques are tone reservation (TR), tone injection (TI) [66], coding [156], and partial transmit sequence (PTS) [157].

Methods like TI, coding and PTS may require side information. The need for side information increases the amount of processing in the receiver,

Table 4.1: Characteristics of PAPR reduction techniques. This table is based on the original PAPR reduction techniques. Improved versions of the original techniques have not been considered.

Technique	Data rate loss	Distortionless	Transmitter complexity	Receiver complexity
Clipping	NO	NO	LOW	LOW
Coding	YES	YES	HIGH	HIGH
TR	YES	YES	HIGH	LOW
TI	NO	YES	HIGH	LOW
PTS	YES	YES	HIGH	MEDIUM
COFDM	NO	YES	HIGH	LOW

and reduces the effective system data rate. Thus, when choosing one PAPR reduction technique, one needs to take into account the amount of PAPR reduction achieved, implementation complexity, the modification of the transmission power, and the data rate loss [27]. Table 4.1 provides a comparison between the methods that will be discussed next.

High PAPR in MIMO systems can be reduced by modifying the conventional PAPR reduction techniques [158–161]. Novel techniques based on spatial shifting has been developed in [162, 163].

4.3.1 Clipping

Clipping is the simplest technique for PAPR reduction, where the signal at the transmitter is clipped to a desired level A_s without modifying the phase information. The amplitude limitation of the time domain signal affects the received signal on all subcarriers (in-band distortion) and creates out-of-band emission.

Intuitively, the probability of clipping is directly related with the PAPR of the signal and the applied back-off. Signals with high PAPR are clipped more frequently than signals with low PAPR. In [71], an analysis of the required PA back-off for a given clipping probability is presented for a class A PA.

As previously discussed, the amount of back-off applied to the input signal will affect the power amplifier efficiency. For a class A power amplifier that achieves linear amplification up to the saturation point, the PAE as a function of the PAPR can be expressed as

$$PAE = \frac{PAE_{max}}{PAPR} \tag{4.3}$$

The maximum power amplifier efficiency (PAE_{max}) of 50 % is obtained

when the amplifier is operating at the saturation point. As an example, [71] reports that to guarantee a clipping probability of 10^{-4} for an OFDM signal of $N = 128$ subcarriers, the efficiency of a class A is only 3.2%.

In [164], an optimal clipping function is derived that maximizes the signal-to-noise-and-distortion ratio (SNDR). The resulting function that maximizes the SNDR is the *soft limiter* including gain. The relationship between the optimal clipping function and capacity is also derived.

4.3.2 Coding

The idea of the coding methods is to generate all possible code words and calculate their resulting PAPR. Then the code words with PAPR exceeding a predefined threshold are eliminated. Block coding is proposed in [156] and cyclic coding in [165]. In [166], a Golay complementary repetition code is proposed to reduce simultaneously the PAPR and peak interference-to-carrier ratio (PICR). A theoretical analysis related with the lower bound on the PAPR of a constant energy code is developed in [167].

The coding methods require an exhaustive search to find the best codes to be transmitted and large lookup tables for coding and decoding. These characteristics limit coding methods to systems with a small number of subcarriers.

4.3.3 Tone reservation

The basic idea of tone reservation technique is to reserve a set of P subcarriers (tones) which are not used for data transmission but for specially designed peak-reduction symbols.

Tone reservation (TR) is a distortionless technique and leads to very simple decoding of data symbols, since the receiver can simply ignore symbols on other carriers than those used for data. The goal is to find the time domain signal $\mathbf{p}(n)$ that when added to the original signal $\mathbf{x}(n)$ minimizes the maximum peak value, i.e.,

$$\min_{\mathbf{p}(n)} \|\mathbf{x}(n) + \mathbf{p}(n)\|_\infty = \min_{\boldsymbol{p}(n)} \left\|\mathbf{x}(n) + \mathbf{Q}_N \boldsymbol{p}(n)\right\|_\infty \tag{4.4}$$

where $\|f\|_\infty$ denotes the ∞-norm of the vector f that is the maximum of the absolute values of its components, n represents the OFDM symbol index, $\boldsymbol{p}(n) \in \mathbb{C}^{N\times 1}$ is the frequency-domain peak reduction symbol with P non-zero tones and $\mathbf{Q}_N$ is the $N \times N$ IDFT matrix.

A block diagram of the implementation of TR technique is shown in Figure 4.3a.

To find the optimal value of the peak-reduction symbol $\boldsymbol{p}(n)$, a convex optimization problem needs to be solved which requires high computational complexity. To reduce the computational complexity, a gradient algorithm can be used [66].

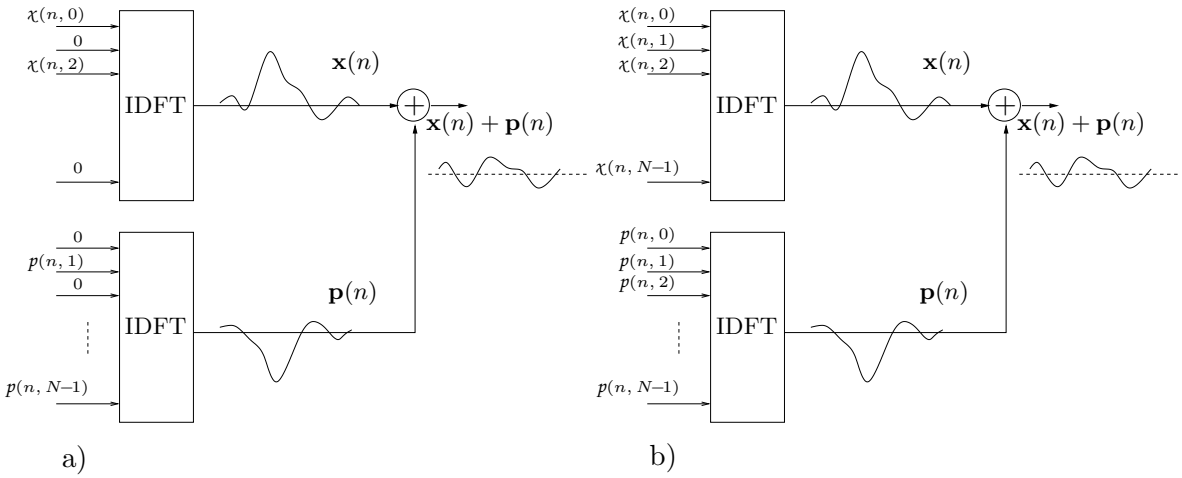

Figure 4.3: a) Tone reservation method b) Tone injection method [66].

A drawback of TR method is the reduction of the effective data rate because P carriers are reserved for peak-reduction symbols. However, if adaptive modulation is used, the overhead can be reduced by employing peak-reduction symbols in tones where the SNR is too low for data transmission.

4.3.4 Tone injection

The basic idea of tone injection (TI) is to increase the original constellation size so that the points in the original constellation can be mapped into several equivalent points in the expanded constellation. The extra degrees of freedom can be exploited for PAPR reduction.

The substitution of the points in the basic constellation by new points in the larger constellation is equivalent to injecting a tone of appropriate amplitude and phase in the OFDM symbol as is illustrated in Figure 4.3b [66]. Assuming that adaptive modulation is used and that the k-th tone is using an M-ary square quadrature amplitude modulation (M-QAM) with a minimum distance between constellation points $d(k)$. The symbol $\mathcal{X}(n,k)$ at subcarrier k can be represented by its real $\mathcal{X}_R(n,k)$ and imaginary $\mathcal{X}_I(n,k)$ components that can take values $\{\pm d(k)/2, \pm 3d(k)/2, \ldots, \pm(\sqrt{M(k)}-1)d(k)/2\}$.

The TI technique modifies the original constellation point $\mathcal{X}(n,k) = \mathcal{X}_R(n,k) + j\mathcal{X}_I(n,k)$ so that

$$\begin{aligned} \overline{\mathcal{X}}(n,k) &= \mathcal{X}(n,k) + \mathcal{P}(n,k) \\ &= [\mathcal{X}_R(n,k) + t(n,k)D(k)] + j[\mathcal{X}_I(n,k) + q(n,k)D(k)] \quad (4.5) \end{aligned}$$

where $t(n,k)$ and $q(n,k)$ are any integer values chosen to minimize the PAPR and $D(k) \geq d(k)\sqrt{M(k)}$.

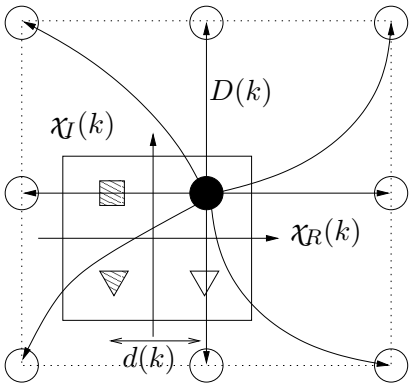

Figure 4.4: Example of mapping applied to the original 4-QAM symbol into a 32-QAM symbol in tone injection method.

Figure 4.4 illustrates the TI method applied to a 4-QAM constellation. The original symbol is represented using a black circle and the equivalent points of the expanded constellation are represented using white circles. The TI technique maps the original symbol to the point among all white circles that minimizes the PAPR.

The constant $p(n,k)$ in Eq. (4.5) can be removed after equalization by performing a simple *modulo*-D operation on the equalized signal.

Equation (4.5) shows that the modified constellation $\overline{\mathcal{X}}(n,k)$ has more energy than the original symbol $\mathcal{X}(n,k)$, whenever $t(n,k) \neq 0$ or $q(n,k) \neq 0$ and $D(k) \geq d(k)\sqrt{M(k)}$. This power increase may create secondary peaks affecting the algorithm performance [66]. Another drawback of TI is the high complexity associated with the minimization algorithm.

4.3.5 Partial transmit sequence

In the partial transmit sequence (PTS) technique, the input data block $\boldsymbol{\mathcal{X}}(n)$ of N symbols is divided into M disjoint vectors $\boldsymbol{\mathcal{X}}_m(n) = [\mathcal{X}_m(n,0), \mathcal{X}_m(n,1) \ldots, \mathcal{X}_m(n,N-1)]^T$, $m = 1,2,\ldots,M$, i.e., $\mathcal{X}_i(n,k)\mathcal{X}_j(n,k) = 0, \ \forall j \neq i$.

The original input data block can be expressed as

$$\boldsymbol{\mathcal{X}}(n) = \sum_{m=1}^{M} \boldsymbol{\mathcal{X}}_m(n) \tag{4.6}$$

Figure 4.5 illustrates an example of $N = 8$ subcarriers where the symbol vector $\boldsymbol{\mathcal{X}}(n)$ is divided into $M = 4$ vectors, each vector with $N/M = 2$ non-zero values. In the example, each vector $\{\boldsymbol{\mathcal{X}}_m(n)\}_{n=1}^{M}$ is allocated a group of N/M consecutive subcarriers. In practice, any combination of subcarriers can be used as long as they result in a disjoint set of vectors.

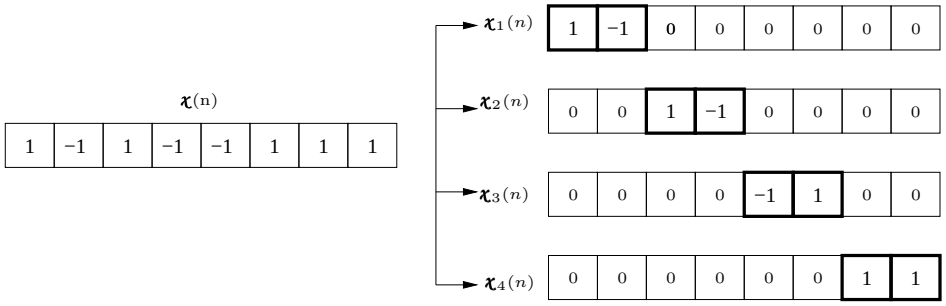

Figure 4.5: Example of $M = 4$ disjoints blocks used with the PTS technique for an OFDM system with $N = 8$ subcarriers.

After the initial division each vector $\boldsymbol{\chi}_m(n)$ is converted to time domain $\mathbf{x}_m(n) = [x_m(n,0), x_m(n,1), \ldots, x_m(n,N-1)]^T$, multiplied by a complex phase, and combined to yield the following time-domain signal

$$\mathbf{x}'(n) = \sum_{m=1}^{M} b_m(n) \cdot \mathbf{x}_m(n) \tag{4.7}$$

where $b_m(n)$ are complex phase factors to be optimized such that the PAPR of $\mathbf{x}'(n)$ is minimized [157].

Thereafter, the low PAPR symbol is transmitted together with the associated phase factors. An schematic diagram of the PTS technique is shown in Figure 4.6. In practice, the phase factors are limited to L values to reduce the search complexity. The amount of PAPR reduction achieved with PTS depends on how the N subcarriers are distributed among the $\{\boldsymbol{\chi}_m(n)\}_{n=1}^{M}$ vectors and the number of allowed phase factors L. A drawback of this approach is that the complexity of the optimization method increases exponentially with M. Some approaches have been proposed to reduce the computational complexity, see [168–171].

4.3.6 Clustered OFDM

In this technique, the N subcarriers are clustered into M blocks and transmitted over separate antennas [172]. The PAPR is reduced since there are only N/M subcarriers per transmitter. This approach has the added advantage of diversity gain provided by the use of multiple antennas.

The performances of clustered OFDM (COFDM) and a variation of COFDM, antenna interleaving OFDM (AIOFDM), have been evaluated in WLANs system employing a nonlinear PA and the results reported in Publication P1.

In AIOFDM, the subcarriers used for transmission at each antenna are spread over the whole frequency bandwidth, thus maximizing the frequency

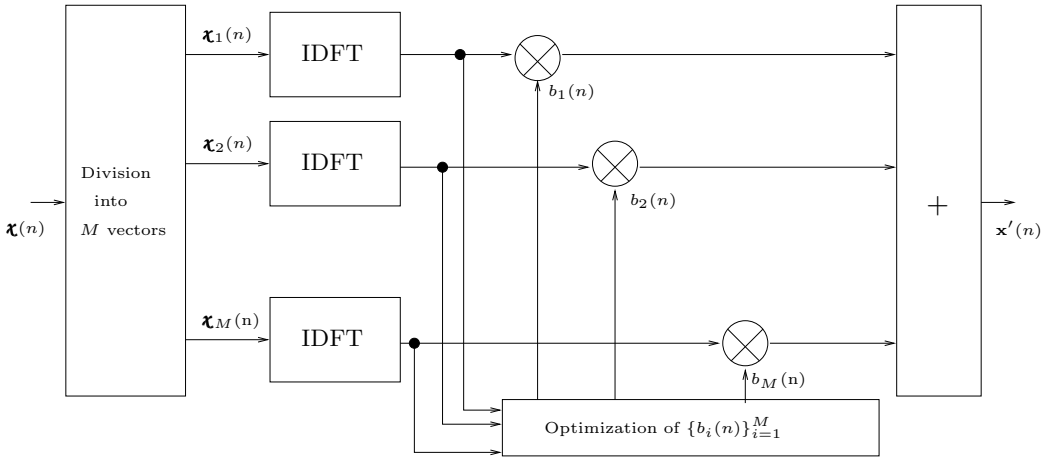

Figure 4.6: Block diagram of the partial transmit sequence technique.

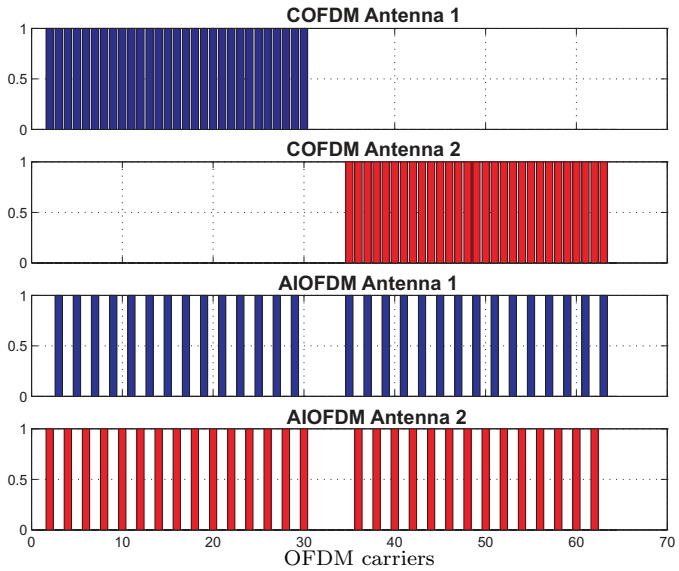

Figure 4.7: Carrier allocation for COFDM and AIOFDM for an OFDM system using $N = 64$ subcarriers and $M = 2$ antennas

diversity and at the same time reducing the PAPR in the same way as COFDM. Figure 4.7 illustrates how the subcarriers are divided between the antennas for COFDM and AIOFDM when using $N = 64$ subcarriers and $M = 2$ antennas.

Simulation results reported in P1 show that COFDM and AIOFDM help to reduce the linearity constraints and power efficiency in the PA design.

4.4 Predistortion

The predistorter (PD) is designed to model the inverse of the nonlinear PA response. The device is then placed before the nonlinear PA such that a linearly amplified signal is obtained at the output of the system, see Figure 4.8.

According to the position of the predistorter, three different categories can be distinguished [29]: 1) the RF predistorter which works directly at carrier frequency, 2) the IF predistorter that operates at the intermediate frequency (IF), and; 3) the baseband predistorter where the predistortion is moved to the baseband frequency allowing the application of DSP techniques. Baseband predistorters that fall within the scope of the thesis will be discussed next.

The most simple predistorter structures are memoryless, in which the current output depends only on the current input. The PA effects, characterized by the AM/AM and AM/PM effects, are compensated by using an expanding nonlinearity corresponding to the PA inverse transfer function. The memoryless predistortion techniques that have been developed during last decade are either look-up-table (LUT) based or parameter based.

In the LUT approach a complete input-output mapping of the PD is stored in memory [173–178]. The extension of LUT method for broadband PA (memory effects) is proposed in [179]. A review of adaptive LUT techniques can be found in [180]. The drawback of the LUT approach is the memory requirements, especially when the LUT is extended to handle a broadband PA with frequency dependent response.

In the parametric approach, the predistorter is described by a nonlinear function, polynomial model, piece-wise linear model or Volterra model. Parametric implementations for a memoryless PA are proposed in, e.g., [181, 182].

Memoryless predistorter structures applied to power amplifiers with memory reach very limited performance [183]. For broadband applications such as OFDM or for high-power amplifiers, memory effects need to be considered in the predistorter design [100]. The models that have been considered for memory PDs are based on Volterra series, Wiener, Hammerstein and memory polynomial models. To design PDs that take in account PA memory, one of the following approaches is often taken:

- Direct adaptation:

  A model of the PA transfer function is first identified. This model is thereafter used to find the inverse [184,185]. Figure 4.9 shows the block diagram of the direct adaptation structure. The PA input $y_{PD}(n)$ and PA output $y(n)$ are used to calculate an estimate of the PA model $\hat{g}(\cdot)$. This estimate is then used to calculate the PA inverse P.

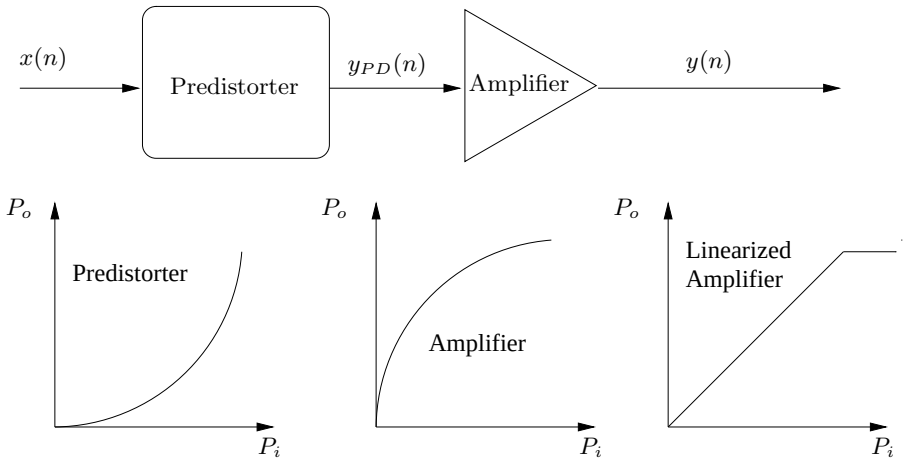

Figure 4.8: Block diagram describing the principle of predistorter. The PD modifies the input signal $x(n)$ such that the PA output $y(n)$ is a linearly amplified version of $x(n)$.

- Indirect learning adaptation:

  The calculation of the inverse of the power amplifier is generally a difficult task. For this reason the indirect learning method, originally adopted for predistortion design in [186], is a popular approach for adaptively finding the predistorter model. In this structure the predistorter is directly designed eliminating the PA estimation step.

  In the structure depicted in Figure 4.10, the predistorter parameters A are obtained by minimizing the error signal $e(n)$ obtained from the training branch output signal $\hat{y}_{PD}(n)$ and the predistorter output signal $y_{PD}(n)$. The parameters obtained in the training branch are directly copied to the predistorter, avoiding the inverse calculation process.

Direct adaptation structures based in Volterra series are addressed in [187–190], where the PA inverse is calculated by applying pth-order inverse techniques [191]. The preliminary work of indirect-learning Volterra predistorter was done in [186]. A similar approach using a multichannel filtering algorithm is presented in [192]. The high implementation complexity related with the high number of parameters and the slow series convergence are two fundamental issues that prevent the implementation of Volterra PDs in real systems. To reduce the number of parameters related with Volterra models while still keeping a good model capability, Wiener, Hammerstein and memory polynomial models can be employed.

The Wiener model has been adopted for PD design in several papers [193–195]. In [196] an adaptive LMS algorithm is derived for Wiener model

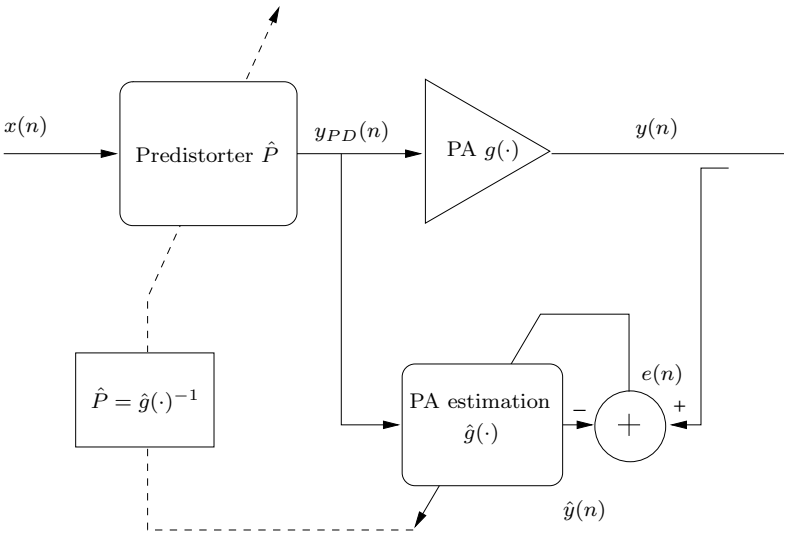

Figure 4.9: Predistorter implementation using direct learning structure

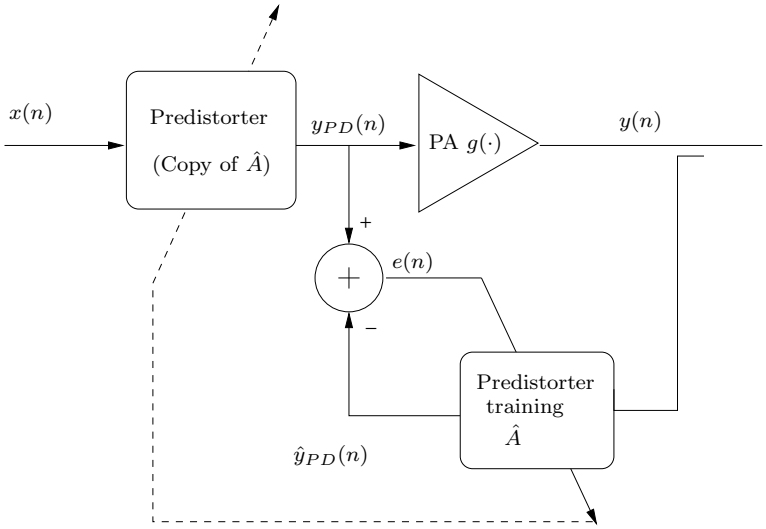

Figure 4.10: Predistorter implementation using indirect learning structure

based PD using an indirect learning structure. A direct learning structure for a Wiener model based PD is presented in [184]. PDs employing a Hammerstein model can be found in [197–199]. A Hammerstein and a memory polynomial predistorter are evaluated in [200], where the memory polynomial predistorter is shown to outperform the Hammerstein structure in the cancellation of out-of-band emission in a WCDMA system.

Indirect learning based PDs using memory polynomials have been presented in [103, 201, 202]. Replacing the conventional polynomial model by an orthogonal polynomial alleviate the numerical problems associated with the estimation of predistorter coefficients [82]. A generalized memory polynomial model that outperform conventional memory polynomials is presented in [100]. Implementations of PDs using neural networks are reported in [203–205].

It is important to note that the implementation of baseband predistorters requires a feedback of the downconverted (RF to baseband) output signal [29]. The distortion created by the nonideal behavior of the analogue components in the feedback path will affect the overall performance of the PD [206].

4.5 Contributions

This section summarizes the contributions of thesis related to transmitter compensation techniques. We first present the carrier-allocation method proposed in publication P2 that reduces the intermodulation distortion (IMD) in a multiuser OFDM system. A similar approach is found in [207, Chapt. 6] where an antenna array was used to reduce the IMD in a switched multibeam FDMA system. In that work, the users of a cellular system are allocated to frequency channels in such way that the IMD is minimized which is shown to outperform a random channel allocation. Finally, we describe the split predistorter (SPD) structure for broadband PA proposed in P6.

4.5.1 Carrier-allocation with reduced IMD

When a two-tone signal is applied in a nonlinear amplifier modelled with an n_{PA}-order polynomial, the frequency components of the output signal are given by

$$f_{IMP} = mf_1 \pm nf_2 \tag{4.8}$$

where f_1 and f_2 are the input signal frequencies and m,n are positive integers such that $m + n = n_{PA}$.

Considering the application of a two-tone signal in a PA exhibiting high-order nonlinearities, the number of harmonics and intermodulation products will be increased. If the power amplifier has a 7-th order nonlinearity, the terms m and n will run between 0 to 7, $m + n \leq 7$. Removing the out-band

products by filtering, the in-band spectrum will include the $3-th$, $5-th$ and $7-th$ harmonics.

For a PA modelled with a third-order polynomial excited with a two-tone signal of frequencies f_1 and f_2, the following frequency components will be generated: $3f_1$, $3f_2$, $2f_1+f_2$, $2f_1-f_2$, f_1+2f_2 and $2f_2-f_1$.

We consider a multiuser OFDM system with N_c carriers and a maximum of U users. The proposed intermodulation minimizing allocation technique (IMAT) assigns to each active user the set of $N = N_c/U$ subcarriers that minimizes the interference over other users created by second and third-order distortion.

The frequency associated with the N_c subcarriers are defined by $\mathbf{F} = \{f_1, f_2, \ldots, f_{Nc}\}$. In this algorithm only the combination of the maximum of three carriers is considered. The IMP by two carriers is given by $f_{IMP} = mf_1 \pm nf_2$ with $m+n=3$. If three carriers are considered, the IMP appears at the frequencies $f_{IMP} = mf_1 \pm nf_2 \pm kf_2$ with $m, n, k \leq 0$ so $m+n+k=3$.

The user allocation technique can be summarized in two basic steps:

Step 1: The first user is randomly allocated N subcarriers distributed across the spectrum.

Step 2: If a new user becomes active in the system, it will be assigned a new group of N carriers. Only the free subcarriers are considered (i.e., not previously assigned).

The allocation criterion for each new carrier f_i can be written as:

$$\text{Find } f_i \in F_f := \min \left| \sum_{j=1}^{J} P_{IM}(f_i) \right| \tag{4.9}$$

where F_f is the set of free carriers, and $P_{IM}(f_i)$ is the power of the IMP generated between the carrier f_i with the J combinations of the active carriers that generate IMP inside the OFDM bandwidth.

The IMP are calculated by combining the previously assigned carriers with all the possible new carriers allowing no more than one user per carrier. The new $N = N_c/U$ carriers that give the minimum power of the IMP on active users carriers are chosen.

If a new user becomes active, the selection process is carried out again with the free carriers.

The above method is suitable for medium or low load systems. In the case of a fully loaded system, the results are the same as with conventional block OFDM or interleaved OFDM methods.

IMAT requires knowledge on the number of active users and their associated subcarriers in order to apply the allocation criterion. The knowledge

Table 4.2: Power amplifier efficiency at a fixed $BER = 10^{-4}$ for IMAT and IAT methods. OFDM system with $N_c = 64$ carriers and two transmit antennas. The number of user is varying between 1 to 7 assigning $N = 8$ carriers per user. A class A PA is considered for PAE calculation. High load and medium load means 7 and 4 active users, respectively.

	PAE_{IMAT}	PAE_{IAT}	$\overline{PAE}_{IMAT}$	$\overline{PAE}_{IAT}$
Medium load, SNR=10dB	22.5%	12.8%	0.45	0.256
High load, SNR=10dB	8.4%	6.3%	0.168	0.126
Medium load, SNR=20dB	29.7%	26.9%	0.594	0.538
High load, SNR=20dB	20.3%	18.2%	0.406	0.364

of the PA model is not required to apply IMAT. It is based on a realistic assumption that the PA can be modelled using a third-order polynomial. Considering practical systems with several users and thousands of subcarriers the complexity of the allocation method is high. However, computationally efficient techniques can be implemented to compute the IMPs [208].

A base station with L antennas and U mobile stations with a single antenna has been simulated to evaluate the performance of IMAT. A pre-IFFT beamforming is implemented in the base station and its weights are calculated in order to maximize the signal to interference ratio (SIR). L transmit antennas have been considered in this application to evaluate the performance of IMAT in a multiple antennas environment. However, the application of IMAT is not restricted to multi-antenna systems.

The system under consideration has $N_c = 64$ carriers and 2 transmit antennas. The number of users is varying between 1 to 7 assigning $N = 8$ carriers per user. Table 4.2 illustrates the PA power efficiency improvements for a class A PA when using the IMAT and when using the interleaved access technique (IAT). Efficiency and normalized efficiency are indicated in the table, where the normalized PA efficiency (PAE) is defined as $\overline{PAE} = PAE/PAE_{max}$, with $PAE_{max} = 50\%$ for class A amplifier. From the Table 4.2 in a medium load system we see that using the IMAT outlined above can improve power efficiency up to 10%.

While IMAT aims to reduce IMP, adaptive resource allocation aims to maximize throughput without taking into account possible intermodulation products. Ideally, both techniques should be implemented jointly. One option is to add a new constraint (minimization of IMP) in adaptive resource allocation problem. A joint implementation of both techniques can be explored in future research.

4.5.2 Split predistorter structure

The SPD is implemented using a low-complexity memoryless predistorter in the transmitter that compensates the nonlinear distortion and a postcompensation filter at the receiver that jointly estimates PA memory and channel effects. This approach has several advantages: the out-of-band distortion is reduced as with the conventional predistorter and the identification of the PA memory can now be easily performed at the receiver jointly with the wireless channel. This feature is particularly attractive because the computationally involved identification and tracking at the transmitter is avoided. Other approach is presented in [148] where memory effects are compensated applying frequency domain pre-equalization (transmitter). The drawback of this technique is that an estimation of the PA memory is required at the transmitter.

The price to pay for joint estimation of PA memory and channel effects is an increase in the minimum number of pilot tones. This is because the effective length of the channel is increased. A conventional OFDM channel technique can be used for tracking the time-varying channel and the PA memory effect in digital domain.

In the following we assume that the broadband PA is modelled using a Wiener structure with a linear filter $\mathbf{h}_a$ and a static nonlinearity $g[\cdot]$, and that the length of the cyclic prefix is enough to compensate the ISI created by the wireless channel and the memory filter. The transmitted signal in frequency domain, after the modulation and amplification processes, can now be written as

$$\mathcal{X}_g(n,k) = K_L \mathcal{H}_a(n,k)\mathcal{X}(n,k) + \mathcal{D}(n,k) \tag{4.10}$$

where $\mathcal{X}(n,k)$ is the transmitted symbol at subcarrier k, $\mathcal{D}(n,k)$ is the value of the nonlinear distortion on subcarrier k, and $\mathcal{H}_a(n,k)$ is the k-th component of the $N \times 1$ frequency response vector of the PA memory.

The $\mathcal{X}_g(n,k)$ signal is transmitted through the wireless channel, and the received signal at subcarrier k, at time n, can be expressed as

$$\begin{aligned} \mathcal{Y}(n,k) &= \mathcal{H}_c(n,k)\mathcal{X}_g(n,k) + \mathcal{N}(n,k) \\ &= K_L \mathcal{H}_{eff}(n,k)\mathcal{X}(n,k) + \mathcal{H}_c(n,k)\mathcal{D}(n,k) + \mathcal{N}(n,k) \end{aligned} \tag{4.11}$$

where $\mathcal{N}(n,k)$ is the additive noise, assumed here to be circular complex Gaussian with variance σ_n^2, and $\mathcal{H}_{eff}(n,k) = \mathcal{H}_a(n,k)\mathcal{H}_c(n,k)$ is the effective channel, where $\mathcal{H}_c(n,k)$ is the channel response at subcarrier k.

The predistorter tasks can now be distributed such that the transmitter compensates for the static nonlinearity, and the receiver equalizes the PA memory.

- Memoryless PD

  A Q-th order polynomial predistorter $P(x)$ is designed to linearize the static nonlinearity,

$$\hat{P}[x(n)] = \sum_{i=0}^{Q} b_i |x(n)|^i \tag{4.12}$$

  Defining a P-th order polynomial model for the static nonlinearity $g(\cdot)$, the output of the predistorter-amplifier combination can be written as

$$y(n) = \sum_{j=0}^{P} a_j \left(\sum_{i=0}^{Q} b_i |x(n)|^i \right)^j \tag{4.13}$$

  The inverse of the power amplifier function can be fitted by another polynomial from training data [181]

$$x_t(n) = g^{-1}[y_t(n)] = \sum_{j=0}^{Q} \beta_j y_t^j(n) \tag{4.14}$$

  where $x_t(n)$ is an input training sequence and $y_t(n)$ is the system output. The coefficients β_i of the polynomial predistorter can be obtained using an LS estimate as

$$\hat{\beta} = \left[\bar{\mathbf{Y}}_t^{\mathrm{H}} \bar{\mathbf{Y}}_t \right]^{-1} \bar{\mathbf{Y}}_t^{\mathrm{H}} \mathbf{X}_t \tag{4.15}$$

  where $\bar{\mathbf{Y}}_n$ is the *Vandermonde* matrix formed by the output signal vector, and $\hat{\beta} = [\beta_0, \beta_1, \ldots, \beta_Q]$ are the estimated coefficients that describe the inverse nonlinearity polynomial $g^{-1}[\cdot]$. Finally, the predistortion function $P(x)$ is given by

$$\hat{P}[x(n)] \quad = \quad g^{-1}(y_t(n)) = \sum_{j=0}^{Q} \beta_j a_1^j x(n)^j = \sum_{j=0}^{Q} b_j x(n)^j$$

  with $b_j = a_1^j \beta_j$.

- Memory equalization

  A joint estimation of the linear part $\hbar_a$ and transmit channel $\hbar_c$ in frequency domain is proposed eliminating the model estimation process at the transmitter. Moreover, tracking capability is included and time variations due to PA memory and wireless channel can be followed because the estimation of the effective channel is carried out for each OFDM symbol.

  We assume a comb-type pilot arrangement where a set of T carriers are dedicated for channel estimation [209]. Furthermore, let $\mathcal{T} =$

$\{k_1, \cdots, k_T\}$ denote the set specifying the T pilot carriers. The channel frequency response on these subcarriers ($k \in \mathcal{T}$) may be estimated as

$$\begin{aligned} \hat{\mathcal{H}}_{eff}(n,k) &= \mathcal{Y}(n,k)/\mathcal{X}(n,k) \\ &= \mathcal{H}_{eff}(n,k)K_L + \mathcal{H}_c(n,k)\frac{\mathcal{D}'(n,k)}{\mathcal{X}(n,k)} + \frac{\mathcal{N}(n,k)}{\mathcal{X}(n,k)} \end{aligned} \tag{4.16}$$

where $\mathcal{D}'(n,k)$ is the residual nonlinear distortion that was not removed by the predistorter, and $\mathcal{X}(n,k)$ is the training symbol.

Collecting the channel estimates obtained at the pilot carriers into vector $\hat{\boldsymbol{\mathcal{H}}}_p(n) = [\hat{\mathcal{H}}_{eff}(n,k_1), \cdots, \hat{\mathcal{H}}_{eff}(n,k_T)]^T$, the whole channel frequency domain response can be obtained through interpolation using truncated DFT matrices [210], as given in the following expression

$$\hat{\boldsymbol{\mathcal{H}}}_{eff}(n) = \mathbf{Q}_N[\mathbf{Q}_{\mathcal{T}}^{\mathrm{H}}\mathbf{Q}_{\mathcal{T}}]^{-1}\mathbf{Q}_{\mathcal{T}}^{\mathrm{H}}\hat{\boldsymbol{\mathcal{H}}}_p(n) \tag{4.17}$$

where matrix $\mathbf{Q}_{\mathcal{T}}$ is formed from the IDFT matrix $\mathbf{Q}_N$ by extracting the T columns associated with the pilot subcarriers and the L_{eff} rows associated with the non-zero time-domain channel taps.

The proposed technique obtains the best performance when the PA can be accurately modelled using a Hammerstein model. However, considering small levels of residual nonlinear distortion, the technique shows excellent performance also for Wiener structures.

The performance of the SPD is evaluated for several PA models and compared with a conventional PD where the linear model is assumed to be known. Linear PA and a nonlinear PA compensated with memoryless PD are included for reference. Figures 4.11 and 4.12 show the BER results for two different PA models. The PA models and simulation parameters are summarized in Table 4.3. Simulation results show that the SPD technique is robust to different PA models reaching a similar performance to the conventional PD (with memory).

Table 4.3: Simulation parameters used for generating Figures 4.11 and 4.12.

System parameters	
Number of subcarriers	512
Cyclic prefix length	16
Modulation	16-QAM
Channel	SUI 3 [211]
Number of pilot carriers	32
PA models	
Model 1 WLAN low-power amplifier	Modelled with a Wiener model. Nonlinear block: 5-th order polynomial. Linear block: FIR filter of 7 taps.
Model 2 Class AB amplifier	Modelled with a Wiener model. Nonlinear block: 5-th order polynomial. Linear block: IIR filter.

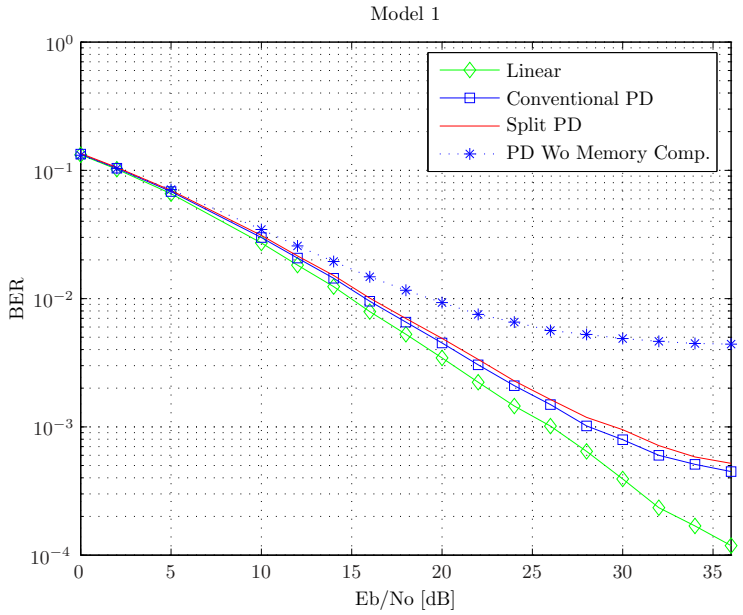

Figure 4.11: BER versus E_b/N_o of an OFDM system with 16-QAM modulation, for split predistortion (SPD), conventional PD with nonlinear PA (model 1 in Table 4.3), and memoryless PD.

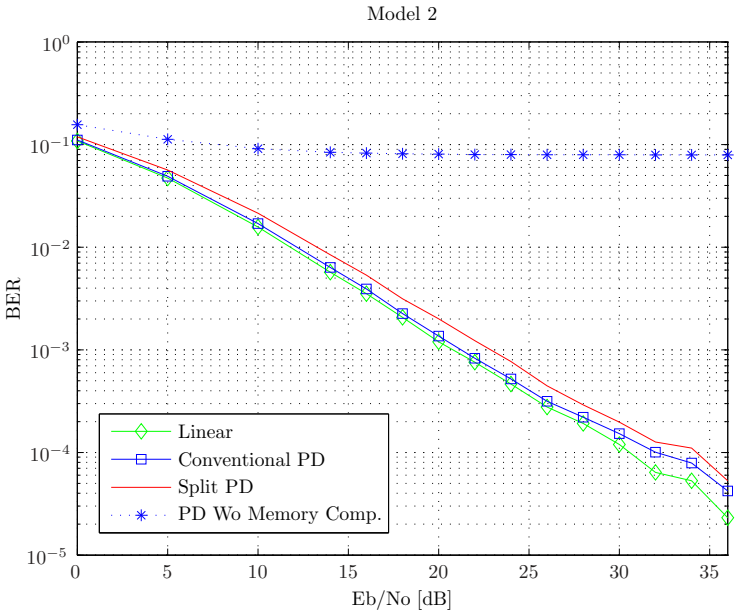

Figure 4.12: BER versus E_b/N_o of an OFDM system with 16-QAM modulation, for split predistortion (SPD), conventional PD with nonlinear PA (model 2 in Table 4.3), and memoryless PD.

Chapter 5

Power amplifier distortion compensation at the receiver

The removal of the PA nonlinear distortion at the transmitter is often preferred to avoid the problems due to the wireless channel that introduces additional memory and has time-variant characteristics [196]. On the other hand, transmitter compensation techniques, like predistorters and PAPR reduction, may render the implementation too complex in small handsets (cellular telephony) or subscriber units (WLAN and WiMAX). This chapter reviews distortion compensation techniques suitable for implementation at the receiver. Finally, the author's contributions are reviewed.

5.1 Introduction

Nonlinear PA distortion compensation at the receiver enables a reduced transmitter complexity when compared with a transmitter compensation solution. Instead, the demanding processing is moved to the receiver. The choice between a receiver or a transmitter implementation depends on system complexity that can be supported. Receiver compensation techniques can be justified at base stations where higher computational complexity, power consumption, and implementation cost are allowed while the mobile transceivers are preferred to be kept simple and power efficient.

As an important note, it is worth mentioning that receiver compensation techniques can only mitigate the effects of in-band distortion. Therefore, the power amplifier operation point needs to be set in a region such that the spectral regrowth, which creates interference on neighboring users satisfies the spectral mask requirement set by the standards.

Receiver compensation techniques include postdistortion methods [1]

[1] In this thesis the term postdistorter refers to the compensation technique implemented after the nonlinearity in the receiver side in contrast with some publications where this term is used for the element placed after the nonlinearity in the transmitter [212–214]

[32,215–217], nonlinear equalization [218–220], and iterative detection methods [33, 34, 221–223]. The first two approaches were developed for single-carriers systems. Iterative detection methods are more recent and have been developed for OFDM systems.

A postdistorter generates a nonlinear distortion signal based on the received signal and is used for cancelling the IMPs in the received signal.

Nonlinear equalization using Volterra series to remove the nonlinear distortion in voiceband data transmission is proposed in [218]. A Volterra equalizer applied in satellite channels is addressed in [219], where the identified channel impulse response is used to reproduce the ISI term and cancel it from the demodulated signal. Later on, the same authors developed an adaptive cancellation of nonlinear ISI in voiceband systems employing a decision feedback equalizer [220]. For an interesting analysis of the performance of predistortion, equalization and ISI cancellation techniques in a transmitter employing a nonlinear PA, see [224].

The development of receiver cancellation techniques for removing nonlinear distortion in multicarrier systems was initiated in the 90's. These techniques mitigate the effects of the clipping operation and are based on iterative detection of the original signal to reconstruct the clipping noise [33,34,221–223]. With the objective of removing nonlinear distortion arising from practical PAs, e.g., SSPA and TWTA, a sub-optimal iterative receiver for distorted OFDM signals was introduced in [225].

Clipping noise cancellation techniques are applied in the receiver to reduce the in-band distortion created by the clipping operation, applied to reduce the PAPR of the time domain OFDM signal [130], performed in the transmitter.

Section 5.2 provides an introduction to the most relevant iterative techniques proposed in the literature. The concept of iterative detection is then extended to a multiuser SDMA-OFDM system in publications P3 and P5 of this thesis. Important practical issues like channel estimation and PA modelling errors are dealt with in publication P4. The extension to broadband PAs is considered in publication P8, where also an adaptive PA parameter estimation is performed at the receiver.

An overview of the contributions of this thesis related to publications P3-P5 and P8 are provided in Section 5.3.

5.2 Detection of clipped OFDM signals

In the following, we briefly describe the iterative detection techniques for clipped OFDM signal presented in [33,34]. A different approach that reconstruct the clipped symbols by using oversampling proposed in [226] is also described.

5.2.1 Decision-aided reconstruction of clipped signals

The first approach to the reconstruction of clipped OFDM signals is the decision-aided reconstruction (DAR) technique proposed in [33].

Considering a soft limiter PA, the signal after clipping operation $x_g(n)$, can be written as

$$x_g(n) = \begin{cases} x(n), & |x(n)| < A_s \\ A_s, & |x(n)| > A_s \end{cases} \tag{5.1}$$

where $x(n)$ is the undistorted time domain input sequence and A_s is the output saturation voltage (clipping level) of the PA.

The clipped signal is transmitted through the channel and after the DFT operation, the received signal in frequency domain is given by

$$\mathcal{Y}(n,k) = \mathcal{H}(n,k)K_L\mathcal{X}(n,k) + \mathcal{U}(n,k) \tag{5.2}$$

where $\mathcal{H}(n,k)$ is the complex channel gain at subcarrier k, $\mathcal{U}(n,k) = \mathcal{H}(n,k)\mathcal{D}(n,k) + \mathcal{N}(n,k)$ is an additive distortion term that includes the clipping noise and the AWGN channel noise, and K_L is the gain factor. For large clipping levels $K_L = 1$ and is, therefore, not included in the reconstruction algorithm summarized below:

Step 1: The soft estimate of the clipped transmitted signal is obtained as $\hat{\mathcal{X}}_g(n,k) = \frac{\mathcal{Y}(n,k)}{\mathcal{H}(n,k)}$ for $k = 0, \cdots, N-1$.

Step 2: For iteration m, the symbol decisions $\hat{\mathcal{X}}^{(m)}(n,k)$ are found according to

$$\hat{\mathcal{X}}^{(m)}(n,k) = \arg\min_{\mathcal{X}} \left| \mathcal{Y}^{(m)}(n,k) - \mathcal{H}(n,k)\mathcal{X} \right|, \ 0 \le k \le N-1 \tag{5.3}$$

where m represents the iteration number and $\hat{\mathcal{Y}}^{(0)}(n,k) = \mathcal{Y}(n,k)$.

Step 3: The soft estimates $\{\hat{\mathcal{X}}_g(n,k)\}_{k=0}^{N-1}$ in Step 1 and symbol decisions $\{\hat{\mathcal{X}}^{(m)}(n,k)\}_{k=0}^{N-1}$ are converted to their corresponding time domain sequences $\{\hat{x}_g(n,i)\}_{i=0}^{N-1}$ and $\{\hat{x}^{(m)}(n,i)\}_{i=0}^{N-1}$ using the IDFT. Clipped samples are detected and a new sequence is generated $\{\tilde{x}_g^{(m)}(n,i)\}_{i=0}^{N-1}$ according to

$$\tilde{x}_g^{(m)}(n,i) = \begin{cases} \hat{x}_g(n,i), & |\hat{x}^{(m)}(n,i)| \le A_s \\ \hat{x}^{(m)}(n,i), & |\hat{x}^{(m)}(n,i)| > A_s \end{cases} \tag{5.4}$$

for $0 \le i \le N-1$.

Step 4: The sequence $\{\tilde{x}_g^{(m)}(n,i)\}_{i=0}^{N-1}$ is converted back to frequency domain obtaining $\{\tilde{\mathcal{X}}_g^{(m)}(n,k)\}_{i=0}^{N-1}$.

Step 5: The index number is increased $m = m + 1$ and $\boldsymbol{y}^{(m)}(n,k)$ is determined by

$$\boldsymbol{y}^{(m)}(n,k) = \boldsymbol{h}(n,k)\tilde{\boldsymbol{\chi}}_g^{(m-1)}(n,k) \tag{5.5}$$

Step 6: Go to Step 2 to refine the symbol estimates.

The DAR technique in [33] was evaluated for a fixed channel and showed good performance for clipping levels larger than 4 dB for the case of 16-QAM modulation. For the case of lower clipping levels, the decision errors degrade the performance. This is a problem associated with most decision-based techniques. The DAR performance in a static channel including the effects of channel estimation errors was also evaluated in [33]. A single chirp sequence with unitary PAPR [227] was used to estimate the static channel.

5.2.2 Iterative clipping noise estimation

If the clipping noise is generated by a known process, it can be regenerated in the receiver and thereafter removed [34]. Assuming a soft limiter PA as in Eq. (5.1), the clipped signal can be modelled as an undistorted attenuated component $K_L\,\mathbf{x}(n)$ plus a distortion noise $\mathbf{d}(n)$

$$\mathbf{x}_g(n) = K_L\,\mathbf{x}(n) + \mathbf{d}(n) \tag{5.6}$$

The received signal in frequency domain can be expressed as

$$\boldsymbol{y}(n,k) = \boldsymbol{h}(n,k)\left[K_L\boldsymbol{\chi}(n,k) + \boldsymbol{d}(n,k)\right] + \boldsymbol{n}(n,k) \tag{5.7}$$

where, as before, $\boldsymbol{h}(n,k)$ is the complex channel gain at subcarrier k and $\boldsymbol{n}(n,k)$ is AWGN noise.

If the receiver knows the clipping level A_s, and assuming a perfect channel knowledge, the clipping noise $\boldsymbol{d}(n,k)$ can be estimated and then canceled from the received signal in Eq. (5.7).

The iterative cancellation process can be summarized as:

Step 1: Using the channel observations $\{\boldsymbol{y}(n,k)\}_{k=0}^{N-1}$, the transmitted symbols are decoded and detected $\{\hat{\boldsymbol{\chi}}(n,k)\}_{k=0}^{N-1}$.

Step 2: The decoded sequence $\{\hat{\boldsymbol{\chi}}(n,k)\}_{k=0}^{N-1}$ is converted to the corresponding time domain sequence $\{\hat{x}(n,i)\}_{i=0}^{N-1}$. The clipped time-domain sequence $\{\hat{x}_g(n,i)\}_{i=0}^{N-1}$ is regenerated by using Eq. (5.1) and converted to frequency-domain obtaining $\{\hat{\boldsymbol{\chi}}_g(n,k)\}_{k=0}^{N-1}$. The attenuated frequency domain symbols $K_L\{\hat{\boldsymbol{\chi}}(n,k)\}_{k=0}^{N-1}$ are also regenerated.

Assuming that K_L is known, the clipping noise can be estimated as

$$\hat{\boldsymbol{d}}(n,k) = \hat{\boldsymbol{\chi}}_g(n,k) - K_L\hat{\boldsymbol{\chi}}(n,k),\ 0 \le k \le N-1 \tag{5.8}$$

Step 3: The estimated clipping noise is subtracted from the received signal, obtaining a refined channel observation

$$\hat{\boldsymbol{y}}(n,k) = \boldsymbol{y}(n,k) - \boldsymbol{h}(n,k)\hat{\boldsymbol{d}}(n,k) \tag{5.9}$$

Step 4: Go to Step 1 and obtain the new symbol estimate with the refined channel observation $\hat{\boldsymbol{y}}(n,k)$

The proposed method estimates and cancels the clipping noise instead of restoring the clipped signal to its unclipped form that is more sensitive to decision errors as done in [33]. The robustness of the technique with respect to channel estimation errors was not addressed. The original technique proposed includes oversampling and implement a clipping-filtering technique to cope with the out-of-band distortion [34, 228].

The previous technique was developed for removing the distortion from soft limiter PA models (i.e., clipping noise). The case of real amplifiers, as memoryless SSPA, were considered in [221, 225]. More details related to the cancellation of nonlinear distortion and practical issues, as channel estimation and PA model estimation, can be found in Section 5.3.

5.2.3 Clipping noise cancellation using oversampling

It is well known that as long as the average sampling rate of a signal is above the Nyquist rate, lost samples can be recovered based on the other samples [229]. Based on this idea, a reconstruction of the clipped samples (lost samples) in an oversampled system was proposed in [226].

The system performance is improved using this method in terms of BER. However, the proposed technique requires a bandwidth expansion between 25% to 100%. Another problem is that the use of oversampling in the transmitter increases the adjacent channel interference reducing the effective SNR due to the adjacent users.

Moreover, instability problems are reported when the number of clipping events is increased (i.e., low clipping levels).

5.3 Contributions

There are two different situations where receiver compensation techniques are applied: 1) to remove the nonlinear distortion induced by deliberate clipping that is applied to reduce the dynamic range of the PA, and 2) to remove the nonlinear distortion created by the nonlinear transfer function of the PA without the implementation of deliberate clipping. In the first case, only the knowledge of the clipping level is required for the implementation of the compensation technique [33, 34]. Publication [P5] assumes that the nonlinear distortion is created by the nonlinear PA itself. In this case,

the compensation technique requires knowledge of the PA parameters, e.g., polynomial coefficients when a polynomial is employed to model the PA response.

In the next subsection, the contributions of this thesis to receiver side cancellation techniques are briefly described. In the first part, the extension of iterative detection techniques to multiuser case presented in P3 and P5 is presented. This work also includes the derivation of channel estimation method for systems affected by nonlinear distortion addressed in publication P4. Finally, the application of the cancellation technique to broadband PAs and adaptive estimation of the PA parameters presented in [P8] is reviewed.

5.3.1 Power amplifier nonlinearities cancellation (PANC) for SDMA-OFDM systems

In this work a combination of multiuser detection and clipping noise mitigation techniques is proposed. We consider an SDMA-OFDM system with N subcarriers, a base station with P antennas and L mobile users with a single transmit antenna, as depicted in Figure 5.1.

Under the assumption that the power amplifier is operating in a bias region where several clipping events occur during an OFDM symbol, the output of the power amplifier can be modelled as a scaled version of the input signal plus an additive distortion term, as was discussed in Chapter 3, Section 3.2.

Including this additive distortion term into the signal model in Eq. (2.13), the received signal on subcarrier k can now be written as

$$\boldsymbol{y}(n,k) = \boldsymbol{\mathcal{H}}(n,k)[K_L\boldsymbol{\chi}(n,k) + \boldsymbol{d}(n,k)] + \boldsymbol{n}(n,k) \tag{5.10}$$

where, as before, $\boldsymbol{y}(n,k) = [y_1(n,k),\ldots,y_P(n,k)]^{\mathrm{T}}$ denote the vector of received signals, $\boldsymbol{\chi}(n,k) = [\chi_1(n,k),\ldots,\chi_L(n,k)]^{\mathrm{T}}$ is the vector containing transmitted signals from each user, $\boldsymbol{n}(n,k) \in \mathbb{C}^{P\times 1}$ is the additive noise assumed to be circular complex Gaussian with $E[\boldsymbol{n}(n,k)\boldsymbol{n}^{\mathrm{H}}(n,k)] = \sigma_n^2\mathbf{I}$, and $\boldsymbol{\mathcal{H}}(n,k) \in \mathbb{C}^{P\times L}$ is the channel transfer matrix given by Eq. (2.14). The new term $\boldsymbol{d}(n,k) = [d_1(n,k)\ \cdots\ , d_L(n,k)]^{\mathrm{T}}$ (compared with Eq. (2.13)) is the vector containing the nonlinear distortion of each user.

The idea of the power amplifier nonlinearities cancellation (PANC) technique is to employ a model of the transmitter nonlinearity $g(\cdot)$ to estimate the nonlinear distortion term $\hat{\boldsymbol{d}}(n,k)$ from the estimated symbols $\{\hat{\boldsymbol{\chi}}(n,k)\}_{k=0}^{N-1}$. The estimated distortion vector is then removed from the original received vector, such that a new refined estimate of $\boldsymbol{\chi}(n,k)$ can be obtained. This process can be performed iteratively until some predefined bound is reached.

The PANC technique is applied after the LS receiver independently for each user using its own PA parameters. In this analysis, K_L is assumed as

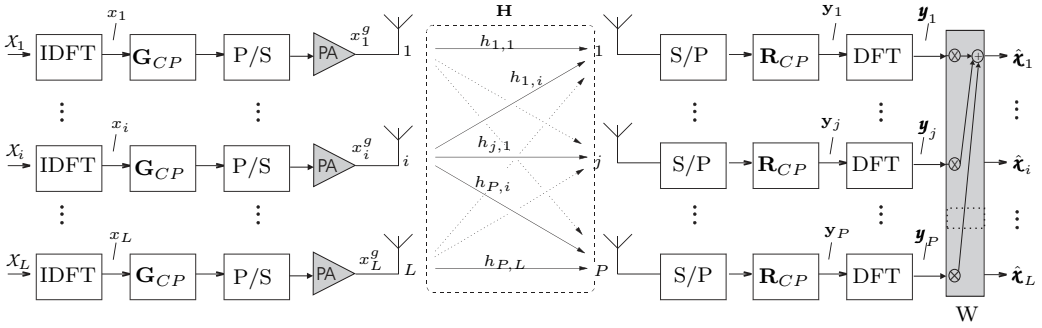

Figure 5.1: Block diagram of an SDMA-OFDM system consisting of one base station equipped with P antennas and L mobile users each with a single antenna element.

a scalar constant to simplify the notation. The PANC algorithm is carried out for each user and can be summarized in three steps:

Step 1: Multiuser detection

Employing the LS detector, defined in Eq. (2.16), the estimation of the jth user signal is given by

$$\begin{aligned}\hat{\boldsymbol{\chi}}_j^{(m)}(n,k) &= \frac{1}{K_L}\left[\boldsymbol{\mathcal{H}}(n,k)\mathrm{col}_j\left\{\left[\boldsymbol{\mathcal{H}}(n,k)^{\mathrm{H}}\boldsymbol{\mathcal{H}}(n,k)\right]^{-1}\right\}\right]^{\mathrm{H}}\boldsymbol{y}(n,k) \\ &- K_L\hat{\boldsymbol{d}}_j^{(m)}(n,k) \end{aligned} \tag{5.11}$$

where $\mathrm{col}_j\{\cdot\}$ denotes the jth column vector of the corresponding matrix. For initialization, we set $\hat{\boldsymbol{d}}_j^{(0)}(n,k) = 0$.

Step 2: Demodulation

Using $\hat{\boldsymbol{\chi}}_j^{(m)}(n) = [\hat{\chi}_j^{(m)}(n,0), \hat{\chi}_j^{(m)}(n,1), \ldots, \hat{\chi}_j^{(m)}(n,N-1)]^T$, an estimate $\boldsymbol{z}_j^{(m)}(n) = [z_j^{(m)}(n,0), z_j^{(m)}(n,1), \ldots, z_j^{(m)}(n,N-1)]^T$ of the original transmitted constellation $\boldsymbol{\chi}_j(n)$ is obtained by applying hard decoding (or more efficient methods if coding is employed). The detection operation can be represented as

$$z_j^{(m)}(n,k) = \left\langle \hat{\chi}_j(n,k) - \hat{d}_j^{(m)}(n,k) \right\rangle \tag{5.12}$$

where $\langle\ ,\rangle$ denotes the symbol decision process in which the decoder chooses the value of $z_j^{(m)}(n,k)$ that is closest in Euclidean distance to $\hat{\chi}_j(n,k)$.

This process is carried out for all active carriers. Using the recovered symbols, the time domain signal of each user is reproduced via IDFT as $\hat{\mathbf{x}}_j^{(m)}(n) = \mathbf{Q}_N \boldsymbol{z}_j^{(m)}(n)$.

Step 3: Distortion removal

If the nonlinear model of the PA, $g[\cdot]$, is known at the receiver, the distortion in time domain can be estimated as

$$\hat{\mathbf{d}}_j(n) = g[\hat{\mathbf{x}}_j^{(m)}(n)] - K_L \hat{\mathbf{x}}_j^{(m)}(n) \tag{5.13}$$

The frequency-domain distortion term is obtained by applying the DFT operator

$$\hat{\boldsymbol{d}}_j^{(m)}(n) = \mathbf{Q}_N^{\mathrm{H}} \left\{ g[\hat{\mathbf{x}}_j^{(m)}(n)] - K_L \hat{\mathbf{x}}_j^{(m)}(n) \right\} \tag{5.14}$$

The distortion $\hat{\boldsymbol{d}}_j^{(m)}(n) = [\hat{d}_j^{(m)}(n,0) \ \cdots, \ \hat{d}_j^{(m)}(n,N-1)]^{\mathrm{T}}$ is then subtracted from the estimated signal $\hat{\boldsymbol{\chi}}_j^{(m)}(n) = [\hat{\chi}_j^{(m)}(n,0) \ \cdots, \ \hat{\chi}_j^{(m)}(n,N-1)]^{\mathrm{T}}$ (in step 1). Using this result, the transmitted constellation is re-estimated in a new decoding/distortion cancellation step.

Simulation results suggest that two or three iteration are sufficient.

In the previous description of the PANC technique, the channel has been assumed known in the receiver. In practice, the channel needs to be estimated. The employed channel estimation scheme will play an important role because estimation errors will degrade user separation and as a consequence affect the performance of nonlinear distortion cancellation. It is, therefore, important to provide accurate channel estimates. On the other hand, the estimation quality is strongly related to the number of dedicated pilots. If only FD channel estimation is used (i.e., pilot carriers), a significant number of pilot tones are required which reduces the effective data rate of the system. Therefore, to enable a practical pilot overhead we consider a channel estimation approach in publication P4 that combines frequency-domain (FD) estimation with time-domain (TD) estimation. The basic idea is to use the equalized signal obtained by using an initial frequency-domain channel estimate to remove the multiuser interference and the nonlinear distortion, and improve the channel estimate in time domain (TD). A block diagram that illustrates the combination of the channel estimation method and PANC is shown in Figure 5.2.

The performance of PANC was evaluated for stationary and time-varying channels. Simulation parameters are summarized in Table 5.1.

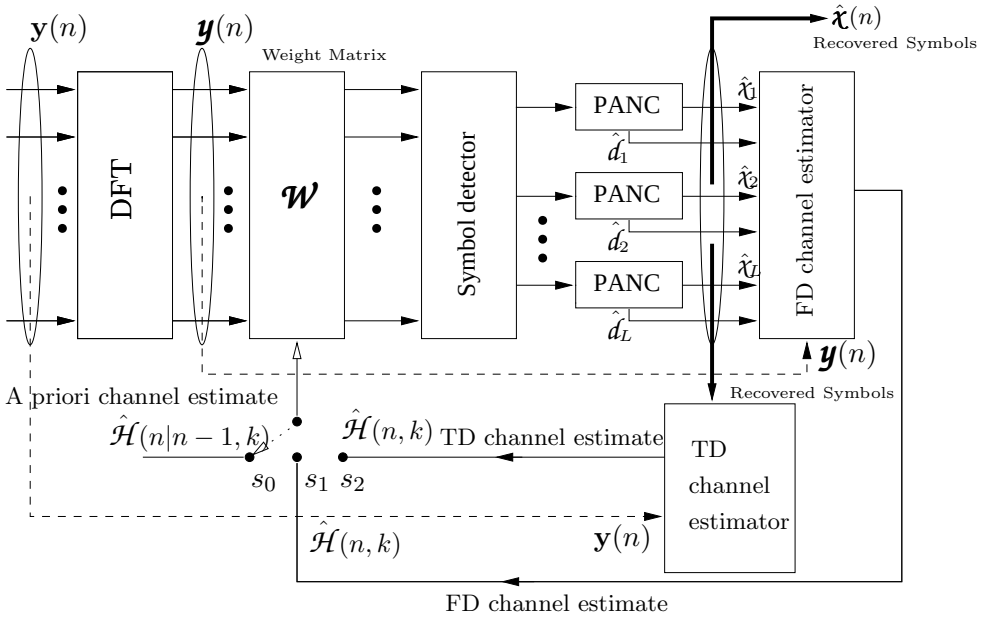

Figure 5.2: Channel estimation with PANC. s_0: Transmitted symbols are recovered using the previous channel estimate, s_1: Transmitted symbols are recovered using the new FD channel estimate obtained after nonlinear distortion cancellation (after PANC), s_2: Transmitted symbols are recovered with a refined TD channel estimate.

Figure 5.3 and 5.4 present a family of BER curves for an SDMA-OFDM system affected by nonlinear distortion assuming perfect channel information (CSI) and using FD-TD channel estimation technique. This curves are obtained using an stationary and a time-varying channels respectively with $L = 2$ active users and $P = 4$ receive antennas and assuming that the PA model is known at the receiver. Figure 5.4 also includes BER curves considering that the PA model is estimated using a 7-th order polynomial. The combination of a memoryless PD with PANC is also evaluated. These BER curves show that PANC is robust to PA modelling errors and channel estimation errors. The combination of PANC with PD do not present an improvement in the BER. However, this combination can be an interesting option because the PD provides a reduction of the out-of-band distortion and PANC reduces the BER.

5.3.2 Power amplifier nonlinearities cancellation (PANC) technique with adaptive PA model estimation

The PANC technique and its predecessors [33] and [34] require the knowledge of the PA model parameters in the receiver. The transmission of PA

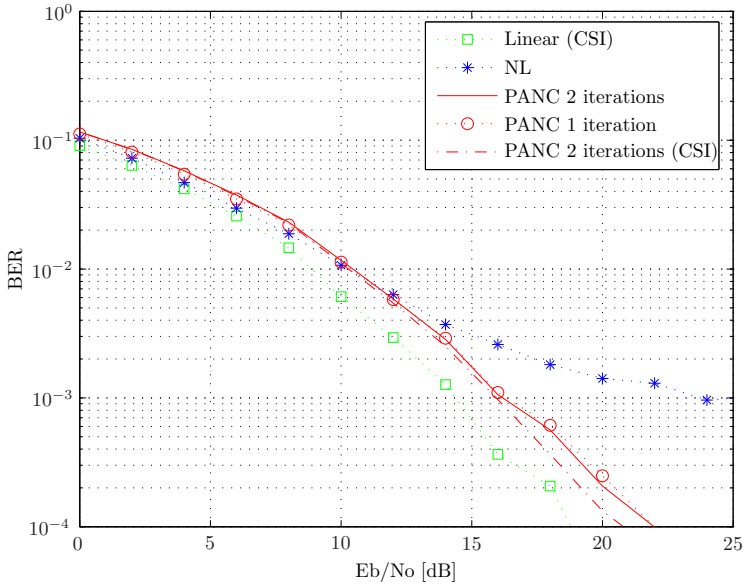

Figure 5.3: BER versus E_b/N_o of a $P \times L$ SDMA-OFDM system $P = 4$ and $L = 2$ with 16-QAM modulation, for PANC with FD-TD channel estimation ($T = 32$ subcarriers per user), stationary channel, and using perfect channel state information (CSI), and LS detector, SSPA PA model with clipping $\nu = 4$ dB. Results obtained with linear PA and nonlinear PA (NL) without PANC are included for reference.

Table 5.1: Simulation parameters used for generating Figures 5.3 and 5.4

System parameters	
Number of subcarriers	512
Cyclic prefix length	8
Modulation	16-QAM
Power amplifier	SSPA
Clipping level	4 dB
Carrier frequency	5 GHZ
Bandwidth	20 MHZ
Channel parameters	
Type	Typical Urban
Channel delay profile	[0,1,2,3] μs
Power loss taps	[0,-1,-3,-9] dB
Mobile speed	5 km/h, 30 km/h

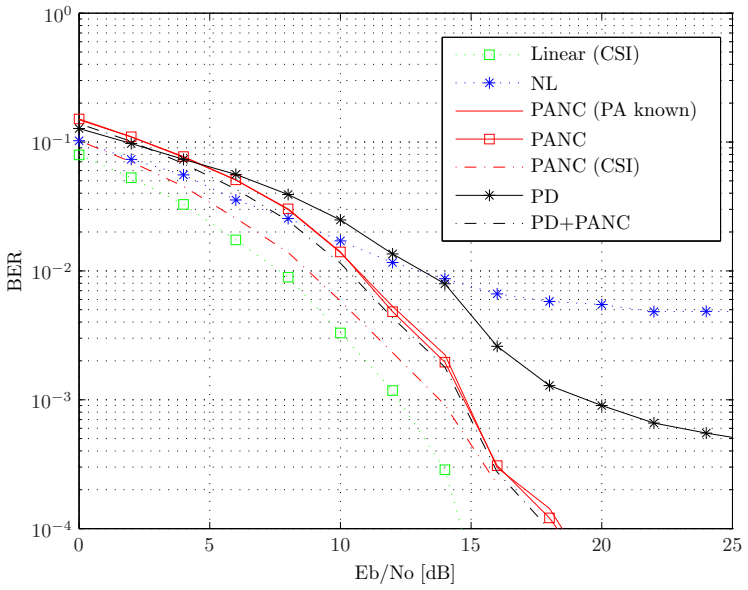

Figure 5.4: BER versus E_b/N_o of a $P \times L$ SDMA-OFDM system $P = 4$ and $L = 2$ with 16-QAM modulation, for PANC with FD-TD channel estimation ($T = 16$ subcarriers per user), time-varying channel, and using perfect channel state information (CSI), and LS detector, SSPA PA model with clipping $\nu = 4$ dB. Results using perfectly known PA model and estimated PA model using a 7-th order polynomial, and linear PA and nonlinear PA (NL) without PANC are included for reference.

parameters can be done in the initialization jointly with channel estimation and synchronization, see P5. In order to simplify the hardware required for the identification and tracking of the PA model in the transmitter unit, publication P8 proposes to move these tasks to the receiver. The new approach has several advantages:

- The computationally involved PA identification and tracking at the transmitter is avoided and the PA model estimation can be done fully in digital domain. In the case of PA identification at the transmitter, the input-output measurements required to estimate and track the PA model need a feedback loop from analog domain (PA output) to digital domain increasing the hardware complexity.

- The technique is applicable for the case of broadband PAs because the proposed PA model estimation approach takes into account the estimation and equalization of the effective time-varying channel (wireless channel plus PA memory).

The system under consideration is a single-user OFDM with N subcarriers where the PA is modelled with a Hammerstein structure, i.e., it is a cascade of a static nonlinearity block denoted by $g(\cdot)$ and a linear filter $\mathbf{c}(n)$, see Section 2.5.2.

Assuming that the cyclic prefix is chosen larger than the effective channel length, i.e., the convolution of the linear part $\mathbf{c}(n) \in \mathbb{C}^{N\times 1}$ of the Hammerstein model and the wireless channel $\mathbf{h}(n)$, the received signal at subcarrier k can be expressed as

$$\mathcal{Y}(n,k) = \mathcal{H}_{eff}(n,k)\left[K_L\mathcal{X}(n,k) + \mathcal{D}(n,k)\right] + \mathcal{N}(n,k) \tag{5.15}$$

where $\mathcal{N}(n,k)$ is the additive noise, assumed here to be circular complex Gaussian with variance σ_n^2, and $\mathcal{H}_{eff}(n,k) = \mathcal{C}(n,k)\mathcal{H}(n,k)$ is the effective channel.

Assuming perfect knowledge of the effective channel, the equalized frequency-domain signal is given by

$$\tilde{\mathcal{Y}}(n,k) = K_L\mathcal{X}(n,k) + \mathcal{D}(n,k) + \mathcal{N}(n,k)/\mathcal{H}_{eff}(n,k) \tag{5.16}$$

We see from Eq. (5.16) that the use of a nonlinear PA affects the detection process adding an additive term and scaling the original signal.

The PANC technique described in Section 5.3.1 can be directly applied to this case. However, the PANC technique requires the knowledge of the static nonlinearity $g[\cdot]$ and the effective channel $\mathcal{H}_{eff}(n,k)$. In P8 we show how to estimate the PA model and the channel in the receiver.

Step 1: Initial channel estimation

In the initialization step, two OFDM pilot symbols are transmitted. The first symbol has a low PAPR to enable accurate estimation of the effective channel $\mathcal{H}_{eff}(n,k)$ without the influence of the nonlinear static block $g[\cdot]$, i.e., we can assume $\mathcal{D}(n,k) = 0$ and $K_L = 1$.

The channel frequency response on the pilot subcarriers can now be obtained as

$$\hat{\mathcal{H}}_p(n,k) = \frac{\mathcal{Y}(n,k)}{\mathcal{X}(n,k)},\ \forall k \in \mathcal{T} \tag{5.17}$$

where $\mathcal{T} = \{k_1, \ldots, k_T\}$ denotes the index set specifying the T pilot carriers with $\{k_p\}_{p=1}^{T}$ taken from the set $\{1, \ldots, N\}$. The whole frequency domain channel response $\hat{\boldsymbol{\mathcal{H}}}_{eff}(n)$ is obtained through interpolation using truncated DFT matrices [210].

Step 2: Initial PA model estimation

A second OFDM pilot symbol designed to have a uniform amplitude distribution is exploited to estimate $g[\cdot]$. The PA modelled with a

P order polynomial whose coefficients $\mathbf{a}(n) = [a_1(n), \cdots, a_P(n)]^T$ can be estimated at the receiver using an LS estimator as

$$\hat{\mathbf{a}}(n) = \left[\mathbf{U}^{\mathrm{H}}(n)\mathbf{U}(n)\right]^{-1}\mathbf{U}^{\mathrm{H}}(n)\tilde{\mathbf{y}}(n) \tag{5.18}$$

where $\tilde{\mathbf{y}}(n)$ is the $N \times 1$ time-domain received signal after equalization (see Eq. (5.16)) that represents the output of the PA, and $\mathbf{U}(n)$ is an $N \times P$ *Vandermonde matrix* constructed with the N input vectors $\{\mathbf{u}(n,j)\}_{j=1}^{N}$ given by $\mathbf{u}(n,j) = \left[1\ |x(n,j)|\ |x(n,j)|^2\ \cdots\ |x(n,j)|^P\right]^{\mathrm{T}}$.

Step 3: PA model and channel tracking

During normal data transmission, the channel estimation needs to be carried out in the presence of nonlinear distortion. The channel estimation technique derived in P4 can be applied here. From Eq. (5.15), we see that during data transmission, the channel is estimated as

$$\hat{\mathcal{H}}_p(n,k) = \frac{\mathcal{Y}(n,k)}{\mathcal{X}(n,k) + \hat{\mathcal{D}}(n,k)},\ \forall k \in \mathcal{T} \tag{5.19}$$

where $\hat{\mathcal{D}}(n,k)$ is obtained from the output of the PANC detector.

The variations in the PA between consecutive OFDM symbols can be tracked by using a normalized least mean-square (NLMS) algorithm operating on the OFDM subsymbols, i.e., sample-by-sample processing.

The proposed technique presents promising results as is illustrated in Figure 5.5, where the BER curves are plotted for a PA modelled using a Hammerstein model. Simulations results have been obtained using the parameters summarized in Table 5.2

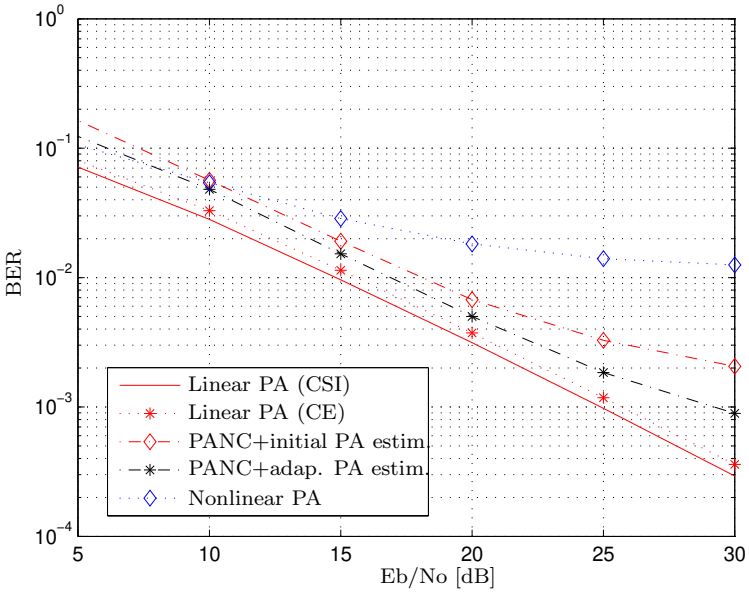

Figure 5.5: BER versus E_b/N_o for PANC with adaptive PA estimation and using initial PA model estimate (no tracking), FD channel estimator ($T = 32$ pilot subcarriers) and time-varying Hammerstein-type PA model. Linear PA with channel estimation (CE) and channel state information (CSI), and nonlinear PA without PANC are included for reference.

Table 5.2: Simulation parameters: PANC with adaptive PA model estimation

System parameters	
Number of subcarriers	512
Cyclic prefix length	16
Pilot carriers	32
Modulation	16-QAM
Power amplifier	SSPA with memory
Clipping level	4 dB
Carrier frequency	5 GHZ
Bandwidth	20 MHZ
Channel parameters	
Type	Typical Urban
Channel delay profile	[0,1,2,3] μ s
Power loss taps	[0,-1,-3,-9] dB
Mobile speed	2 km/h

Chapter 6

Conclusion

6.1 Summary

In order to exploit fully the benefits provided by OFDM, advanced signal processing techniques are required to cope with several practical issues, e.g., accurate channel estimation, compensation of power amplifier nonlinearities, I/Q mismatch, phase noise, and synchronization. At the same time, implementation complexity should remain low and the PA power efficiency needs to be maximized. The PA dominates the power consumption of the whole system. This means that the operating time in a terminal greatly depends on the efficiency of the PA. Base stations also require high power efficiency in order to achieve low power consumption and avoid problems of overheating.

The power efficiency of OFDM communication systems is limited by two key factors: the high PAPR levels of the OFDM signals (high amplitude fluctuations), and the nonlinearity of the PAs. The high dynamic range of the OFDM signal requires that the PAs are operated with high back-off to avoid nonlinear distortion. However, reducing the average operating power results in a poor power efficiency. Increasing the average operating power increases the power amplifier efficiency by allowing the PA to operate in its nonlinear region. The resulting nonlinear distortion degrades the system performance. This trade off between power efficiency and nonlinear distortion has been the main driver in the development of new signal processing techniques for reducing the PA induced nonlinear distortion.

This thesis analyzes the performance degradation due to nonlinear amplifiers in multicarrier systems, and proposes cost-effective solutions for the cancellation of nonlinear distortion effects.

The influence of nonlinear amplification in multi-antenna OFDM systems is studied when employing memoryless and broadband PAs. We derive closed-form expressions for bit error probability (BEP) and capacity for multi-antenna OFDM systems that employ nonlinear memoryless PAs. The

special case of SDMA-OFDM systems is studied but the results are readily extended to other OFDM systems with diversity. In the case of broadband systems, where memoryless PA models cannot be considered anymore, a closed-form BEP expression is derived for an OSTBC-OFDM system that includes the effects of nonlinear distortion and imperfect PA memory estimation. The results show that even for the case when the nonlinear distortion is removed, PA memory estimation errors increase substantially the BEP levels. That is, memory compensation is not a minor issue and must be solved in practical OFDM implementations.

The performance analyses carried out in this thesis motivate the implementation of nonlinearity compensation techniques to obtain tolerable levels of bit error rate (BER) and capacity. Several techniques have been proposed in this thesis including low PAPR OFDM implementations, receiver cancellation techniques implemented for memoryless and broadband PAs, transmitter compensation techniques and a hybrid solution that distributes the compensation tasks between the transmitter and the receiver.

Initially, we propose a transmitter technique suitable for a multiuser OFDM system where the subcarriers are distributed among the users to minimize the intermodulation distortion created by nonlinear PAs. The proposed intermodulation minimizing allocation technique (IMAT) assigns the subcarriers to each user such that the resulting second- and third-order intermodulation distortion that interfere with other users is minimized. IMAT reports good BER results and improvements in the PA power efficiency.

Thereafter, a novel receiver technique that is able to cancel the nonlinear PA distortion, referred to as power amplifier nonlinearities cancellation (PANC), is developed. The proposed technique combines multiuser detection and nonlinear distortion mitigation techniques. When applied in an SDMA-OFDM system, the PANC technique reduces drastically the effects of the nonlinear amplification and improves the power efficiency. Its robustness in a realistic scenario, which includes channel estimation and PA modelling errors, was evaluated showing excellent results. The challenging scenario of time-varying (and frequency selective) channels that need to be tracked during transmission is addressed. The channel estimation scheme needs to be carefully designed because estimation errors will degrade user separation and affect the nonlinear distortion cancellation performance. On the other hand, the estimation quality is strongly related to the number of dedicated pilots symbols. A combined frequency-domain and time-domain channel estimation strategy that incorporates the distortion estimates from PANC into the estimation procedure is proposed. The combined channel estimation and PANC approach enables a practical pilot overhead and is not affected by the nonlinear distortion.

PANC is an attractive technique for uplink transmission because the computationally intensive tasks are implemented in the receiver (base station) where more resources are available. The PANC technique requires a

model of the PA to be known at the receiver. Initially we considered the more simple case where the PA model is estimated in the transmitter and sent to the receiver during initialization. We then consider the more practical approach to estimate and track the PA parameters in the receiver. The modified technique also considers the case of broadband PA.

Finally, a split predistorter (SPD) structure is introduced to cope with nonlinear distortion from a broadband PA. The goal is to alleviate the high complexity related with the conventional predistorter design. The SPD method avoids PA memory estimation at the transmitter enabling a reduced complexity broadband PA distortion compensation. The idea of the SPD is to distribute the predistorter tasks such that the transmitter compensates for the static nonlinearity using a low complexity PD, and the receiver identifies and compensates the PA memory jointly with the wireless channel.

The techniques presented in this thesis to compensate the harmful effects of nonlinear PAs can be implemented together with other techniques like PAPR reduction or linearization techniques to get even higher power efficiency maintaining a reduced performance degradation.

6.2 Future work

Possible topics of future research include

- The problem of PA model estimation at the receiver for more general broadband models like Wiener-Hammerstein and generalized polynomial models. This topic is at present time under research with the objective to provide a general cancellation technique that covers the different PAs used in real-world communication systems.

- Theoretical derivation of BEP after PANC. PANC is based on a decision-feedback structure, and its performance depends on the accuracy of the initial estimation and the number of detected errors. As a consequence, the theoretical analysis of the performance of PANC is not trivial. However, it will be very useful for predicting when the iterative technique can be applied with good results.

- The evaluation of the proposed compensation techniques using real-world signals (measurements).

- Compensation of carrier frequency offset in an OFDM system affected by other RF impairments.

- Optimization of the developed compensation techniques to be implemented in Digital Signal Processors (DSP), Field Programmable Gate Array (FPGA) or Application Specific Integrated Circuits (ASIC) are other open issues to be explored in real-world systems.

Bibliography

[1] IEEE, *Wireless LAN Medium Access control (MAC) and physical layer (PHY) specifications: High Speed Physical Layer in the 5 Ghz Band*, IEEE Std 802.11a-1999.

[2] IEEE, *Wireless LAN Medium Access Control (MAC) and Physical Layer (PHY) specifications. Further Higher-Speed Physical Layer Extension in the 2.4GHz Band*, IEEE Std 802.11g-2003.

[3] ETSI, *Broadband radio access networks (BRAN); HIPERLAN type 2; Physical (PHY) layer*, TS 101 475 V1.1.1, 2000-2004.

[4] ETSI, *Radio Broadcasting Systems; Digital Audio Broadcasting (DAB) to mobile, portable and fixed receivers*, EN 300 401 V1.3.3, May 2001.

[5] ETSI, *Digital Video Broadcasting (DVB); framing structure, channel coding and modulation for digital terrestrial television*, EN 300 744 V1.5.1, Nov. 2004.

[6] ITU, *Asymmetrical Digital Subscriber Line (ADSL) Transceivers: Transmission media and System*, G.992.1, July 1998.

[7] ECMA, "High rate ultra wideband PHY and MAC standard, standard ECMA-368 , Geneva 1st edition," Dec. 2005.

[8] A. Batra, J. Balakrishnan, G. R. Aiello, J. R. Foerster, and A. Dabak, "Design of a multiband OFDM system for realistic UWB channel environments," *IEEE Trans. Microw. Theory Tech.*, vol. 52, no. 9, pp. 2123 – 2138, Sept. 2004.

[9] L. Yang and G. B. Giannakis, "Ultra-wideband communications: An idea whose time has come," *IEEE Signal Process. Mag.*, vol. 21, no. 6, pp. 26 – 54, Nov. 2004.

[10] L. Hanzo, W. Webb, and T. Keller, *Single- and Multi-carrier Quadrature Amplitude Modulation*, John Wiley Sons, LTD, 2000.

[11] R. D. van Nee and R. Prasad, *OFDM for Wireless Multimedia Communications*, Artech House, 2000.

[12] T. Keller and L. Hanzo, "Adaptive multicarrier modulation: A convenient framework for time-frequency processing in wireless communications," *Proc. IEEE*, vol. 88, no. 5, pp. 611 – 640, May 2000.

[13] P. Chow, J. Cioffi, and J. Bingham, "A practical discrete multitone transceiver loading algorithm for data transmission over spectrally shaped channels," *IEEE Trans. Commun.*, vol. 43, no. 2, pp. 772 – 775, Feb. - Apr. 1995.

[14] J. Louveaux, L. Vandendorpe, and T. Sartenaer, "Cyclic prefixed single carrier and multicarrier transmission: bit rate comparison," *IEEE Commun. Lett.*, vol. 3, no. 4, pp. 180 – 182, Apr. 2003.

[15] F. R. Micolau, *Feedback-Channel and adaptative MIMO coded-modulations*, Ph.D. thesis, Universitat Politecnica de Catalunya, Barcelona, Spain, Nov. 2005.

[16] J. Heiskala and J. Terry, *OFDM Wireless LANs: A Theoretical and Practical Guide*, Sams Publishing, 2002.

[17] H. Sampath, S. Talwar, J. Tellado, V. Erceg, and A. Paulraj, "A fourth generation of MIMO-OFDM broadband wireless system: Design, performance and field trail results," *IEEE Commun. Mag.*, vol. 40, no. 9, pp. 141 – 149, Sept. 2002.

[18] H. Ekstrom, A. Furuskar, J. Karlsson, M. Meyer, S. Parkvall, J. Torsner, and M. Wahlqvist, "Technical solutions for the 3G Long-Term Evolution," *IEEE Commun. Mag.*, vol. 44, no. 3, pp. 141 – 149, Mar. 2006.

[19] Y. Li, J. H. Winters, and N. R. Sollenberger, "MIMO-OFDM for wireless communications: Signal detection with enhanced channel estimation," *IEEE Trans. Commun.*, vol. 50, no. 9, pp. 1471 – 1477, Sept. 2002.

[20] A. Paulraj, D. Gore, R. Nabar, and H. Bolscskei, "An overview of MIMO communications - a key to gigabit wireless," *Proc. IEEE*, vol. 92, no. 2, pp. 198 – 218, Feb. 2004.

[21] G. Stuber, J. Barry, S. McLaughlin, Y. Li, M. Ingram, and T. Pratt, "Broadband MIMO-OFDM wireless communications," *Proc. IEEE*, vol. 92, no. 2, pp. 271–294, Feb. 2004.

[22] P. Vandenameele, *Space division multiple access for wireless local area networks*, Kluwer, 2001.

[23] C. Y. Zhang, "An efficient resource allocation scheme for spatial multiuser access in MIMO-OFDM systems," *IEEE Trans. Commun.*, vol. 53, no. 1, pp. 107 – 116, Jan. 2005.

[24] H. Bolcskei, "Dynamic multiuser resource allocation and adaptation for wireless systems," *IEEE Trans. Wireless Commun.*, vol. 13, no. 4, pp. 38–47, Aug. 2006.

[25] P. Arun, R. Venkatesh, S. Karthikeyan, and S. Srikanth, "Multiple access schemes for OFDM based indoor wireless systems," in *Proc. 8th National Conference on Communications*, Jan. 2002, pp. 488–492, Mumbai, India.

[26] D. Wulich, "Definition of efficient PAPR in OFDM," *IEEE Commun. Lett.*, vol. 9, no. 9, pp. 832 – 834, Sept. 2005.

[27] S. H. Han and J. H. Lee, "An overview of peak-to-average power ratio reduction techniques for multicarrier transmission," *IEEE Trans. Wireless Commun.*, vol. 12, no. 2, pp. 56–65, Apr. 2005.

[28] P. B. Kenington, "Linearized transmitters: an enabling technology for software defined radio," *IEEE Commun. Mag.*, vol. 40, no. 2, pp. 156 – 162, Feb. 2002.

[29] P. Kenington, *High-Linearity RF amplifier Design*, Artech House, 2000.

[30] S. Cripps, *Advanced techniques in RF power amplifiers design*, Artech, 2002.

[31] A. Katz, "Linearization: reducing distortion in power amplifiers," *IEEE Microw. Mag.*, vol. 2, no. 4, pp. 37–49, Dec. 2001.

[32] L. D. Quach and S. Stapleton, "A postdistortion receiver for mobile communications," *IEEE Trans. Veh. Technol.*, vol. 42, no. 4, pp. 604 – 616, Nov. 1993.

[33] D. Kim and G. L. Stuber, "Clipping noise mitigation for OFDM by decision-aided reconstruction," *IEEE Commun. Lett.*, vol. 3, no. 1, pp. 4 – 6, Jan. 1999.

[34] H. Chen and A. Haimovich, "Iterative estimation and cancellation of clipping noise for OFDM signals," *IEEE Commun. Lett.*, vol. 7, no. 7, pp. 305 – 307, July 2003.

[35] L. Hanzo, M. Munster, B. J. Choi, and T. Keller, *OFDM and MC-CDMA for broadband multi-user communication , WLANs and broadcasting*, Wiley, 2003.

[36] D. Dardari, "Ordered subcarrier selection algorithm for OFDM-based high-speed WLANs," *IEEE Trans. Wireless Commun.*, vol. 3, no. 5, pp. 1452 – 1458, Sept. 2004.

[37] A. Armada, "A simple multiuser bit loading algorithm for multicarrier WLAN," in *Proc. IEEE International Conference on Communications, ICC'01*, June 2001, vol. 4, pp. 1168 – 1171, Helsinki, Finland.

[38] L. Cimini, "Analysis and simulation of a digital mobile channel using orthogonal frequency division multiplexing," *IEEE Trans. Commun.*, vol. 33, no. 7, pp. 665–675, July 1985.

[39] S. B. Weinstein and P. M. Ebert, "Data transmission by frequency division multiplexing using the discrete Fourier transform," *IEEE Trans. Commun. Tech.*, vol. 19, no. 10, pp. 628–634, Oct. 1971.

[40] J. Binghman, "Multicarrier modulation for data transmission: An idea whose time has come," *IEEE Commun. Mag.*, vol. 28, no. 5, pp. 5–14, May 1990.

[41] A. Peled and A. Ruiz, "Frequency domain data transmission using reduced computational complexity algorithms," in *Proc. IEEE Int. Conf. Acoust. Speech, Signal Process., ICASSP'80*, Apr. 1980, pp. 964–967, Denver, USA.

[42] B. Hirosaki, "An orthogonally multiplexed QAM system using the discrete Fourier transform," *IEEE Trans. Commun.*, vol. 29, no. 7, pp. 983–989, July 1981.

[43] T. Starr, J. Cioffi, and P. Silverman, *Understanding Digital Subscriber Lines*, Prentice Hall, 1999.

[44] 3GPP, "Technical specification Group Radio Access Network. physical layer aspect for evolved UTRA," *3GPP TR 25.814, R7.*

[45] F. Ivanek, "Convergence and competition on the way toward 4G: Where are we going?," in *Proc. IEEE Radio and Wireless Symposium*, Jan. 2007, pp. 265 – 268, California, USA.

[46] "Mobile WiMAX - Part 1: A technical overview and performance evaluation," *WiMAX Forum*, Aug. 2006.

[47] J. Shapira and S. Miller, *CDMA Radio with Repeaters*, Springer, 2006.

[48] Z. Wang and G. Giannakis, "Wireless multicarrier communications," *IEEE Signal Process. Mag.*, vol. 17, no. 3, pp. 29 – 48, May 2000.

[49] B. Muquet, Z. Wang, G. Giannakis, M. de Courville, and P. Duhamel, "Cyclic prefixing or zero padding for wireless multicarrier transmissions?," *IEEE Trans. Commun.*, vol. 50, no. 12, pp. 2136 – 2148, Dec. 2002.

[50] A. Pandharipande, "Principles of OFDM," *IEEE Potentials*, vol. 21, no. 12, pp. 16 – 19, Apr.-May 2002.

[51] P. W. Wolniansky, G. J. Foschini, G. D. Golden, and R. A. Valenzuela, "V-BLAST : An architecture for realizing very high data rates over the rich-scattering wireless channel," in *Proc. URSI International Symposium on Signals, Systems and Electronics*, Jan. 1998, pp. 295 – 300, Pisa, France.

[52] G. D. Golden, G. J. Foschini, R. A. Valenzuela, and P. W. Wolniansky, "Detection algorithm and initial laboratory results using V-BLAST space-time communication architecture," *IEE Electronics Lett.*, vol. 35, no. 1, pp. 14 – 16, Jan. 1999.

[53] S. Thoen, L. Deneire, L. Van der Perre, M. Engels, and H. De Man, "Constrained least squares detector for OFDM/SDMA-based wireless networks," *IEEE Trans. Wireless Commun.*, vol. 2, no. 1, pp. 129 – 135, Jan. 2003.

[54] M. Jiang, S. X. Ng, and L. Hanzo, "Hybrid iterative multiuser detection for channel coded space division multiple access OFDM systems," *IEEE Trans. Vehic. Tech.*, vol. 55, no. 1, pp. 115 – 127, Jan. 2006.

[55] P. Vandenameele, L. Van Der Perre, M. Engels, B. Gyselinckx, and H. De Man, "A combined OFDM-SDMA approach," *IEEE J. Sel. Area Commun.*, vol. 18, no. 11, pp. 2312 – 2321, Nov. 2000.

[56] N. Dawod, I. Marsland, and R. Hafez, "Improved transmit steering for MIMO-OFDM downlinks with distributed base station antenna arrays," *IEEE J. Sel. Areas Commun.*, vol. 24, no. 3, pp. 419 – 426, Mar. 2006.

[57] Y. Wu, T. Cui, and C. Tellambura, "Optimal low-complexity detection for space division multiple access wireless systems," *IEEE Commun. Lett.*, vol. 10, no. 3, pp. 156 – 158, Mar. 2006.

[58] A. F. Molisch, M. Z. Win, and J. H. Winters, "Space-time-frequency (STF) coding for MIMO-OFDM systems," *IEEE Commun. Lett.*, vol. 6, no. 9, pp. 370 – 372, Sept. 2002.

[59] R. Blum, Y. G. Li, J. Winters, and Q. Yan, "Improved space-time coding for MIMO-OFDM wireless communications," *IEEE Trans. Commun.*, vol. 49, no. 11, pp. 1873 – 1878, Nov. 2001.

[60] A. Paulraj, R. Nabar, and D. Gore, *Introduction to Space-Time Wireless Communications*, Cambridge, University Press, UK, 2003.

[61] H. Bolcskei, "MIMO-OFDM wireless systems: basics, perspectives, and challenges," *IEEE Trans. Wireless Commun.*, vol. 13, no. 4, pp. 31–37, Aug. 2006.

[62] S. Verdu, *Multiuser Detection*, Cambridge University Press, 1998.

[63] Duel-Hallen, J. Holtzman, and Z. Zvonar, "Multiuser detection for CDMA systems," *IEEE Personal Commun.*, vol. 2, no. 2, pp. 46 – 58, Apr. 1995.

[64] X. Wang and H. V. Poor, "Space-time multiuser detection in multipath CDMA channels," *IEEE Trans. Signal Process.*, vol. 47, no. 9, Sept. 1999.

[65] M. Honig and M. K. Tsatsanis, "Adaptive techniques for multiuser CDMA receivers," *IEEE Signal Process. Mag.*, vol. 17, no. 3, pp. 49 – 61, May 2000.

[66] J. Tellado, *Multicarrier Modulation with Low PAR: Applications to DSL and Wireless*, Boston, Kluwer Academic, 2000.

[67] J. Vuolevi and T. Rahkonen, *Distortion in RF Power Amplifiers*, Norwood Artech House, 2003.

[68] R. Prasad, *OFDM for Wireless Communications Systems*, Boston Artech House, 2004, 2004.

[69] H. Ochiai and H. Imai, "On the distribution of the peak-to-average power ratio in OFDM signals," *IEEE Trans. Commun.*, vol. 49, no. 2, pp. 282 – 289, Feb. 2001.

[70] R. van Nee and A. de Wild, "Reducing the peak-to-average power ratio of OFDM," in *Proc. IEEE Vehicular Technology Conference, VTC'98*, May 1998, vol. 3, pp. 2072 – 2076, Ottawa, Canada.

[71] R. Baxley and G. T. Zhou, "Power savings analysis of peak-to-average power ratio in OFDM," *IEEE Trans. Consum. Electron.*, vol. 50, no. 3, pp. 792 – 798, Aug. 2004.

[72] S. Akamatsu, C. Baylis, and L. Dunleavy, "Accurate simulation models yield high-efficiency power amplifier design," *IEEE Microw. Mag.*, vol. 6, no. 4, pp. 114 – 124, Dec. 2005.

[73] S. Boumaiza and F. Ghannouchi, "Thermal memory effects modeling and compensation in RF power amplifiers and predistortion linearizers," *IEEE Trans. Microw. Theory Tech.*, vol. 51, no. 12, pp. 2427 – 2433, Dec. 2003.

[74] A. A. M. Saleh, "Frequency-independent and frequency-dependent nonlinear models of TWT amplifiers," *IEEE Trans. Commun.*, vol. 29, no. 11, pp. 1715–1720, Nov. 1981.

[75] T. Nguyen, J. Yoh, C. Lee, H. Tran, and D. Johnson, "Modeling of HPA and HPA linearization through a predistorter: Global broadcasting service applications,," *IEEE Trans. Broadcast.*, vol. 49, no. 2, pp. 132 – 141, June 2003.

[76] A. Ghorbani and M. Sheikhan, "The effect of solid state power amplifiers (SSPAs) nonlinearities on MPSK and M-QAM signal transmission," in *Proc. Sixth International Conference on Digital Processing of Signals in Communications*, Sept. 1991, vol. 1, pp. 193–197, Leicestershire, UK.

[77] C. Rapp, "Effects of HPA nonlinearity on a 4-DPSK/OFDM signal for a digital sound broadcasting system," in *Proc. European Conference on Satellite Communications*, Oct. 1991, vol. 1, pp. 179–184, Liege, Belgium.

[78] G. T. Zhou, H. Qian, L. Ding, and R. Raich, "On the baseband representation of a bandpass nonlinearity," *IEEE Trans. Signal Process.*, vol. 53, no. 8, pp. 2953–2957, Aug. 2005.

[79] L. Ding, *Digital Predistortion of Power Amplifiers for Wireless Applications*, Ph.D. thesis, School of Electrical and Computer Engineering, Georgia Institute of Technology, Mar. 2004.

[80] R. Raich, *Nonlinear System Identification and Analysis with Applications to Power Amplifier Modeling and Power Amplifier Predistortion*, Ph.D. thesis, School of Electrical and Computer Engineering, Georgia Institute of Technology, Mar. 2004.

[81] W. Bosch and G. Gatti, "Measurements and simulation of memory effects in predistortion linearizers," *IEEE Trans. Microw. Theory Tech.*, vol. 37, no. 12, pp. 1885 – 1890, Dec. 1989.

[82] R. Raich, H. Qian, and G. T. Zhou, "Orthogonal polynomials for power amplifier modeling and predistorter design," *IEEE Trans. Veh. Technol.*, vol. 53, no. 5, pp. 1468–1479, Sept. 2004.

[83] L. Ding, H. Qian, N. Chen, and G. T. Zhou, "A memory polynomial predistorter implemented using TMS320C67," in *Proc. Texas Instruments Developer Conference*, Feb. 2004, Houston, USA.

[84] J. J. Bussgang, "Cross correlation function of amplitude-distorted Gaussian input signals," *Res. Lab Electron., M.I.T., Cambridge, MA, Tech. Rep. 216*, vol. 3, Mar. 1952.

[85] J. Minkoff, "The role of AM-to-PM conversion in memoryless nonlinear systems," *IEEE Trans. Commun.*, vol. 33, no. 2, pp. 139 – 144, Feb. 1985.

[86] A. Bahai, M. Singh, A. Goldsmith, and B. Saltzberg, "A new approach for evaluating clipping distortion in multicarrier systems," *IEEE J. Sel. Areas Commun.*, vol. 20, no. 5, pp. 1037–1046, June 2002.

[87] D. Dardari, V. Tralli, and A. Vaccari, "A theoretical characterization of nonlinear distortion effects in OFDM systems," *IEEE Trans. Commun.*, vol. 48, no. 10, pp. 1755– 1764, Oct. 2000.

[88] I. Santamaria, J. Ibanez, M. Lazaro, C. Pantaleon, and L. Vielva, "Modeling nonlinear power amplifiers in OFDM systems from subsampled data: A comparative study using real measurements," *EURASIP Journal on Applied Signal Processing*, vol. 2003, no. 12, pp. 1219–1228, 2003.

[89] H. Ku, *Behavioral modeling of nonlinear RF power amplifiers for digital wireless communication systems with implications for predistortion linearization systems*, Ph.D. thesis, School of Electrical and Computer Engineering, Georgia Institute of Technology, Dec. 2003.

[90] J. Vuolevi, *Analysis, measurement and cancellation of the bandwidth and amplitude dependence of intermodulation distortion in RF power amplifiers*, Ph.D. thesis, University of Oulu, Finland, Oct. 2001.

[91] H. Ku and J. Kenney, "Behavioral modeling of nonlinear RF power amplifiers considering memory effects," *IEEE Trans. Microw. Theory Tech.*, vol. 51, no. 12, pp. 2495– 2504, Dec. 2003.

[92] J. Wood and D. E. Root, *Fundamentals of nonlinear behavioral modeling for RF and microwave design*, Artech, 2005.

[93] T. Turlington, *Behavioral modeling of nonlinear RF and microwave devices*, Artech, 2000.

[94] J. Pedro and S. Maas, "A comparative overview of microwave and wireless power-amplifier behavioral modeling approaches," *IEEE Trans. Microw. Theory Tech.*, vol. 53, no. 4, pp. 1150– 1163, Apr. 2005.

[95] M. Isaksson, D. Wisell, and D. Ronnow, "A comparative analysis of behavioral models for RF power amplifiers," *IEEE Trans. Microw. Theory Tech.*, vol. 54, no. 1, pp. 348–349, Jan. 2006.

[96] E. Aschbacher, *Digital Predistortion of Microwave Power Amplifiers*, Ph.D. thesis, Technishe Universitat Wien, Mar. 2004.

[97] C. Crespo-Cadenas, J. Reina-Tosina, and M. J. Madero-Ayora, "Volterra behavioral model for wideband RF amplifiers," *IEEE Trans. Microw. Theory Tech.*, vol. 55, no. 3, pp. 449 – 457, Mar. 2007.

[98] R. Hacioglu and G. A. Williamson, "Reduced complexity volterra models for nonlinear system identification," *EURASIP Journal on Applied Signal Processing*, vol. 2001, no. 4, pp. 257–265, 2001.

[99] M. Isaksson and D. Ronnow, "A Kautz-Volterra behavioral model for RF power amplifiers," in *Proc. IEEE Int. Microwave Symp. Dig., MTT-S'06*, June 2006, pp. 485 – 488, San Francisco, USA.

[100] D. Morgan, Z. Ma, J. Kim, M. Zierdt, and J. Pastalan, "A generalized memory polynomial model for digital predistortion of RF power amplifiers," *IEEE Trans. Signal Process.*, vol. 54, no. 10, pp. 3852–3860, Oct. 2006.

[101] J. Cousseau, J. Figueroa, S. Werner, and T. Laakso, "Efficient nonlinear Wiener model identification using a complex-valued simplicial canonical piecewise linear filter," *IEEE Trans. Signal Process. Part 1*, vol. 55, no. 5, pp. 1780 – 1792, May 2007.

[102] A. Hagenblad, "Aspects of the identification of Wiener models," M.S. thesis, Division of Automatic Control, Department of Electrical Engineering Linkopings universitet, 1999.

[103] L. Ding, G. T. Zhou, D. R. Morgan, Z. Ma, J. S. Kenney, J. Kim, and C. R. Giardina, "A robust digital baseband predistorter constructed using memory polynomials," *IEEE Trans. Commun.*, vol. 52, no. 1, pp. 159–165, Jan. 2004.

[104] A. Tarighat and A. H. Sayed, "MIMO OFDM receivers for systems with IQ imbalances," *IEEE Trans. Signal Process.*, vol. 53, no. 9, pp. 3583 – 3596, Sept. 2005.

[105] A. Tarighat, R. Bagheri, and A. H. Sayed, "Compensation schemes and performance analysis of IQ imbalances in OFDM receivers," *IEEE Trans. Signal Process.*, vol. 53, no. 8, pp. 3257 – 3268, Aug. 2005.

[106] J. Tubbax, B. Come, L. Van der Perre, L. Deneire, S. Donnay, and M. Engels, "Compensation of IQ imbalance in OFDM systems," in *Proc. IEEE International Conference on Communications, ICC'03*, May 2003, vol. 5, pp. 3403 – 3407, Anchorage, Alaska.

[107] C. Muschallik, "Influence of RF oscillators on an OFDM signal," *IEEE Trans. Consum. Electron.*, vol. 41, no. 3, pp. 592 – 603, Aug. 1995.

[108] M. Valkama, *Advanced I/Q signal processing for wideband receivers: Models and algorithms*, Ph.D. thesis, Tampere University of Technology, Dec. 2001.

[109] M. Valkama, A. Ghadam, L. Anttila, and M. Renfors, "Advanced digital signal processing techniques for compensation of nonlinear distortion in wideband multicarrier radio receivers," *IEEE Trans. Microw. Theory Tech.*, vol. 54, no. 6, pp. 2356 – 2366, June 2006.

[110] L. Piazzo and P. Mandarini, "Analysis of phase noise effects in OFDM modems," *IEEE Trans. Commun.*, vol. 50, no. 10, pp. 1696–1705, Oct. 2003.

[111] T. Pollet, M. Moeneclaey, I. Jeanclaude, and H. Sari, "Effect of carrier phase jitter on single-carrier and multi-carrier QAM systems," in *Proc. IEEE International Conference on Communications, ICC'95*, June 1995, pp. 1046 – 1050, Seatle, USA.

[112] T. Pollet, M. V. Bladel, and M. Moeneclaey, "BER sensitivity of OFDM systems to carrier frequency offset and wiener phase noise," *IEEE Trans. Commun.*, vol. 43, no. 10, pp. 191–193, Feb. - Apr. 1995.

[113] S. Wu and Y. Bar-Ness, "OFDM systems in the presence of phase noise: consequences and solutions," *IEEE Trans. Commun.*, vol. 52, no. 11, pp. 1988 – 1996, Nov. 2004.

[114] H.-G. Ryu, Y. S. Li, and J.-S. Park, "Nonlinear analysis of the phase noise in the OFDM communication system," *IEEE Trans. Consum. Electron.*, vol. 50, no. 1, pp. 54 – 63, Feb. 2004.

[115] R. Rao and B. Daneshrad, "Analog impairments in MIMO-OFDM systems," *IEEE Trans. Wireless Commun.*, vol. 50, no. 12, pp. 3382 – 3387, Dec. 2006.

[116] B. Ai, Z.-X. Yang, C.-Y. Pan, J.-H. Ge, Y. Wang, and Z. Lu, "On the synchronization techniques for wireless OFDM systems," *IEEE Trans. Broadcast.*, vol. 52, no. 2, pp. 236 – 244, Mar. 2006.

[117] M. Morelli, C.-C. Jay Kuo, and M. O. Pun, "Synchronization techniques for orthogonal frequency division multiple access (OFDMA): A tutorial review," *Proceedings of the IEEE*, vol. 95, no. 7, pp. 1394 – 1427, July 2007.

[118] T. Roman, *Advanced Receiver Structures for mobile MIMO Multicarrier Communication Systems*, Ph.D. thesis, Helsinki University of Technology, March. 2006.

[119] J. Li, G. Liu, and G. B. Giannakis, "Carrier frequency offset estimation for OFDM-based WLANs," *IEEE Signal Process. Lett.*, vol. 8, no. 3, pp. 80 – 82, 2001.

[120] A. Coulson, "Maximum likelihood synchronization for OFDM using a pilot symbol algorithms," *IEEE J. Sel. Areas Commun.*, vol. 19, no. 12, pp. 2486 – 2494, Dec. 2001.

[121] F. Yan, W.-P. Zhu, and M. O. Ahmad, "Carrier frequency offset estimation and I/Q imbalance compensation for OFDM systems," *EURASIP Journal on Advances in Signal Processing*, vol. 2007, pp. Article ID 45364, 11 pages, 2007, doi:10.1155/2007/45364.

[122] P. Moose, "A technique for orthogonal frequency division multiplexing frequency offset correction," *IEEE Trans. Commun.*, vol. 42, no. 10, pp. 2908–2914, Oct. 1994.

[123] N. Lashkarian and S. Kiaei, "Class of cyclic-based estimators for frequency-offset estimation of OFDM systems," *IEEE Trans. Commun.*, vol. 48, no. 12, pp. 2139 – 2149, Dec. 2000.

[124] J. J. V. D. Beek, M. Sandell, and P. O. Borjesson, "ML estimation of time and frequency offset in OFDM systems," *IEEE Trans. Signal Process.*, vol. 45, no. 7, pp. 1800 – 1805, July 1997.

[125] X. Ma, C. Tepedelenlioglu, G. B. Giannakis, and S. Barbarossa, "Non-data-aided carrier offset estimators for OFDM with null subcarriers: identifiability, algorithms, and performance," *IEEE J. Sel. Areas Commun.*, vol. 19, no. 12, pp. 2504 – 2515, Dec. 2001.

[126] E. Costa and S. Pupolin, "M-QAM-OFDM System performance in the presence of a nonlinear amplifier and phase noise," *IEEE Trans. Commun.*, vol. 50, no. 3, pp. 462–472, Mar. 2002.

[127] H. Ochiai, "Performance analysis of peak power and band-limited OFDM system with linear scaling," *IEEE Trans. Wireless Commun.*, vol. 2, no. 5, pp. 1055 – 1065, Sept. 2003.

[128] M. Friese, "On the degradation of OFDM-signals due to peak-clipping in optimally predistorted power amplifiers," in *Proc. IEEE Global Communications Conference, GLOBECOM 98*, Nov. 1998, vol. 2, pp. 939–944, Sidney.

[129] P. Banelli and S. Capocardi, "Theoretical analysis and performance of OFDM signals in nonlinear AWGN channels," *IEEE Trans. Commun.*, vol. 48, no. 3, pp. 430 – 441, Mar. 2000.

[130] H. Ochiai and H. Imai, "Performance analysis of deliberately clipped OFDM signals," *IEEE Trans. Commun.*, vol. 50, no. 1, pp. 89 – 101, Jan. 2002.

[131] I. Gradshteyn and I. Ryzhik, *Table of integrals, Series and products*, Academic Press, 1994.

[132] R. F. Baum, "The correlation function of smoothly limited gaussian noise," *IRE Trans. Inform. Theory*, vol. 3, pp. 193 – 196, Sept. 1957.

[133] O. Shimbo, "Effects of intermodulation, AM-PM conversion and additive noise in multicarrier TWT systems," *Proc. IEEE*, vol. 59, no. 2, pp. 230 – 238, Feb. 1971.

[134] K. Gard, H. Gutierrez, and M. Steer, "Characterization of spectral regrowth in microwave amplifiers based on the nonlinear transformation of a complex gaussian process," *IEEE Trans. Microw. Theory Tech.*, vol. 47, no. 7, pp. 1059 – 1069, July 1999.

[135] K. Gard, L. Larson, and M. Steer, "The impact of RF front-end characteristics on the spectral regrowth of communications signals," *IEEE Trans. Microw. Theory Tech.*, vol. 53, no. 6, pp. 2179 – 2186, June 2005.

[136] G. T. Zhou and J. S. Kenney, "Predicting spectral regrowth of nonlinear power amplifiers," *IEEE Trans. Commun.*, vol. 50, no. 5, pp. 718 – 722, May 2002.

[137] G. T. Zhou, "Analysis of spectral regrowth of weakly nonlinear power amplifiers," *IEEE Commun. Lett.*, vol. 4, no. 11, pp. 357 – 359, Nov. 2000.

[138] G. T. Zhou and R. Raich, "Spectral analysis of polynomial nonlinearity with applications to RF power amplifiers," *EURASIP Journal on Applied Signal Processing*, vol. 2004, no. 12, pp. 1831 – 1840, 2004.

[139] B. Baytekin and R. G. Meyer, "Analysis and simulation of spectral regrowth in radio frequency power amplifiers," *IEEE J. Solid-State Circuits*, vol. 40, no. 2, pp. 370 – 381, Feb. 2005.

[140] S. A. Maas, "Volterra analysis of spectral regrowth," *IEEE Microwave and Guided Waves Lett.*, vol. 7, no. 7, pp. 192 – 193, July 1997.

[141] J. Winters, J. Salz, and R. D. Gitlin, "The impact of antenna diversity on the capacity of wireless communication systems," *IEEE Trans. Commun.*, vol. 42, no. 2, pp. 1740–1751, Feb-Apr. 1994.

[142] T. Schenk, *RF Impairments in Multiple Antenna OFDM - Influence and Mitigation*, Ph.D. thesis, TU Eindhoven, The Netherlands, Nov. 2006.

[143] T. Schenk, X.-J. Tao, P. Smulders, and E. Fledderus, "A two-step modeling approach for the influence of radio-system impairments in multicarrier MIMO systems," in *Proc. IEEE Personal, Indoor and Mobile Radio Communications, PIMRC 2005*, Sept. 2005, vol. 11, pp. 176 – 180, Berlin, Germany.

[144] T. Schenk, P. Smulders, and E. Fledderus, "Impact of nonlinearities in multiple antenna OFDM transceivers," in *Proc. IEEE Symp. Benelux Chapter on Communications and Vehicular Technology (SCVT-2006)*, Nov. 2006, vol. 11, pp. 53 – 56, Liege, Belgium.

[145] F. Gregorio, S. Werner, T. Laakso, and J. Cousseau, "Analysis of SDMA-OFDM system BER performance in presence of power amplifier nonlinearities," in *Proc. IEEE Signal Processing Advances in Wireless Communications, SPAWC 2006*, May 2006, Cannes, France.

[146] M. Abramowitz and I. Stegun, *Handbook of mathematical functions with formulas, graphs, and mathematical tables*, Norwich (NY) Knovel 2002.

[147] I. Gradshteyn and I. Ryzhik, *Table of integrals and products*, Academic Press, 1965.

[148] A. Chaker, M. Atiaudo, I. Fijalkow, and J. Gautier, "Precompensation of the frequency-dependence of a non-linear amplifier in a multi-carrier transmission," in *Proc. IEEE International Conference on Communications, ICC'04*, June 2004, vol. 4, pp. 2464–2467, Paris, France.

[149] P. Garcia, A. Ortega, J. de Mingo, and A. Valdovinos, "Nonlinear distortion cancellation using LINC transmitters in OFDM systems," *IEEE Trans. Broadcast.*, vol. 51, no. 1, pp. 84 – 93, Mar. 2005.

[150] D. Jennings and J. McGeehan, "A high-efficiency RF transmitter using VCO-derived synthesis: CALLUM," *IEEE Trans. Microw. Theory Tech.*, vol. 47, no. 6, pp. 715 – 721, June 1999.

[151] N. Chen, G. T. Zhou, and H. Qian, "Power efficiency improvements through peak-to-average power ratio reduction and power amplifier linearization," *EURASIP Journal on Advances in Signal Processing*, vol. 2007, pp. ID 20463, 7 pages, 2007.

[152] X. Huang, J. Lu, J. Zheng, K. Letaief, and J. Gu, "Companding transform for reduction in peak-to-average power ratio of OFDM signals," *IEEE Trans. Wireless Commun.*, vol. 3, no. 6, pp. 2030 – 2039, Nov. 2004.

[153] T. Pratt, N. Jones, L. Smee, and M. Torrey, "OFDM link performance with companding for PAPR reduction in the presence of non-linear amplification," *IEEE Trans. Broadcast.*, vol. 52, no. 2, pp. 261 – 267, June 2006.

[154] S. Mann, M. Beach, P. Warr, and J. McGeehan, "Increasing the talk-time of mobile radios with efficient linear transmitter architectures," *Electronics Communication Engineering Journal*, vol. 13, no. 2, pp. 65 – 76, Apr. 2001.

[155] Hittite Microwave Corporation, *http://www.hittite.com*.

[156] D. Wulich, "Reduction of peak to mean ratio of multicarrier modulation using cyclic coding," *IEE Electronics Lett.*, vol. 32, no. 5, pp. 432–433, Feb. 1996.

[157] S. H. Muller and J. B. Huber, "OFDM with reduced peak-to-average power ratio by optimum combination of partial transmit sequences," *IEE Electronics Lett.*, vol. 33, no. 5, pp. 368 – 369, Feb. 1997.

[158] M. Tan, Z. Latinovic, and Y. Bar-Ness, "STBC MIMO-OFDM peak-to-average power ratio reduction by cross-antenna rotation and inversion," *IEEE Commun. Lett.*, vol. 9, pp. 592 – 594, July 2005.

[159] K. W. Park and Y. S. Cho, "A PAPR reduction method for MIMO-OFDM systems using subband permutation," *IEICE Trans. Commun.*, vol. E89-B, pp. 220 – 222, Jan. 2006.

[160] Y. L. Lee, Y. H. You, W. G. Jeon, J. H. Paik, and H. K. Song, "Peak-to-average power ratio in MIMO-OFDM systems using selective mapping," *IEEE Commun. Lett.*, vol. 7, no. 12, pp. 1885 – 1890, Dec. 2003.

[161] A. Venkataraman, H. Reddy, and T. M. Duman, "Space-time coded OFDM with low PAPR," *EURASIP Journal on Applied Signal Processing*, vol. 2006, pp. Article ID 87125, 9 pages, 2006.

[162] T. Schenk, P. Smulders, and E. Fledderus, "The application of spatial shifting for peak-to-average power ratio reduction in MIMO OFDM systems," in *Proc. IEEE Vehicular Technology Conference, VTC'06-Spring*, May 2006, vol. 11, pp. 1859 – 1863, Melbourne, Australia.

[163] T. Schenk, P. Smulders, and E. Fledderus, "Peak-to-average power reduction in space division multiplexing based OFDM systems through spatial shifting," *Electronics Letters*, vol. 41, no. 15, pp. 860 – 861, July 2005.

[164] R. Raich, H. Qian, and G. T. Zhou, "Optimization of SNDR for amplitude-limited nonlinearities," *IEEE Trans. Commun.*, vol. 53, no. 11, pp. 1964 – 1972, Nov. 2005.

[165] A. E. Jones, T. A. Wilkinson, and S. K. Barton, "Block coding scheme for reduction of peak to mean envelope power ratio of multicarrier transmission schemes," *IEE Electronics Lett.*, vol. 30, no. 25, pp. 2098–2099, Dec. 1994.

[166] K. Sathananthan and C. Tellambura, "Coding to reduce both PAR and PICR of an OFDM signal," *IEEE Commun. Lett.*, vol. 6, no. 8, pp. 316– 318, Aug. 2002.

[167] K. Paterson and V. Tarokh, "On the existence and construction of good codes with low peak-to-average power ratios," *IEEE Trans. Inf. Theory*, vol. 46, no. 6, pp. 1974–1987, Sept. 2000.

[168] C. Tellambura, "Improved phase factor computation for the PAPR reduction of an OFDM signal using PTS," *IEEE Commun. Lett.*, vol. 5, no. 4, pp. 135 – 137, Apr. 2001.

[169] D. W. Lim, S. J. Heo, J. S. No, and H. Chung;, "A new PTS OFDM scheme with low complexity for PAPR reduction," *IEEE Trans. Broadcast.*, vol. 52, no. 1, pp. 77 – 82, Mar. 2006.

[170] S. H. Han and J. H. Lee, "PAPR reduction of OFDM signals using a reduced complexity PTS technique," *IEEE Signal Process. Lett.*, vol. 11, no. 11, pp. 887 – 890, Nov. 2006.

[171] A. D. S. Jayalath and C. Tellambura, "An adaptive PTS approach for the reduction of peak-to-average power ratio of an OFDM signal," *IEE Electronics Lett.*, vol. 36, pp. 1161–1163, July 2000.

[172] L. J. Cimini, B. Daneshrad, and N. Sollenberger, "Clustered OFDM with transmitter diversity and coding," in *Proc. IEEE Global Communications Conference, GLOBECOM 96*, Nov. 1996, vol. 1, pp. 703–707, London.

[173] J. Cavers, "Amplifier linearization using a digital predistorter with fast adaptation and low memory requirements," *IEEE Trans. Veh. Technol.*, vol. 39, no. 4, pp. 374–382, Nov. 2000.

[174] A. A. M. Saleh and J. Salz, "Adaptive linearization of power amplifiers in digital radio systems," *Bell Syst. Tech. J.*, vol. 62, no. 4, pp. 1019–1033, Apr. 1983.

[175] W. G. Jeon, K. H. Chang, and Y. S. Cho, "An adaptive data predistorter for compensation of nonlinear distortion in OFDM systems," *IEEE Trans. Commun.*, vol. 45, no. 10, pp. 1167–1172, Oct. 1997.

[176] A. D'Andrea, V. Lottici, and R. Reggiannini, "Nonlinear predistortion of OFDM signals over frequency-selective fading channels," *IEEE Trans. Commun.*, vol. 49, no. 5, pp. 837 – 843, May 2001.

[177] M. Faulkner and M. Johansson, "Adaptive linearization using predistortion-experimental results," *IEEE Trans. Veh. Technol.*, vol. 43, no. 2, pp. 323 – 332, May 1994.

[178] H.-H. Chen, C.-H. Lin, P.-C. Huang, and J.-T. Chen, "Joint polynomial and look-up-table predistortion power amplifier linearization," *IEEE Trans. Circuits Syst. II*, vol. 53, no. 8, pp. 612 – 616, Aug. 2006.

[179] H. Zhi-yong, G. Jian-hua, G. Shu-jian, and W. Gang;, "An improved look-up table predistortion technique for HPA with memory effects in OFDM systems," *IEEE Trans. Broadcast.*, vol. 52, no. 1, pp. 87 – 91, Mar. 2006.

[180] K. Muhonen, M. Kavehrad, and R. Krishnamoorthy, "Look-up table techniques for adaptive digital predistortion: a development and comparison," *IEEE Trans. Veh. Technol.*, vol. 39, no. 3, pp. 1995 – 2002, Sept. 2000.

[181] Y. Guo and J. Cavallaro, "Enhanced power efficiency of mobile OFDM radio using predistortion and post-compensation," in *Proc. IEEE Vehicular Technology Conference, VTC'02-Fall*, Sept. 2002, vol. 1, pp. 214 – 218, Vancouver, Canada.

[182] M. Y. Cheong, S. Werner, and T. I. Laakso, "Design of predistorters for power amplifiers in future mobile communications systems," in *Nordic Signal Processing Symposium NORSIG'04*, June 2004, Espoo, Finland.

[183] J. S. Kenney, W. Woo, L. Ding, R. Raich, H. Ku, and G. T. Zhou, "The impact of memory effects on predistortion linearization of RF power amplifiers," in *Proc. 8th Int. Microwave Opt. Technol. Symp.*, June 2001, pp. 189 – 193, Montreal, Canada.

[184] H. Kang, Y. Cho, and D. Youn, "On compensating nonlinear distortions of an OFDM system using an efficient adaptive predistorter," *IEEE Trans. Commun.*, vol. 47, no. 4, pp. 522–526, Apr. 1999.

[185] D. Zhou and V. E. DeBrunner, "Novel adaptive nonlinear predistorters based on the direct learning algorithm," *IEEE Trans. Signal Process.*, vol. 55, no. 1, pp. 120 – 133, Jan. 2007.

[186] C. Eun and E. J. Powers, "A new Volterra predistorter based on the indirect learning architecture," *IEEE Trans. Signal Process.*, vol. 45, no. 1, pp. 223 – 227, Jan. 1997.

[187] K. F. To, P. Ching, and K. M. Wong, "Compensation of amplifier nonlinearities on wavelet packet division multiplexing," in *Proc. IEEE Int. Conf. Acoust., Speech, Signal Process., ICASSP'01*, May 2001, vol. 4, pp. 2669 – 2672, Utah, USA.

[188] J. Tsimbinos and K. Lever, "Nonlinear system compensation based on orthogonal polynomial inverses," *IEEE Trans. Circuits Syst. I: Fundam. Theory Appl.*, vol. 48, no. 4, pp. 406 – 417, Apr. 2006.

[189] C. Tseng and E. J. Powers, "Nonlinear channel equalization in digital satellite systems," in *Proc. IEEE Global Telecommunications Conference, GLOBECOM 1993*, Nov. 1993, vol. 1, pp. 1639–1643, Houston.

[190] E. Biglieri, S. Barberis, and M. Catena, "Analysis and compensation of nonlinearities in digital transmission systems," *IEEE J. Sel. Areas Commun.*, vol. 6, no. 1, pp. 42 – 51, Jan. 1988.

[191] M. Schetzen, *The Volterra and Wiener Theories of Nonlinear Systems*, J. Wiley Sons, 1980.

[192] A. Zhu and T. Brazil, "An adaptive volterra predistorter for the linearization of RF high power amplifiers," in *Proc. IEEE Int. Microwave Symp. Dig., MTT-S'02*, June 2002, vol. 1, pp. 461 – 464, Seattle, USA.

[193] H. W. Kang, Y. S. Cho, and D. H. Youn, "Adaptive precompensation of Wiener systems," *IEEE Trans. Signal Process.*, vol. 46, no. 10, pp. 2825 – 2829, Oct. 1998.

[194] T. Liu, S. Boumaiza, and F. Ghannouchi, "Pre-compensation for the dynamic nonlinearity of wideband wireless transmitters using augmented Wiener predistorters," in *Proc. Asia-Pacific Microwave Conference, APMC 2005*, Dec. 2005, Suzhou, China.

[195] P. Gilabert, G. Montoro, and E. Bertran, "On the Wiener and Hammerstein models for power amplifier predistortion," in *Proc. Asia-Pacific Microwave Conference, APMC 2005*, Dec. 2005, Suzhou, China.

[196] E. Aschbacher and M. Rupp, "Modeling and identification of a nonlinear power-amplifier with memory for nonlinear digital adaptive predistortion," in *Proc. IEEE Signal Processing Advances in Wireless Communications, SPAWC 2003*, June 2003, vol. 1, pp. 658 – 662, Rome, Italy.

[197] T. Liu, S. Boumaiza, and F. Ghannouchi, "Augmented Hammerstein predistorter for linearization of broad-band wireless transmitters," *IEEE Trans. Microw. Theory Tech.*, vol. 54, no. 4, pp. 1340 – 1349, June 2006.

[198] D. Zhou and V. Debrunner, "A simplified adaptive nonlinear predistorter for high power amplifiers based on the direct learning algorithm," in *Proc. IEEE Int. Conf. Acoust. Speech, Signal Process., ICASSP'04*, May 2004, vol. 4, pp. IV– 1037–40, Montreal, Canada.

[199] L. Ding, R. Raich, and G. T. Zhou, "A Hammerstein predistortion linearization design based on the indirect learning architecture," in *Proc. IEEE Int. Conf. Acoust., Speech, Signal Process., ICASSP'02*, May 2002, vol. 3, pp. III 2689 – 2692, Florida, USA.

[200] T. Liu, S. Boumaiza, and F. Ghannouchi, "Identification and precompensation of the electrical memory effects in wireless transceivers," in *Proc. IEEE Radio and Wireless Symp.*, Jan. 2006, pp. 535 – 538, San Diego, USA.

[201] J. Kim and K. Konstantinou, "Digital predistortion of wideband signals based on power amplifier model with memory," *IEE Electronics Lett.*, vol. 37, pp. 1417–1418, Nov. 2001.

[202] L. Ding, Z. Ma, D. Morgan, M. Zierdt, and J. Pastalan, "A least-squares/Newton method for digital predistortion of wideband signals," *IEEE Trans. Commun.*, vol. 54, no. 5, pp. 833– 840, May 2006.

[203] B. Watkins and R. North, "Predistortion of nonlinear amplifiers using neural networks," in *Proc. IEEE Military Communications Conference, MILCOM '96*, Oct. 1996, vol. 1, pp. 316 – 320.

[204] N. Naskas and Y. Papananos, "Neural-network-based adaptive baseband predistortion method for RF power amplifiers," *IEEE Trans. Circuits Syst. II,*, vol. 51, no. 11, pp. 619–623, Nov. 2004.

[205] M. Isaksson, D. Wisell, and D. Ronnow, "Wide-band dynamic modeling of power amplifiers using radial-basis function neural networks," *IEEE Trans. Microw. Theory Tech.*, vol. 53, no. 11, pp. 3422 – 3428, Nov. 2005.

[206] A. Mansell and A. Bateman, "Practical implementation issues for adaptive predistortion transmitter linearisation," in *IEE Colloquium on Linear RF Amplifiers and Transmitters*, April 1994, vol. 11.

[207] M.Wennström, *On MIMO Systems and Adaptive Arrays for Wireless Communication. Analysis and Practical Aspects*, Ph.D. thesis, Uppsala University, Oct. 2002.

[208] B. G., G. Reali, and S. Cacopardi, "A modified algorithm for the fast computation of even and odd order intermodulation products," *IEEE Commun. Lett.*, vol. 51, pp. 121–123, feb. 2005.

[209] S. Werner, M. Enescu, and V. Koivunen, "Combined frequency and time domain channel estimation in mobile MIMO-OFDM systems," in *Proc. IEEE Int. Conf. Acoust., Speech, Signal Process., ICASSP'06*, May 2006, pp. IV 373–376, Toulouse, France.

[210] L. Deneire, P. Vandenameele, L. van der Perre, B. Gyselinckx, and M. Engels, "A low-complexity ML channel estimator for OFDM," *IEEE Trans. Commun.*, vol. 51, no. 2, pp. 135–140, Feb. 2003.

[211] V. Erceg and e. a. K. Hari, "Channel models for fixed wireless applications," *Tech. rep., IEEE 802.16 Broadband Wireless Access Working Group*, Jan. 2001.

[212] R. Marsalek, P. Jardin, and G. Baudoin, "From post-distortion to predistortion for power amplifiers linearization," *IEEE Commun. Lett.*, vol. 7, no. 7, pp. 308 – 310, July 2003.

[213] J.-H. Han and S. Nam;, "Power amplifier linearisation using postdistortion error canceller based on complex envelope transfer characteristics," *Electronics Lett.*, vol. 36, no. 19, pp. 1665 – 1666, Sept. 2000.

[214] Y. Miar, M. Vaezi, and A. Momen, "A new post distorter of WLAN amplifiers using Hammerstein filter," in *Proc. Canadian Conference on Electrical and Computer Engineering, 2005*, May 2005, vol. 1, pp. 1701 – 1703, Saskatchewan, Canada.

[215] S. Stapleton and L. Quach, "Reduction of adjacent channel interference using postdistortion," in *Proc. IEEE Vehicular Technology Conference, VTC'02-Fall*, May 1992, vol. 2, pp. 915 – 918, Vancouver, Canada.

[216] C. H. Lee, V. Postoyalko, and T. O'Farrell, "Enhanced performance of rof link for cellular mobile systems using postdistortion compensation," in *Proc. IEEE Personal, Indoor and Mobile Radio Communi-*

cations, PIMRC 2004, Sept. 2004, vol. 4, pp. 2772 – 2776, Barcelona, Spain.

[217] J. Macdonald, "Nonlinear distortion reduction by complementary distortion," *IRE Trans. Audio*, vol. 7, no. 5, pp. 128 – 133, Sept. 1959.

[218] D. D. Falconer, "Adaptive equalization of channel nonlinearities in QAM data transmission systems," *Bell Syst. Tech.*, vol. 57, pp. 2589 – 2611, Sept. 1978.

[219] S. Benedetto and E. Biglieri, "Nonlinear equalization of digital satellite channels," *IEEE J. Sel. Areas Commun.*, vol. 1, no. 1, pp. 57 – 62, Jan. 1983.

[220] S. Benedetto, A. Gersho, R. D. Gitlin, and T. L. Lim, "Adaptive cancellation of nonlinear intersymbol interference for voiceband data transmission," *IEEE J. Sel. Areas Commun.*, vol. 2, no. 5, pp. 765 – 777, Sept. 1984.

[221] J. Tellado, L. Hoo, and J. Cioffi, "Maximum-likelihood detection of nonlinearly distorted multicarrier symbols by iterative decoding," *IEEE Trans. Commun.*, vol. 51, pp. 218–228, Feb. 2003.

[222] Y. Xiao, S. Li, X. Lei, and Y. Tang;, "Clipping noise mitigation for channel estimation in OFDM systems," *IEEE Commun. Lett.*, vol. 10, no. 6, pp. 474 – 476, June 2006.

[223] R. AliHemmati and P. Azmi, "Iterative reconstruction-based method for clipping noise suppression in OFDM systems," *IEE Commun. Proc.*, vol. 152, no. 4, pp. 452 – 456, Aug. 2005.

[224] G. Karam and H. Sari, "Analysis of predistortion, equalization, and ISI cancellation techniques in digital radio systems with nonlinear transmit amplifiers," *IEEE Trans. Commun.*, vol. 37, no. 12, pp. 1245 – 1253, Dec. 1989.

[225] S. Zhidkov, "Receiver synthesis for nonlinearly amplified OFDM signal," in *Proc. IEEE Workshop on Signal Processing Systems, SIPS 2003*, Aug. 2003, pp. 387 – 392, Seoul, Korea.

[226] H. Saeedi, M. Sharif, and F. Marvasti, "Clipping noise cancellation in OFDM systems using oversampled signal reconstruction," *IEEE Commun. Lett.*, vol. 6, no. 2, pp. 73 – 75, Feb. 2002.

[227] J. M. Cioffi and J. Binghman, "A data-driven multitone echo canceller," *IEEE Trans. Commun.*, vol. 42, no. 10, pp. 2853 – 2869, Oct. 1994.

[228] X. Li and L. J. Cimini, "Effects of clipping and filtering on the performance of OFDM," in *Proc. IEEE Vehicular Technology Conference, VTC'97*, May 1997, pp. 1634 – 1638, Arizona, USA.

[229] F. Marvasti, *Nonuniform Sampling: Theory and Practice*, New York: Kluwer Academic/Plenum, 2001.